

High-throughput annotation of full-length long noncoding RNAs with Capture Long-Read Sequencing (CLS)

Authors

Julien Lagarde^{*1,2}, Barbara Uszczyńska-Ratajczak^{*1,2,6}, Silvia Carbonell³, Sílvia Pérez-Lluch^{1,2}, Amaya Abad^{1,2}, Carrie Davis⁴, Thomas R. Gingeras⁴, Adam Frankish⁵, Jennifer Harrow^{5,7}, Roderic Guigo^{#1,2}, Rory Johnson^{#1,2,8}

* Equal contribution

Corresponding authors: rory.johnson@dkf.unibe.ch, roderic.guigo@crg.cat

Author affiliations

¹ Centre for Genomic Regulation (CRG), Barcelona Institute of Science and Technology (BIST), Dr. Aiguader 88, 08003 Barcelona, Spain.

² Universitat Pompeu Fabra (UPF), Barcelona, Spain.

³ R&D Department, Quantitative Genomic Medicine Laboratories (qGenomics), Barcelona, Spain.

⁴ Functional Genomics Group, Cold Spring Harbor Laboratory, 1 Bungtown Road, Cold Spring Harbor, New York 11724, USA.

⁵ Wellcome Trust Sanger Institute, Hinxton, Cambridgeshire, UK CB10 1HH.

⁶ Present address: International Institute of Molecular and Cell Biology, Ks. Trojdena 4, 02-109 Warsaw, Poland

⁷ Present address: Illumina, Cambridge, UK.

⁸ Present address: Department of Clinical Research, University of Bern, Murtenstrasse 35, 3010 Bern, Switzerland.

1

2
3
4

5

6
7
8
9
10
11
12
13
14
15

Keywords

Long non-coding RNA; lncRNA; lincRNA; RNA sequencing; transcriptomics; GENCODE; annotation; CaptureSeq; third generation sequencing; long read sequencing; PacBio; KANTR.

Abbreviations

bp: base pair
FL: full length
nt: nucleotide
ROI: read of insert, *i.e.* PacBio reads
SJ: splice junction
SMRT: single-molecule real-time
TM: transcript model

Abstract

Accurate annotations of genes and their transcripts is a foundation of genomics, but no annotation technique presently combines throughput and accuracy. As a result, current reference gene collections remain far from complete: many genes models are fragmentary, while thousands more remain uncatalogued—particularly for long noncoding RNAs (lncRNAs). To accelerate lncRNA annotation, the GENCODE consortium has developed RNA Capture Long Seq (CLS), combining targeted RNA capture with third generation long-read sequencing. We present an experimental re-annotation of the entire GENCODE intergenic lncRNA population in matched human and mouse tissues. CLS approximately doubles the annotated complexity of targeted loci, in terms of validated splice junctions and transcript models, outperforming existing short-read techniques. The full-length transcript models produced by CLS enable us to definitively characterize the genomic features of lncRNAs, including promoter- and gene-structure, and protein-coding potential. Thus CLS removes a longstanding bottleneck of transcriptome annotation, generating manual-quality full-length transcript models at high-throughput scales.

Introduction

Long noncoding RNAs (lncRNAs) represent a vast and largely unexplored component of the mammalian genome. Efforts to assign lncRNA functions rest on the availability of high-quality transcriptome annotations. At present such annotations are still rudimentary: we have little idea of the total lncRNA count, and for those that have been identified, transcript structures remain largely incomplete.

The number and size of available lncRNA annotations have grown rapidly thanks to projects using diverse approaches. Early gene sets, deriving from a mixture of FANTOM cDNA sequencing efforts and public databases (1,2) were joined by the “lincRNA” (long intergenic non-coding RNA) sets, discovered through analysis of chromatin signatures (3). More recently, studies have applied *de novo* transcript-reconstruction software, such as *Cufflinks* (4) and *Scripture* (5) to identify novel genes in short-read RNA sequencing (RNAseq) datasets (6-10). However the reference for lncRNAs, as for protein-coding genes, has become the regularly-updated, manual annotations from GENCODE, which are based on curation of cDNAs and ESTs by human annotators (11,12). GENCODE has been adopted by most international genomics consortia(13-17).

At present, annotation efforts are caught in a trade-off between throughput and quality. *De novo* methods deliver large annotations with low hands-on time and financial investment. In contrast, manual annotation is relatively slow and requires long-term funding. However the quality of *de novo* annotations is often doubtful, due to the inherent difficulty of reconstructing transcript structures from much shorter sequence reads. Such structures tend to be incomplete, often lacking terminal exons or omitting splice junctions between adjacent exons (18). This particularly affects lncRNAs, whose low expression results in low read coverage (12). The outcome is a growing divergence between automated annotations of large size but uncertain quality (*e.g.* 101,700 genes for NONCODE (9), and smaller but highly-curated “conservative” annotations of GENCODE (15,767 genes for version 25) (12).

Annotation incompleteness takes two forms. First, genes may be entirely missing from the annotation. Many genomic regions are suspected to transcribe RNA but presently contain no annotation, including “orphan” small RNAs with presumed long precursors (19), enhancers (20)

and ultraconserved elements (21,22). Similarly, thousands of single-exon predicted transcripts may be valid, but are generally excluded owing to doubts over their origin (12). The second form of incompleteness refers to missing or partial gene structures in already-annotated lncRNAs. Start and end sites frequently lack independent supporting evidence (12), and lncRNAs as annotated have shorter spliced lengths and fewer exons than mRNAs (8,12,23). Recently, RACE-Seq was developed to complete lncRNA annotations, but at relatively low throughput (23).

One of the principal impediments to lncRNA annotation arises from their low steady-state levels (3,12). To overcome this, targeted transcriptomics, or “RNA Capture Sequencing” (CaptureSeq) (24) is used to boost the concentration of known or suspected low-abundance transcripts in cDNA libraries. These studies have relied on Illumina short read sequencing and *de novo* transcript reconstruction (24-26), with accompanying doubts over transcript structure quality. Thus, while CaptureSeq achieves high throughput, its transcript structures lack the confidence required for inclusion in GENCODE.

In order to harness the power of CaptureSeq while eliminating *de novo* transcript assembly, we have developed RNA Capture Long Seq (CLS). CLS couples targeted RNA capture with third generation long-read cDNA sequencing. We used CLS to interrogate the GENCODE catalogue of intergenic lncRNAs, together with thousands of suspected novel loci, in six tissues each of human and mouse. CLS dramatically extends known annotations with high-quality novel structures. These data can be combined with other genomic data indicating 5’ and 3’ transcript termini to yield full-length transcript models in an automated way, allowing us to describe fundamental lncRNA promoter and gene structure properties for the first time. Thus CLS represents a significant advance in transcriptome annotation, and the dataset produced here advances our understanding of lncRNA’s basic properties.

Results

Capture Long Seq approach to extend the GENCODE lncRNA annotation

Our aim was to develop an experimental approach to improve and extend reference transcript annotations, while minimizing human intervention and avoiding *de novo* transcript assembly. We designed a method, Capture Long Seq (CLS), which couples targeted RNA capture to Pacific Biosciences (“PacBio”) Third Generation long-read sequencing (Figure 1A). The novelty of CLS is that it captures full-length, unfragmented cDNAs: this enables the targeted sequencing of low-abundance transcripts, while avoiding the uncertainty of assembled transcript structures from short-read sequencing.

CLS may be applied to two distinct objectives: to improve existing gene models, or to identify novel loci (blue and orange in Figure 1A, respectively). Although the present study focuses mainly on the first objective of improving existing lncRNA annotations, we demonstrate also that novel loci can be captured and sequenced. With this in mind, we created a comprehensive capture library targeting the set of intergenic GENCODE lncRNAs in human and mouse. It should be noted that annotations for human are presently more complete than for mouse, and this accounts for the differences in the annotation sizes throughout (9,090 vs 6,615 genes, respectively). It should also be noted that GENCODE annotations probed in this study are principally multi-exonic transcripts based on polyA+ cDNA and EST libraries, and hence are not likely to include many “enhancer RNAs” (11,27). To these we added tiled probes targeting loci that may produce lncRNAs: small RNA genes (28), enhancers (29) and ultraconserved elements (30). For mouse we also added orthologue predictions of human lncRNAs from PipeR (31). Numerous control probes were added, including a series targeting half of the ERCC synthetic spike-ins (32). Together, these sequences were used to design capture libraries of temperature-matched and non-repetitive oligonucleotide probes (Figure 1B).

To access the maximal breadth of lncRNA diversity, we chose a set of transcriptionally-complex and biomedically-relevant organs from mouse and human: whole brain, heart, liver and testis (Figure 1C). To these we added two deeply-studied ENCODE human cell lines, HeLa and K562 (33), and two mouse embryonic time-points (E7 and E15).

We designed a protocol to capture full-length, oligo-dT-primed cDNAs (full details can be found in Materials and Methods). Barcoded, unfragmented cDNAs were pooled and captured. Preliminary tests using quantitative PCR indicated strong and specific enrichment for targeted regions (Supplementary Figure 1). PacBio sequencing tends to favour shorter templates in a mixture (34). Therefore pooled, captured cDNA was size-selected into three ranges (1-1.5kb, 1.5-2.5kb, >2.5kb) (Supplementary Figure 2), and used to construct sequencing libraries for PacBio SMRT (single-molecular real-time) technology (35).

CLS yields an enriched long-read transcriptome

Samples were sequenced on altogether 130 SMRT cells, yielding ~2 million reads in total in each species (Figure 2A). PacBio sequence reads, or “reads of insert” (ROIs) were demultiplexed to retrieve their tissue of origin and mapped to the genome (see Materials and Methods for details). We observed high mapping rates (>99% in both cases), of which 86% and 88% were unique, in human and mouse, respectively (Supplementary Figure 3). For brevity, all data are henceforth quoted in order of human then mouse. The use of short barcodes meant that, for ~30% of reads, the tissue of origin could not be retrieved (Supplementary Figure 4). This may be remedied in future by the use of longer barcode sequences. Representation was evenly distributed across tissues, with the exception of testis (Supplementary Figure 5). The ROIs had a median length of 1 - 1.5 kb (Figure 2B) consistent with previous reports (34) and longer than typical lncRNA annotation of ~0.5 kb (12).

Capture performance is assessed in two ways: by “on-target” rate – the proportion of reads originating from probed regions – and by enrichment, or increase of on-target rate following capture (36). To estimate this, we sequenced pre- and post-capture libraries using MiSeq. CLS achieved on-target rates of 29.7% / 16.5%, representing 19- / 11-fold increase over pre-capture cDNA (Figure 2C, D and Supplementary Figure 6). The majority of off-target signal arises from non-targeted, annotated protein-coding genes (Figure 2C).

CLS on-target rates were lower than previous studies using fragmented cDNA (36). Side-by-side comparisons showed that this is likely due to the lower efficiency of capturing long

cDNA fragments (Supplementary Figure 7), as observed by others (26), and thus representing a future target for protocol optimization.

Synthetic spike-in sequences at known concentrations were used to assess CLS sensitivity and quantitiveness. We compared the relationship of sequence reads to starting concentration for the 42 probed (green) and 50 non-probed (violet) synthetic ERCC sequences in pre- and post-capture samples (Figure 2E, top and bottom rows). Given the low sequencing depth, CLS is surprisingly sensitive, extending detection sensitivity by two orders of magnitude, and capable of detecting molecules at approximately 5×10^{-3} copies per cell (Materials and Methods). As expected, it is less quantitative than conventional CaptureSeq (26), particularly at higher concentrations where the slope falls below unity. This suggests saturation of probes by cDNA molecules during hybridisation. A degree of noise, as inferred by the coefficient of determination (R^2) between read counts and template concentration, is introduced by the capture process (R^2 of 0.63 / 0.87 in human post-capture and pre-capture, respectively).

CLS expands the complexity of known and novel lncRNAs

CLS discovers a wealth of novel transcript structures within annotated lncRNA loci. A good example is the *SAMMSON* oncogene (*LINC01212*) (13), where we discover a variety of new exons, splice sites, and transcription termination sites that are not present in existing annotations (Figure 3A, more examples in Supplementary Figures 8, 9, 10). The existence of substantial additional downstream structure in *SAMMSON* could be validated by RT-PCR (Figure 3A).

Gathering the non-redundant union of all ROIs, we measured the amount of new complexity discovered in targeted lncRNA loci. CLS detected 58% and 45% of targeted lncRNA nucleotides, and extended these annotations by 6.3 / 1.6 Mb nucleotides (86% / 64% increase compared to existing annotations) (Supplementary Figure 11). CLS discovered 45,673 and 11,038 distinct splice junctions (SJs), of which 36,839 and 26,715 are novel (Figure 3B and Supplementary Figure 12, left bars). The number of novel, high-confidence human SJs amounted to 20,327 when using a deeper human SJ reference catalogue composed of both GENCODE v20 and miTranscriptome (8) as a reference (Supplementary Figure 13). For independent validation,

and given the relatively high sequence indel rate detected in PacBio reads (Supplementary Figure 14) (see Methods for analysis of sequencing error rates), we deeply sequenced captured cDNA by Illumina HiSeq at an average depth of 35 million / 26 million pair-end reads per tissue sample. Split reads from this data exactly matched 78% / 75% SJs from CLS. These “high-confidence” SJs alone represent a 160% / 111% increase over the existing, probed GENCODE annotations (Figure 3B, Supplementary Figure 12). Novel high-confidence lncRNA SJs are rather tissue-specific, with greatest numbers observed in testis (Supplementary Figure 15), and were also discovered across other classes of targeted and non-targeted loci (Supplementary Figure 16). We observed a greater frequency of intron retention events in lncRNAs, compared to protein-coding transcripts (Supplementary Figure 17).

To evaluate the biological significance of novel lncRNA SJs, we computed their strength using standard position weight matrix models from donor and acceptor sites (37) (Figure 3C, Supplementary Figure 18). High-confidence novel SJs from lncRNAs (orange, upper panel) far exceed the predicted strength of background SJ-like dinucleotides (bottom panels), and are essentially indistinguishable from annotated SJs in protein-coding and lncRNA loci (pink, upper and middle panels). Even unsupported, novel SJs (black) tend to have high scores in excess of background, although with a significant low-scoring tail. Although they display little evidence of sequence conservation using standard measures (similar to lncRNA SJs in general) (Supplementary Figure 19), novel SJs also display weak but non-random evidence of selected function between human and mouse (Supplementary Figure 20).

We estimated how close these sequencing data are to saturation of true gene structures, that is, to reaching a definitive lncRNA annotation. In each tissue sample, we tested the rate of novel splice junction and transcript model discovery as a function of increasing depth of randomly-sampled ROIs (Figure 3D, Supplementary Figures 21, 22). We observed an ongoing gain of novelty with increasing depth, for both low- and high-confidence SJs, up to that presented here. Similarly, no SJ discovery saturation plateau was reached at increasing simulated HiSeq read depth (Supplementary Figure 23). Thus, considerable additional sequencing is required to fully define the complexity of annotated GENCODE lncRNAs.

Beyond lncRNA characterization, CLS can be of utility to characterize many other types of transcriptional units. As an illustration, we searched for precursor transcripts of small RNAs

(microRNAs, snoRNAs and snRNAs), whose annotation remains poor (19). We probed 1 kb windows around all “orphan” small RNAs, *i.e.* those with no annotated overlapping transcript. Note that, although mature snoRNAs are non-polyadenylated, they tend to be processed from polyA⁺ precursor transcripts (38). We identified more than one hundred likely exonic primary transcripts, and hundreds more potential precursors harbouring small RNAs within their introns (Figure 3E). One intriguing example was the cardiac-enriched hsa-mir-143 (Supplementary Figure 24). We previously identified a standalone lncRNA in the same locus, *CARMEN1*, which is necessary for cardiac precursor cell differentiation (39). CLS identifies a new RT-PCR-supported isoform that overlaps hsa-mir-143, suggesting it is a bifunctional lncRNA directing a complex auto-regulatory feedback loop in cardiogenesis.

Assembling a full-length lncRNA annotation

A unique benefit of the CLS approach is the ability to identify full-length transcript models with confident 5’ and 3’ termini. ROIs of oligo-dT-primed cDNAs carry a fragment of the poly(A) tail, which can identify the polyadenylation site with basepair precision (34). Using conservative filters, 73% / 64% of ROIs had identifiable polyA sites (Supplementary Table S1) representing 16,961 / 12,894 novel polyA sites when compared to end positions of all GENCODE annotations. Both known and novel polyA sites were accompanied by canonical polyadenylation motifs (Supplementary Figure 25). Similarly, the 5’ completeness of ROIs was confirmed by proximity to methyl-guanosine caps identified by CAGE (Cap Analysis of Gene Expression) (17) (Supplementary Figure 26). Together, TSS and polyA sites were used to define the 5’ / 3’ completeness of all ROIs (Figure 4A).

We developed a pipeline to merge ROIs into a non-redundant collection of transcript models (TMs). In contrast to previous approaches (4), our “anchored merging” method respects confirmed internal TSS or polyA sites (Figure 4B). Applying this to captured ROIs results in a greater number of unique TMs than would be identified otherwise (Figure 4C, Supplementary Figure 27). Specifically, we identified 179,993 / 129,556 transcript models across all biotypes (Supplementary Table S2), 86 / 87% of which displayed support of their entire intron chain by captured HiSeq split reads (Supplementary Table S3). The *CCAT1* locus is an example where

several novel transcripts are identified, each with CAGE and polyA support of 5' and 3' termini, respectively (Figure 4D). CLS here suggests that adjacent *CCAT1* and *CASC19* gene models are in fact fragments of the same underlying gene, a conclusion supported by RT-PCR (Figure 4D)(40).

Merged TMs can be defined by their end support: full length (5' and 3' supported), 5' only, 3' only, or unsupported (Figure 4B, E). We identified a total of 65,736 / 44,673 full length (FL) transcript models (Figure 4E and Supplementary Figure 28, left panels): 47,672 (73%) / 37,244 (83%) arise from protein coding genes, and 13,071 (20%) / 5,329 (12%) from lncRNAs (Supplementary Table S2). An additional 3,742 (6%) / 1,258 (3%) represent FL models that span loci of different biotypes (listed in Figure 1B), usually including one protein-coding gene ("Multi-Biotype"). Of the remaining non-coding FL transcript models, 295 / 434 are novel, arising from unannotated gene loci. Altogether, 11,429 / 4,350 full-length structures arise from probed lncRNA loci, of which 8,494 / 3,168 (74% / 73%) are novel (Supplementary Table S2). We identified at least one FL TM for 19% / 12% of the originally-probed lncRNA annotation (Figure 4F, Supplementary Figure 29). Independent evidence for gene promoters from DNaseI hypersensitivity sites, supported the accuracy of our 5' identification strategy (Figure 4G). Human lncRNAs with mouse orthologues had significantly more FL transcript models, although the reciprocal was not observed (Supplementary Figure 30).

In addition to probed lncRNA loci, CLS also discovered several thousand novel TMs originating from unannotated regions, mapping to probed (blue in Figure 1B) or unprobed regions (Supplementary Figures 31, 32). These TMs tended to have lower detection rates (Supplementary Figure 33) consistent with their low overall expression (Supplementary Figure 34) and lower rates of 5' and 3' support than probed lncRNAs, although a small number are full length ("other" in Figure 4E and Supplementary Figure 28, right panels).

We next compared CLS performance to the conventional CaptureSeq methodology using short-read data. We took advantage of our HiSeq analysis (212/156 million reads, in human/mouse) of the same captured cDNA samples, to make a fair comparison between methods. Short-read methods depend on *de novo* transcriptome assembly: we found, using PacBio reads as a reference, that the recent *StringTie* tool consistently outperforms *Cufflinks*, which has been used in previous CaptureSeq projects (Supplementary Figure 35)(26,41). Using

intron chains to compare annotations, we found that CLS identifies 69% / 114% more novel TMs than *StringTie* assembly (Figure 4H and Supplementary Figure 36), despite sequencing 272-fold fewer nucleotides in the PacBio library. Although *StringTie* TMs are slightly longer (Figure 4I), they are far less likely to be full-length than CLS (Supplementary Figure 36). CLS also provided an advantage over short reads in the detection of transcribed genome repeats, identifying in human approximately 20% more nucleotides in repeats being transcribed (Supplementary Figure 37).

Together, these findings show that CLS is effective in creating large numbers of full-length transcript annotations for probed gene loci, in a highly scalable way.

Re-defining lncRNA promoter and gene characteristics with full-length annotations

With a full-length lncRNA catalogue, we could revisit the question of fundamental differences of lncRNA and protein-coding genes. Existing lncRNA transcripts, as annotated, are significantly shorter and have less exons than mRNAs (6,12). However it has remained unresolved whether this is a genuine biological trend, or simply the result of annotation incompleteness (23). Considering FL TMs, we find that the median lncRNA transcript to be 1108 / 1067 nt, similar to mRNAs mapped by the same criteria (1240 / 1320 nt) (Figure 5A, Supplementary Figure 38). This length difference of 11% / 19% is statistically significant ($P < 2 \times 10^{-16}$ for human and mouse, Wilcoxon test). These measured lengths are still shorter than most annotated protein-coding transcripts (median 1,543 nt in GENCODE v20), but much larger than annotated lncRNAs (median 668 nt). There are two factors that preclude our making firm statements regarding relative lengths of lncRNAs and mRNAs: first, the upper length limitation of PacBio reads (Figure 2B); and second, the fact that our size-selection protocol selects against shorter transcripts. Nevertheless we do not find evidence that lncRNAs are substantially shorter (12). Indeed, transcript annotation length estimates are likely to be strongly biased by lncRNAs' lower expression, which would be manifested in less complete annotations by both manual and *de novo* approaches. We expect that this issue will be definitively answered with future nanopore sequencing approaches.

We previously observed a striking enrichment for two-exon genes in lncRNAs, which was not observed in mRNAs (12). However, we have found that this is clearly an artefact arising from annotation incompleteness: the mean number of exons for lncRNAs in the FL models is 4.27, compared to 6.69 for mRNAs (Figure 5B, Supplementary Figure 38). This difference is explained by lncRNAs' longer exons, although they peak at approximately 150 bp, or one nucleosomal turn (Supplementary Figure 39).

The usefulness of TSS annotation used here is demonstrated by the fact that FL transcripts' TSS are, on average, closer than existing annotations to expected promoter features, including promoters and enhancers predicted by genome segmentations (42) and CpG islands, although not evolutionarily-conserved elements or phenotypic GWAS sites (43) (Figure 5C). More accurate mapping of lncRNA promoters in this way may provide new hypotheses for the latter's mechanism of action. For example, an improved 5' annotation strengthens the link between GWAS SNP rs246185, correlating with QT-interval and lying in the promoter of heart- and muscle-expressed RP11-65J2 (ENSG00000262454), for which it is an expression quantitative trait locus (eQTL) (Supplementary Figure 40) (44).

The improved 5' definition provided by CLS transcript models also enables us to compare lncRNA and mRNA promoters. Recent studies, based on the start position of gene annotations, have claimed to observe strong apparent differences across a range of features (45,46). To make fair comparisons between gene sets, we created an expression-matched set of mRNAs in HeLa and K562 cells, and removed bidirectional promoters. These were compared across a variety of datasets from ENCODE (47) (Supplementary Figures 41, 42).

We observe a series of similar and divergent features of lncRNAs' and mRNAs' promoters. For example, activating promoter histone modifications such as H3K4me3 (Figure 5D) and H3K9ac (Figure 5E), are essentially indistinguishable between full-length lncRNAs (dark blue) and protein-coding genes (red), suggesting that, when accounting for expression differences, active promoter architecture of lncRNAs is not unique. The contrast of these findings with previous reports, suggest that the latter's reliance on annotations alone led to inaccurate promoter identification (45,46).

On the other hand, and as observed previously, lncRNA promoters are distinguished by elevated levels of repressive chromatin marks, such as H3K9me3 (Figure 5F) and H3K27me3

(Supplementary Figures 41, 42) (45). This may be the consequence of elevated recruitment to lncRNAs of Polycomb Repressive Complex, as evidenced by its subunit Ezh2 (Figure 5G). Surprisingly, we also observed that the promoters of lncRNAs are distinguished from those of protein-coding genes by a localised peak of insulator protein CTCF binding (Figure 5H). Finally, there is a clear signal of evolutionary conservation at lncRNA promoters, although lower than for protein-coding genes (Figure 5G).

Two conclusions are drawn from this analysis. First, that CLS-inferred TSS have greater density of expected promoter features, compared to corresponding GENCODE annotations, implying that CLS improves TSS annotation. And second, that when adjusting for expression, lncRNA have comparable activating histone modifications, but distinct repressive modifications, compared to protein-coding genes.

Discovery of new potential open reading frames

Recently a number of studies have suggested that many lncRNA loci encode peptide sequences through unannotated open reading frames (ORFs) (48,49). We searched for signals of protein-coding potential in FL models using two complementary methods, based on evolutionary conservation and intrinsic sequence features (Figure 6A, Materials and Methods, Supplementary Data File 1) (50,51). This analysis finds evidence for protein-coding potential in a small fraction of lncRNA FL TMs ($109/1271=8.6\%$), with a similar number of protein-coding FL TMs displaying no evidence of encoding protein ($2900/42,758=6.8\%$) (Figure 6B).

CLS FL models may lead to reclassification of protein-coding potential for seven cases in five distinct gene loci (Figure 6C, Supplementary Figure 43, Supplementary Data File 2). A good example is the *KANTR* locus, where CLS (supported by independent RT-PCR) identifies an unannotated exon harbouring a placental mammal-conserved 76aa ORF with no detectable protein orthologue, composed of two sequential transmembrane domains (Figure 6D, Supplementary Figure 44) (52). This region derives from the antisense strand of a LINE1 transposable element. Another case is *LINC01138*, linked with prostate cancer, where a potential 42 aa ORF is found in the extended transcript (53). This ORF has no identifiable domains or orthologues. We could not find peptide evidence for translation of either ORF (see Materials and

1 Methods). Whole-cell expression, as well as cytoplasmic-to-nuclear distributions, also showed
2 that potentially protein-coding lncRNAs' behaviour is consistently more similar to annotated
3 lncRNAs than to mRNAs (Supplementary Figures 45, 46, 47). Together, these findings
4 demonstrate the utility of CLS in improving the biotype annotation of the small minority of
5 lncRNAs that may encode proteins.

Discussion

We have introduced an annotation methodology that resolves the competing needs of quality and throughput. Capture Long Read Sequencing produces transcript models with quality approaching that of human annotators, yet with throughput comparable to *de novo* transcriptome assembly. In fact, by incorporating 5' and 3' mapping, CLS advances beyond all contemporary annotation methods by providing full-length transcript models.

In the context of GENCODE, CLS will be used to accelerate annotation pipelines. Transcript models, accompanied by meta-data describing 5', 3' and splice junction support, will be stratified by confidence level. These will receive attention from human annotators as a function of their incompleteness, with FL TMs passed directly to published annotations. Future workflows will utilise *de novo* models from short read data from diverse cell types and developmental time points to perform new rounds of CLS. This approach lays the path towards a truly comprehensive human transcriptome annotation.

CLS is appropriate for virtually any class of RNA transcript. CLS' versatility and throughput makes it suited to rapid, low-cost transcriptome annotation in non-model organisms. Preliminary bioinformatic homology screens for potential genes (including protein-coding, lncRNAs, microRNAs etc.), in newly-sequenced genomes, or first-pass short read RNA-Seq, could be used to design capture libraries. Resulting annotations would be substantially more accurate than those produced by current pipelines based on homology and short-read data.

In economic terms, CLS is also competitive. Using conservative estimates, with 2016 prices (\$2460 for 1 lane of PE125bp HiSeq, \$500 for 1 SMRT), and including the cost of sequencing alone, we estimate that CLS yielded one novel, full-length lncRNA structure for every \$8 spent, compared to \$27 for conventional CaptureSeq. This difference is accounted for vastly greater rate of full-length transcript discovery by CLS.

CLS could also be applied to personal genomics studies. Targeted sequencing of gene panels, perhaps those with medical relevance, could examine the little-studied question of alternative transcript variability across individuals—i.e. whether there exist isoforms that are private to given individuals or populations.

Despite its advantages, CLS remains to be optimised in several respects. First, the capture efficiency for long cDNAs will need to be improved to levels presently observed for short fragments. Second, a combination of technical factors limit the completeness of CLS transcript models (TMs), including: sequencing reads that remain shorter than many transcripts; incomplete reverse transcription of the RNA template; degradation of RNA molecules before reverse transcription. Resolving these issues will be important objectives of future protocol improvements, and only then can we make definitive judgements about lncRNA transcript properties.

Full-length annotations have provided the most confident view to date of lncRNA gene properties. These are more similar to mRNAs than previously thought, in terms of spliced length and exon count (12,54). A similar trend is seen for promoters: when lncRNA promoters are accurately mapped by CLS and compared to matched protein-coding genes, we find them to be surprisingly similar for activating modifications. This suggests that previous studies, which placed confidence in annotations of TSS, should be reassessed (45,46). On the other hand lncRNA promoters do have unique properties, including elevated levels of repressive histone modification, recruitment of Polycomb group proteins, and interaction with the insulator protein CTCF. To our knowledge, this is the first report to suggest a relationship between lncRNAs and insulator elements. Overall, these results suggest that lncRNA gene features *per se* are generally comparable to mRNAs, after normalising for their differences in overall expression. Finally, extended TMs do not yield evidence for widespread protein-coding capacity encoded in lncRNAs.

Despite success in mapping novel structure in annotated lncRNAs, we observed surprisingly low numbers of transcript models originating in the relatively fewer numbers of unannotated loci that we probed, including ultraconserved elements and developmental enhancers. This would suggest that, at least in the tissue samples probed here, such elements are not giving rise to substantial numbers of lncRNA-like, polyadenylated transcripts.

In summary, by resolving a longstanding roadblock in lncRNA transcript annotation, the CLS approach promises to dramatically accelerate our progress towards an eventual “complete” mammalian transcriptome annotation. These updated lncRNA catalogues represent a valuable

- 1 resource to the genomic and biomedical communities, and address fundamental issues of
- 2 lncRNA biology.

Figure legends

Figure 1: Capture Long Seq approach to extend the GENCODE lncRNA annotation

- (A) Strategy for automated, high-quality transcriptome annotation. CLS may be used to complete existing annotations (blue), or to map novel transcript structures in suspected loci (orange). Capture oligonucleotides (black bars) are designed to tile across targeted regions. PacBio libraries are prepared for from the captured molecules. Illumina HiSeq short-read sequencing can be performed for independent validation of predicted splice junctions. Predicted transcription start sites can be confirmed by CAGE clusters (green), and transcription termination sites by non-genomically encoded polyA sequences in PacBio reads. Novel exons are denoted by lighter coloured rectangles.
- (B) Summary of human and mouse capture library designs. Shown are the number of individual gene loci that were probed. “PipeR pred.”: orthologue predictions in mouse genome of human lncRNAs, made by PipeR (31); “UCE”: ultraconserved elements; “Prot. coding”: expression-matched, randomly-selected protein-coding genes; “ERCC”: spike-in sequences; “Ecoli”: randomly-selected *E. coli* genomic regions. Enhancers and UCEs are probed on both strands, and these are counted separately. “Total nts”: sum of targeted nucleotides.
- (C) RNA samples used.

Figure 2: CLS yields an enriched, long-read transcriptome

- (A) Summary statistics for long-read sequencing. ROI = “Read Of Insert”, or PacBio reads.
- (B) Length distributions of ROIs. Sequencing libraries were prepared from three size-selected cDNA fractions (see Supplementary Figure 2).
- (C) Breakdown of sequenced reads by gene biotype, pre- (left) and post-capture (right), for human (equivalent mouse data are found in Supplementary Figure 48). Colours denote the on/off-target status of the genomic region from which the reads originate, namely: Grey: reads originating from annotated but not targeted features; green: reads from

targeted features, including lncRNAs; yellow: reads from unannotated, non-targeted regions. The ERCC class comprises only those ERCC spike-ins that were probed in this experiment. Note that when a given read overlapped more than one targeted class of regions, it was counted in each of these classes separately.

(D) Summary of capture performance. The y-axis shows the percent of all mapped ROIs originating from a targeted region (“on-target”). Enrichment is defined as the ratio of this value in Post- and Pre-capture samples. Note that Pre- and Post-capture on-target rates were calculated using MiSeq and PacBio reads, respectively, although similar results were obtained when using MiSeq also for the Post-capture samples.

(E) Response of read counts in captured cDNA to input RNA concentration. Upper panels: Pre-capture; lower panels: Post-capture. Left: human; right: mouse. Note the log scales for each axis. Each point represents one of 92 spiked-in synthetic ERCC RNA sequences. 42 were probed in the capture design (green), while the remaining 50 were not (violet). Lines represent linear fits to each dataset, whose parameters are shown above. Given the log-log representation, a linear response of read counts to template concentration should yield an equation of type $y = c + mx$, where m is 1.

Figure 3: Extending known lncRNA gene structures

(A) Novel transcript structures from the *SAMMSON* (*LINC01212*) locus. Annotation as present in GENCODE v20 is shown in green, capture probes in grey, CLS reads in black (confirming known structure) and red (novel structures). A sequence amplified by independent RT-PCR is also shown.

(B) Novel splice junction (SJ) discovery. The y-axis denotes counts of unique SJs for human (equivalent mouse data in Supplementary Figure 12). Only “on-target” junctions originating from probed lncRNA loci are considered. Grey represents GENCODE-annotated SJs that are not detected. Dark green represents annotated SJs that are detected by CLS. Light green represent novel SJs that are identified by CLS but not annotated. The left column represents all SJs, and the right column represents only high-confidence SJs (supported by at least one split-read from Illumina short read sequencing). See also Supplementary Figure 13 for a comparison of CLS SJs to the *miTranscriptome* catalogue.

- (C) Splice junction (SJ) motif strength. Panels plot the distribution of predicted SJ strength, for acceptors (left) and donors (right). Data shown are for human, equivalent analysis for mouse may be found in Supplementary Figure 18. The strength of the splice sites were computed using standard position weight matrices used by GeneID (37). Data are shown for non-redundant SJs from CLS transcript models from targeted lncRNAs (top), all annotated protein-coding genes (middle), or a background distribution sampled from randomly-selected AG (acceptor-like) and GT (donor-like) dinucleotides.
- (D) Novel splice junction discovery as a function of sequencing depth in human. Each panel represents the number of novel splice junctions (SJs) discovered (y-axis) in simulated analysis where increasing numbers of ROIs (x-axis) were randomly sampled from the experiment. The SJs retrieved at each read depth were further stratified by level of sequencing support (Dark brown: all PacBio SJs; Orange: HiSeq-supported PacBio SJs; Black: HiSeq-unsupported PacBio SJs). Each randomization was repeated fifty times, and a boxplot summarizes the results at each simulated depth. The highest y value represents the actual number of novel SJs discovered. Equivalent data for mouse can be found in Supplementary Figure 21, and for rates of novel transcript model discovery in Supplementary Figure 22.
- (E) Identification of putative precursor transcripts of small RNA genes. For each gene biotype, the figures show the count of unique genes in each group. “Orphans” are those with no annotated same-strand overlapping transcript in GENCODE, and were used for capture probe design in this project. “Pot. Precursors” (potential precursors) represent orphan small RNAs that reside in the intron of and on the same strand as a novel transcript identified by CLS; “Precursors” represent those that reside in the exon of a novel transcript.

Figure 4: Full-length transcript annotation

- (A) The 5' (transcription start site, TSS) and 3' (polyA site) termini of new transcript models can be inferred using CAGE clusters and sequenced polyA tails, respectively. The latter correspond to polyA fragments identified at ROI 3' ends that are not genomically-encoded.

- (B)** “Anchored” merging of ROIs to create transcript models, while respecting their TSS and polyA sites. In conventional merging (left), transcripts’ TSS and polyA sites are lost when they overlap exons of other transcripts. Anchored merging (right) respects and does not collapse TSS and polyA sites that fall within exons of other transcripts.
- (C)** Anchored merging yields more distinct transcript models. The y-axis represents total counts of ROIs (pink), anchor-merged transcript models (brown) and conventionally-merged transcript models (turquoise). Transcript models were merged irrespective of tissue-origin.
- (D)** Example of full-length, TSS- and polyA-mapped transcript models at the human *CCAT1* / *CASC19* locus. GENCODE v20 annotation is shown in green, novel full-length CLS models in red. Note the presence of a CAGE-supported TSS (green star) and multiple distinct polyA sites (red stars). Also shown is the sequence obtained by RT-PCR and Sanger sequencing (black).
- (E)** The total numbers of anchor-merged transcript models identified by CLS for human. The y-axis of each panel shows unique transcript model (TM) counts. Left panel: All merged TMs, coloured by end-support. Middle panel: Full length (FL) TMs, broken down by novelty with respect to existing GENCODE annotations. Green areas are novel and multi-exonic: “overlap” intersect an annotation on the same strand, but do not respect all its splice junctions; “intergenic” overlap no annotation on the same strand; “extension” respect all of an annotation’s splice junctions, and add novel ones. Right panel: Novel FL TMs, coloured by their biotype. “Other” refers to transcripts not mapping to any GENCODE protein-coding or lncRNA annotation. Note that the majority of “multi-biotype” models link a protein-coding gene to another locus. Equivalent data for mouse are found in Supplementary Figure 28.
- (F)** The total numbers of probed lncRNA loci giving rise to CLS transcript models (TMs), novel TMs, full-length CLS TMs (FL TMs) and novel FL TMs in human at increasing minimum cutoffs for each category. Equivalent mouse data can be found in Supplementary Figure 29.
- (G)** Coverage of CLS transcript TSSs with ENCODE DNaseI-hypersensitive sites (DHS) in HeLa-S3. “CAGE+” / “CAGE-“ denote CLS transcript models with / without CAGE-supported 5’ ends, respectively. “GENCODE lncRNA” represent the annotated 5’ ends of

probed lncRNA transcript annotations. “GENCODE protein-coding” corresponds to the TSSs of a subset of annotated protein-coding genes, expression-matched to CLS TMs in HeLa-S3.

(H) Comparison of non-redundant transcript catalogues from GENCODE annotation, CLS, and *de novo* models produced by *StringTie* software within probed lncRNA regions. The latter was run on short reads sequenced from the same captured cDNA as CLS. The identity of transcripts was defined by their intron chain coordinates; as a result only spliced transcripts are reported here. Equivalent mouse data can be found in Supplementary Figure 36.

(I) Spliced length distributions of indicated non-redundant transcript catalogues. “FL” indicates the subset of transcripts from each catalogue that has 5’ support from CAGE, and 3’ support from PacBio-identified polyA sites. The median spliced length of each population is indicated by a vertical dotted line. Equivalent mouse data can be found in Supplementary Figure 36.

Figure 5: Discovery of novel lncRNA transcripts

(A) The mature, spliced transcript length of: CLS full-length transcript models from targeted lncRNA loci (dark blue); transcript models from the targeted and detected GENCODE lncRNA loci (light blue); CLS full-length transcript models from protein-coding loci (red).

(B) The numbers of exons per full length transcript model, from the same groups as in (A). Dotted lines represent medians.

(C) Distance of annotated transcription start sites (TSS) to genomic features. Each cell displays the mean distance to nearest neighbouring feature for each TSS. TSS sets correspond to the classes from (A). “Shuffled” represent FL lincRNA TSS randomly placed throughout genome.

(D) – (I) Comparing promoter profiles across gene sets. The aggregate density of various features is shown across the TSS of indicated gene classes. Note that overlapping TSS were merged within classes, and TSSs belonging to bi-directional promoters were discarded (see Methods). The y-axis denotes the mean signal per TSS, and grey fringes

represent the standard error of the mean. Gene sets are: Dark blue, full-length lncRNA models from CLS; Light blue, the GENCODE annotation models from which the latter were probed; Red, a subset of protein-coding genes with similar expression in *HeLa* as the CLS lncRNAs.

Figure 6: Properties of full-length lncRNAs

(A) The predicted protein-coding potential of all full-length transcript models mapped to lncRNA (left) or protein-coding loci (right). Each point represents a single full length (FL) transcript model (TM). The y-axis displays the coding likelihood according to *PhyloCSF*, based on multiple genome alignments, while the x-axis displays that calculated by CPAT, an alignment-free method. Red lines indicate score thresholds, above which transcript models are considered protein-coding. Models mapping to multiple different biotypes were not considered.

(B) The numbers of classified transcript models (TMs) from (A).

(C) Discovery of new protein-coding transcripts as a result of full-length CLS reads, using *PhyloCSF*. For each probed lncRNA locus, we calculated the transcript isoform with highest scoring ORF (x-axis). From each locus, we identified the full-length transcript model with high scoring ORF (y-axis). LncRNA loci from existing GENCODE v20 annotation predicted to encode proteins are highlighted in yellow. LncRNA loci where new ORFs are discovered as a result of CLS transcript models are highlighted in red.

(D) *KANTR*, an example of an annotated lncRNA locus where CLS discovers novel protein-coding sequence. The upper panel shows the structure of the lncRNA and the associated ORF (highlighted region) falling within two novel full-length CLS transcripts (red). Note how this ORF lies outside existing GENCODE annotation (green), and its overlap with a highly-conserved region (see green *PhyloCSF* conservation track, below). Also shown is the sequence obtained by RT-PCR and Sanger sequencing (black). The lower panel, generated by *CodAlignView* (55), reveals conservative substitutions in the predicted ORF of 76 aa consistent with a functional peptide product. High-confidence

- 1 predicted SMART (56) domains are shown as coloured bars below. The entire ORF lies
- 2 within and antisense to a L1 transposable element (grey bar).

Author contributions

RJ, RG, JH, AF, BU-R and JL designed the experiment. SC generated cDNA libraries and performed the Capture. CD and TRG performed the PacBio sequencing of Capture libraries. JL and BU-R analysed the data under the supervision of RG and RJ. RJ wrote the manuscript, with contributions from JL, BU-R and RG. SP-L and AA performed the RT-PCR experiments.

Competing financial interests

The author declare no competing financial interest.

Acknowledgements

We thank members of the Guigó laboratory for their valuable input and help when handling samples, analysing data and writing the manuscript, including Emilio Palumbo, Ferran Reverter, Alessandra Breschi, Dmitri Pervouchine, Carme Arnan and Francisco Camara. We wish to thank Lluís Armengol (qGenomics) for advice on RNA capture, Diego Garrido (CRG) for help with eQTL analysis, Sarah Bonnín (CRG) for help with data manipulation in R, Irwin Jungreis (MIT) for advice on PhyloCSF. James Wright and Jyoti Choudhary (Sanger Institute) helped in searching for peptide hits to putative coding regions. Sarah Djebali (INRA, France) kindly made available the *Compmerge* utility. This work and publication were supported by the National Human Genome Research Institute of the National Institutes of Health (grant numbers U41HG007234, U41HG007000 and U54HG007004) and the Wellcome Trust (grant number WT098051). RJ was supported by Ramón y Cajal RYC-2011-08851. Work in laboratory of RG was supported by Awards Number U54HG0070, R01MH101814 and U41HG007234 from the National Human Genome Research Institute. This research was partly supported by the NCCR RNA & Disease funded by the Swiss National Science Foundation (to RJ). We thank Romina Garrido (CRG) for administrative support. We acknowledge support of the Spanish Ministry of Economy and Competitiveness, ‘Centro de Excelencia Severo Ochoa 2013-2017’, SEV-2012-0208.

Data availability

Raw and processed data is deposited in the Gene Expression Omnibus under accession GSE93848. RT-PCR validation sequences are available in Supplementary Data File 3. Genome-aligned data were assembled into a public Track Hub, which can be loaded into the UCSC Genome Browser (pre-loaded URL: http://genome-euro.ucsc.edu/cgi-bin/hgTracks?hubUrl=http://public_docs.crg.es/rguigo/CLS/data/trackHub//hub.txt). In addition, a supplementary data portal is available on the web at https://public_docs.crg.es/rguigo/CLS/.

References

1. Carninci, P., Kasukawa, T., Katayama, S., Gough, J., Frith, M.C., Maeda, N., Oyama, R., Ravasi, T., Lenhard, B., Wells, C. *et al.* (2005) The transcriptional landscape of the mammalian genome. *Science*, **309**, 1559-1563.
2. Jia, H., Osak, M., Bogu, G.K., Stanton, L.W., Johnson, R. and Lipovich, L. (2010) Genome-wide computational identification and manual annotation of human long noncoding RNA genes. *RNA*, **16**, 1478-1487.
3. Guttman, M., Amit, I., Garber, M., French, C., Lin, M.F., Feldser, D., Huarte, M., Zuk, O., Carey, B.W., Cassady, J.P. *et al.* (2009) Chromatin signature reveals over a thousand highly conserved large non-coding RNAs in mammals. *Nature*, **458**, 223-227.
4. Trapnell, C., Roberts, A., Goff, L., Pertea, G., Kim, D., Kelley, D.R., Pimentel, H., Salzberg, S.L., Rinn, J.L. and Pachter, L. (2012) Differential gene and transcript expression analysis of RNA-seq experiments with TopHat and Cufflinks. *Nature protocols*, **7**, 562-578.
5. Guttman, M., Garber, M., Levin, J.Z., Donaghey, J., Robinson, J., Adiconis, X., Fan, L., Koziol, M.J., Gnirke, A., Nusbaum, C. *et al.* (2010) Ab initio reconstruction of cell type-specific transcriptomes in mouse reveals the conserved multi-exonic structure of lincRNAs. *Nature biotechnology*, **28**, 503-510.
6. Cabili, M.N., Trapnell, C., Goff, L., Koziol, M., Tazon-Vega, B., Regev, A. and Rinn, J.L. (2011) Integrative annotation of human large intergenic noncoding RNAs reveals global properties and specific subclasses. *Genes & development*, **25**, 1915-1927.
7. Hangauer, M.J., Vaughn, I.W. and McManus, M.T. (2013) Pervasive Transcription of the Human Genome Produces Thousands of Previously Unidentified Long Intergenic Noncoding RNAs. *PLoS genetics*, **9**, e1003569.
8. Iyer, M.K., Niknafs, Y.S., Malik, R., Singhal, U., Sahu, A., Hosono, Y., Barrette, T.R., Prensner, J.R., Evans, J.R., Zhao, S. *et al.* (2015) The landscape of long noncoding RNAs in the human transcriptome. *Nature genetics*.
9. Zhao, Y., Li, H., Fang, S., Kang, Y., Wu, W., Hao, Y., Li, Z., Bu, D., Sun, N., Zhang, M.Q. *et al.* (2016) NONCODE 2016: an informative and valuable data source of long non-coding RNAs. *Nucleic acids research*, **44**, D203-208.
10. Trapnell, C., Williams, B.A., Pertea, G., Mortazavi, A., Kwan, G., van Baren, M.J., Salzberg, S.L., Wold, B.J. and Pachter, L. (2010) Transcript assembly and quantification by RNA-Seq reveals unannotated transcripts and isoform switching during cell differentiation. *Nature biotechnology*, **28**, 511-515.
11. Harrow, J., Frankish, A., Gonzalez, J.M., Tapanari, E., Diekhans, M., Kokocinski, F., Aken, B.L., Barrell, D., Zadissa, A., Searle, S. *et al.* (2012) GENCODE: the reference human genome annotation for The ENCODE Project. *Genome research*, **22**, 1760-1774.
12. Derrien, T., Johnson, R., Bussotti, G., Tanzer, A., Djebali, S., Tilgner, H., Guernec, G., Martin, D., Merkel, A., Knowles, D.G. *et al.* (2012) The GENCODE v7 catalog of human long noncoding RNAs: analysis of their gene structure, evolution, and expression. *Genome research*, **22**, 1775-1789.
13. Leucci, E., Vendramin, R., Spinazzi, M., Laurette, P., Fiers, M., Wouters, J., Radaelli, E., Eyckerman, S., Leonelli, C., Vanderheyden, K. *et al.* (2016) Melanoma addiction to the long non-coding RNA SAMMSON. *Nature*, **531**, 518-522.
14. (2012) An integrated encyclopedia of DNA elements in the human genome. *Nature*, **489**, 57-74.

15. Chen, L., Kostadima, M., Martens, J.H., Canu, G., Garcia, S.P., Turro, E., Downes, K., Macaulay, I.C., Bielczyk-Maczynska, E., Coe, S. *et al.* (2014) Transcriptional diversity during lineage commitment of human blood progenitors. *Science*, **345**, 1251033.
16. Kundaje, A., Meuleman, W., Ernst, J., Bilenky, M., Yen, A., Heravi-Moussavi, A., Kheradpour, P., Zhang, Z., Wang, J., Ziller, M.J. *et al.* (2015) Integrative analysis of 111 reference human epigenomes. *Nature*, **518**, 317-330.
17. Forrest, A.R., Kawaji, H., Rehli, M., Baillie, J.K., de Hoon, M.J., Haberle, V., Lassmann, T., Kulakovskiy, I.V., Lizio, M., Itoh, M. *et al.* (2014) A promoter-level mammalian expression atlas. *Nature*, **507**, 462-470.
18. Steijger, T., Abril, J.F., Engstrom, P.G., Kokocinski, F., Hubbard, T.J., Guigo, R., Harrow, J. and Bertone, P. (2013) Assessment of transcript reconstruction methods for RNA-seq. *Nature methods*, **10**, 1177-1184.
19. Georgakilas, G., Vlachos, I.S., Paraskevopoulou, M.D., Yang, P., Zhang, Y., Economides, A.N. and Hatzigeorgiou, A.G. (2014) microTSS: accurate microRNA transcription start site identification reveals a significant number of divergent pri-miRNAs. *Nature communications*, **5**, 5700.
20. Orom, U.A., Derrien, T., Beringer, M., Gumireddy, K., Gardini, A., Bussotti, G., Lai, F., Zytynicki, M., Notredame, C., Huang, Q. *et al.* (2010) Long noncoding RNAs with enhancer-like function in human cells. *Cell*, **143**, 46-58.
21. Ferdin, J., Nishida, N., Wu, X., Nicoloso, M.S., Shah, M.Y., Devlin, C., Ling, H., Shimizu, M., Kumar, K., Cortez, M.A. *et al.* (2013) HINCUTs in cancer: hypoxia-induced noncoding ultraconserved transcripts. *Cell death and differentiation*, **20**, 1675-1687.
22. Calin, G.A., Liu, C.G., Ferracin, M., Hyslop, T., Spizzo, R., Sevignani, C., Fabbri, M., Cimmino, A., Lee, E.J., Wojcik, S.E. *et al.* (2007) Ultraconserved regions encoding ncRNAs are altered in human leukemias and carcinomas. *Cancer cell*, **12**, 215-229.
23. Lagarde, J., Uszczyńska-Ratajczak, B., Santoyo-Lopez, J., Gonzalez, J.M., Tapanari, E., Mudge, J.M., Steward, C.A., Wilming, L., Tanzer, A., Howald, C. *et al.* (2016) Extension of human lncRNA transcripts by RACE coupled with long-read high-throughput sequencing (RACE-Seq). *Nature communications*, **7**, 12339.
24. Mercer, T.R., Gerhardt, D.J., Dinger, M.E., Crawford, J., Trapnell, C., Jeddelloh, J.A., Mattick, J.S. and Rinn, J.L. (2012) Targeted RNA sequencing reveals the deep complexity of the human transcriptome. *Nature biotechnology*, **30**, 99-104.
25. Bussotti, G., Leonardi, T., Clark, M.B., Mercer, T.R., Crawford, J., Malquori, L., Notredame, C., Dinger, M.E., Mattick, J.S. and Enright, A.J. (2016) Improved definition of the mouse transcriptome via targeted RNA sequencing. *Genome research*, **26**, 705-716.
26. Clark, M.B., Mercer, T.R., Bussotti, G., Leonardi, T., Haynes, K.R., Crawford, J., Brunck, M.E., Cao, K.A., Thomas, G.P., Chen, W.Y. *et al.* (2015) Quantitative gene profiling of long noncoding RNAs with targeted RNA sequencing. *Nature methods*, **12**, 339-342.
27. Andersson, R., Gebhard, C., Miguel-Escalada, I., Hoof, I., Bornholdt, J., Boyd, M., Chen, Y., Zhao, X., Schmidl, C., Suzuki, T. *et al.* (2014) An atlas of active enhancers across human cell types and tissues. *Nature*, **507**, 455-461.
28. Kozomara, A. and Griffiths-Jones, S. (2014) miRBase: annotating high confidence microRNAs using deep sequencing data. *Nucleic acids research*, **42**, D68-73.
29. Visel, A., Minovitsky, S., Dubchak, I. and Pennacchio, L.A. (2007) VISTA Enhancer Browser--a database of tissue-specific human enhancers. *Nucleic acids research*, **35**, D88-92.
30. Dimitrieva, S. and Bucher, P. (2013) UCNEbase--a database of ultraconserved non-coding elements and genomic regulatory blocks. *Nucleic acids research*, **41**, D101-109.

31. Bussotti, G., Raineri, E., Erb, I., Zytnicki, M., Wilm, A., Beaudoin, E., Bucher, P. and Notredame, C. (2011) BlastR--fast and accurate database searches for non-coding RNAs. *Nucleic acids research*, **39**, 6886-6895.
32. Kralj, J.G. and Salit, M.L. (2013) Characterization of in vitro transcription amplification linearity and variability in the low copy number regime using External RNA Control Consortium (ERCC) spike-ins. *Analytical and bioanalytical chemistry*, **405**, 315-320.
33. Djebali, S., Davis, C.A., Merkel, A., Dobin, A., Lassmann, T., Mortazavi, A., Tanzer, A., Lagarde, J., Lin, W., Schlesinger, F. *et al.* (2012) Landscape of transcription in human cells. *Nature*, **489**, 101-108.
34. Sharon, D., Tilgner, H., Grubert, F. and Snyder, M. (2013) A single-molecule long-read survey of the human transcriptome. *Nature biotechnology*, **31**, 1009-1014.
35. Quail, M.A., Smith, M., Coupland, P., Otto, T.D., Harris, S.R., Connor, T.R., Bertoni, A., Swerdlow, H.P. and Gu, Y. (2012) A tale of three next generation sequencing platforms: comparison of Ion Torrent, Pacific Biosciences and Illumina MiSeq sequencers. *BMC genomics*, **13**, 341.
36. Mercer, T.R., Clark, M.B., Crawford, J., Brunck, M.E., Gerhardt, D.J., Taft, R.J., Nielsen, L.K., Dinger, M.E. and Mattick, J.S. (2014) Targeted sequencing for gene discovery and quantification using RNA CaptureSeq. *Nature protocols*, **9**, 989-1009.
37. Blanco, E., Parra, G. and Guigo, R. (2007) Using geneid to identify genes. *Current protocols in bioinformatics / editorial board, Andreas D. Baxeavanis ... [et al.]*, **Chapter 4**, Unit 4 3.
38. Smith, C.M. and Steitz, J.A. (1998) Classification of gas5 as a multi-small-nucleolar-RNA (snoRNA) host gene and a member of the 5'-terminal oligopyrimidine gene family reveals common features of snoRNA host genes. *Molecular and cellular biology*, **18**, 6897-6909.
39. Ounzain, S., Micheletti, R., Arnan, C., Plaisance, I., Cecchi, D., Schroen, B., Reverter, F., Alexanian, M., Gonzales, C., Ng, S.Y. *et al.* (2015) CARMEN, a human super enhancer-associated long noncoding RNA controlling cardiac specification, differentiation and homeostasis. *Journal of molecular and cellular cardiology*, **89**, 98-112.
40. Nissan, A., Stojadinovic, A., Mitran-Rosenbaum, S., Halle, D., Grinbaum, R., Roistacher, M., Bochem, A., Dayanc, B.E., Ritter, G., Gomceli, I. *et al.* (2012) Colon cancer associated transcript-1: a novel RNA expressed in malignant and pre-malignant human tissues. *International journal of cancer. Journal international du cancer*, **130**, 1598-1606.
41. Perte, M., Perte, G.M., Antonescu, C.M., Chang, T.C., Mendell, J.T. and Salzberg, S.L. (2015) StringTie enables improved reconstruction of a transcriptome from RNA-seq reads. *Nature biotechnology*, **33**, 290-295.
42. Marques, A.C., Hughes, J., Graham, B., Kowalczyk, M.S., Higgs, D.R. and Ponting, C.P. (2013) Chromatin signatures at transcriptional start sites separate two equally populated yet distinct classes of intergenic long noncoding RNAs. *Genome biology*, **14**, R131.
43. Welter, D., MacArthur, J., Morales, J., Burdett, T., Hall, P., Junkins, H., Klemm, A., Flicek, P., Manolio, T., Hindorff, L. *et al.* (2014) The NHGRI GWAS Catalog, a curated resource of SNP-trait associations. *Nucleic acids research*, **42**, D1001-1006.
44. Arking, D.E., Pulit, S.L., Crotti, L., van der Harst, P., Munroe, P.B., Koopmann, T.T., Sotoodehnia, N., Rossin, E.J., Morley, M., Wang, X. *et al.* (2014) Genetic association study of QT interval highlights role for calcium signaling pathways in myocardial repolarization. *Nature genetics*, **46**, 826-836.
45. Alam, T., Medvedeva, Y.A., Jia, H., Brown, J.B., Lipovich, L. and Bajic, V.B. (2014) Promoter analysis reveals globally differential regulation of human long non-coding RNA and protein-coding genes. *PloS one*, **9**, e109443.

46. Mele, M., Mattioli, K., Mallard, W., Shechner, D.M., Gerhardinger, C. and Rinn, J.L. (2016) Chromatin environment, transcriptional regulation, and splicing distinguish lincRNAs and mRNAs. *Genome research*.
47. Consortium, E. (2012) An integrated encyclopedia of DNA elements in the human genome. *Nature*, **489**, 57-74.
48. Mackowiak, S.D., Zaubner, H., Bielow, C., Thiel, D., Kutz, K., Calviello, L., Mastrobuoni, G., Rajewsky, N., Kempa, S., Selbach, M. *et al.* (2015) Extensive identification and analysis of conserved small ORFs in animals. *Genome biology*, **16**, 179.
49. Bazzini, A.A., Johnstone, T.G., Christiano, R., Mackowiak, S.D., Obermayer, B., Fleming, E.S., Vejnar, C.E., Lee, M.T., Rajewsky, N., Walther, T.C. *et al.* (2014) Identification of small ORFs in vertebrates using ribosome footprinting and evolutionary conservation. *The EMBO journal*, **33**, 981-993.
50. Wang, L., Park, H.J., Dasari, S., Wang, S., Kocher, J.P. and Li, W. (2013) CPAT: Coding-Potential Assessment Tool using an alignment-free logistic regression model. *Nucleic acids research*, **41**, e74.
51. Lin, M.F., Jungreis, I. and Kellis, M. (2011) PhyloCSF: a comparative genomics method to distinguish protein coding and non-coding regions. *Bioinformatics*, **27**, i275-282.
52. Sauvageau, M., Goff, L.A., Lodato, S., Bonev, B., Groff, A.F., Gerhardinger, C., Sanchez-Gomez, D.B., Hacisuleyman, E., Li, E., Spence, M. *et al.* (2013) Multiple knockout mouse models reveal lincRNAs are required for life and brain development. *eLife*, **2**, e01749.
53. Wan, X., Huang, W., Yang, S., Zhang, Y., Pu, H., Fu, F., Huang, Y., Wu, H., Li, T. and Li, Y. (2016) Identification of androgen-responsive lincRNAs as diagnostic and prognostic markers for prostate cancer. *Oncotarget*.
54. Ruiz-Orera, J., Messeguer, X., Subirana, J.A. and Alba, M.M. (2014) Long non-coding RNAs as a source of new peptides. *eLife*, **3**, e03523.
55. I Jungreis, M Lin and Kellis, M. CodAlignView: a tool for visualizing protein-coding constraint. *In Preparation*.
56. Letunic, I., Doerks, T. and Bork, P. (2015) SMART: recent updates, new developments and status in 2015. *Nucleic acids research*, **43**, D257-260.

Figure 1
bioRxiv preprint doi: <https://doi.org/10.1101/105064>; this version posted June 16, 2017. The copyright holder for this preprint (which was not certified by peer review) is the author/funder, who has granted bioRxiv a license to display the preprint in perpetuity. It is made available under aCC-BY 4.0 International license.

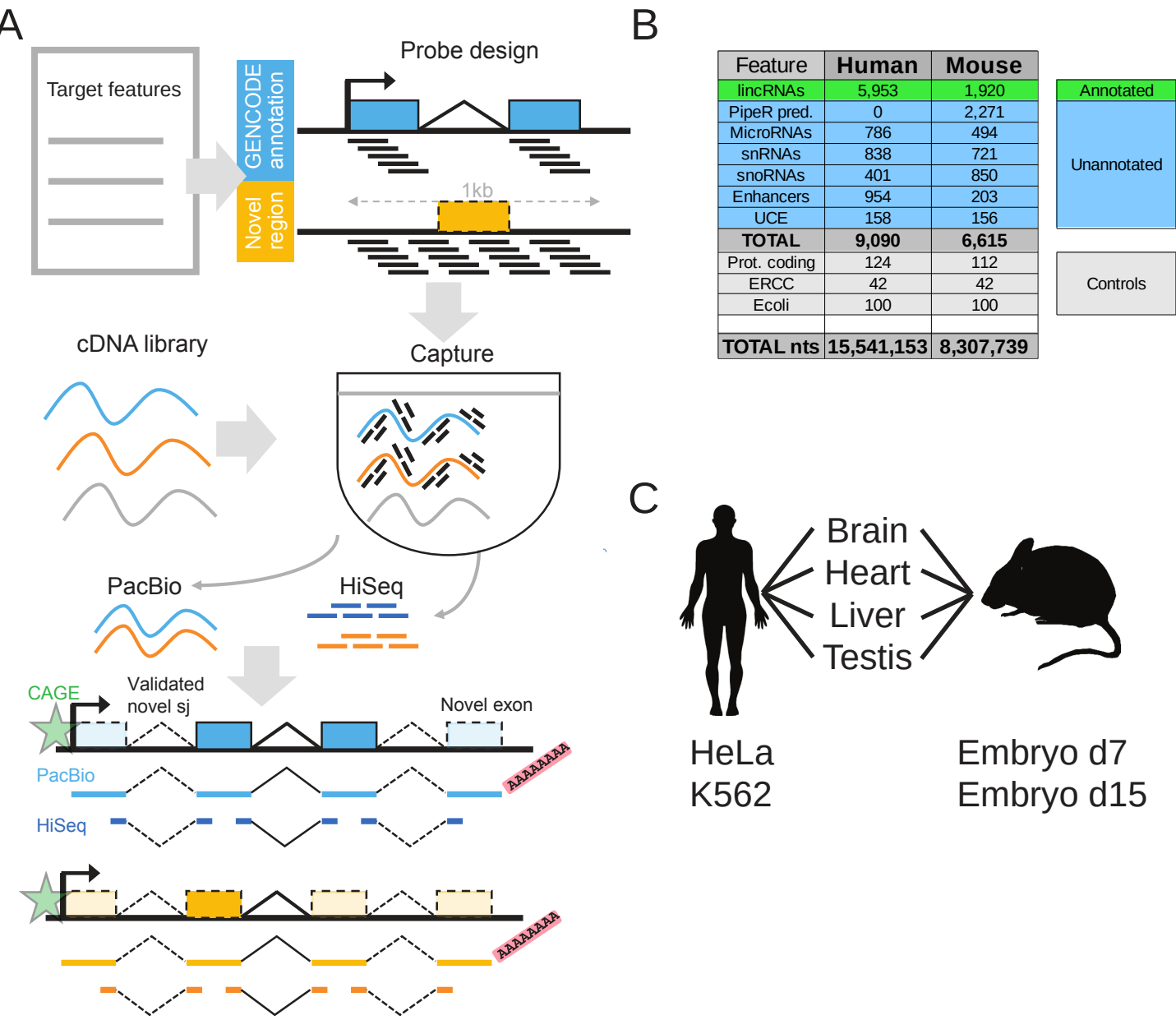


Figure 2

bioRxiv preprint doi: <https://doi.org/10.1101/105064>; this version posted June 16, 2017. The copyright holder for this preprint (which was not certified by peer review) is the author/funder, who has granted bioRxiv a license to display the preprint in perpetuity. It is made available under aCC-BY 4.0 International license.

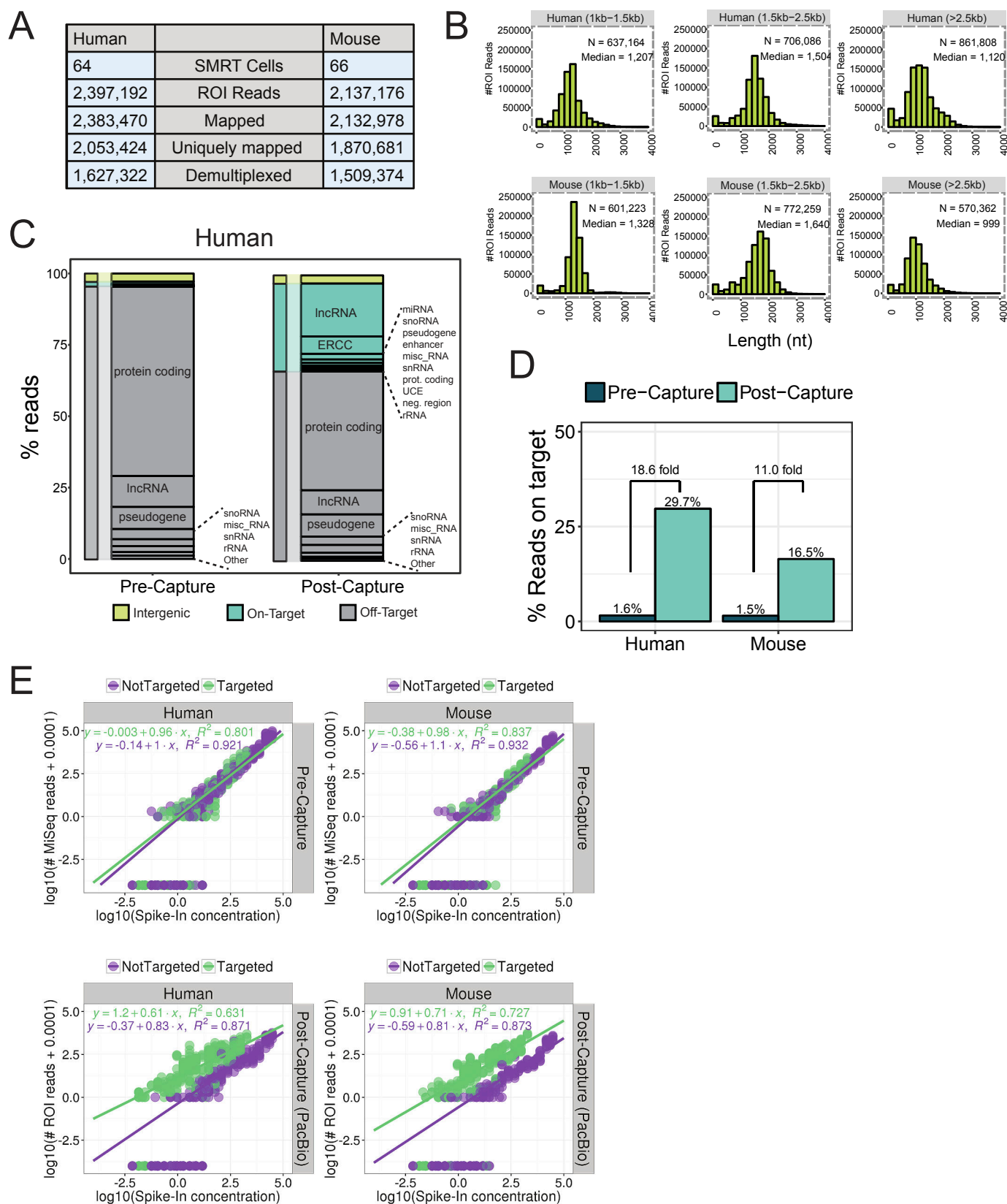


Figure 3 bioRxiv preprint doi: <https://doi.org/10.1101/105064>; this version posted June 16, 2017. The copyright holder for this preprint (which was not certified by peer review) is the author/funder, who has granted bioRxiv a license to display the preprint in perpetuity. It is made available under aCC-BY 4.0 International license.

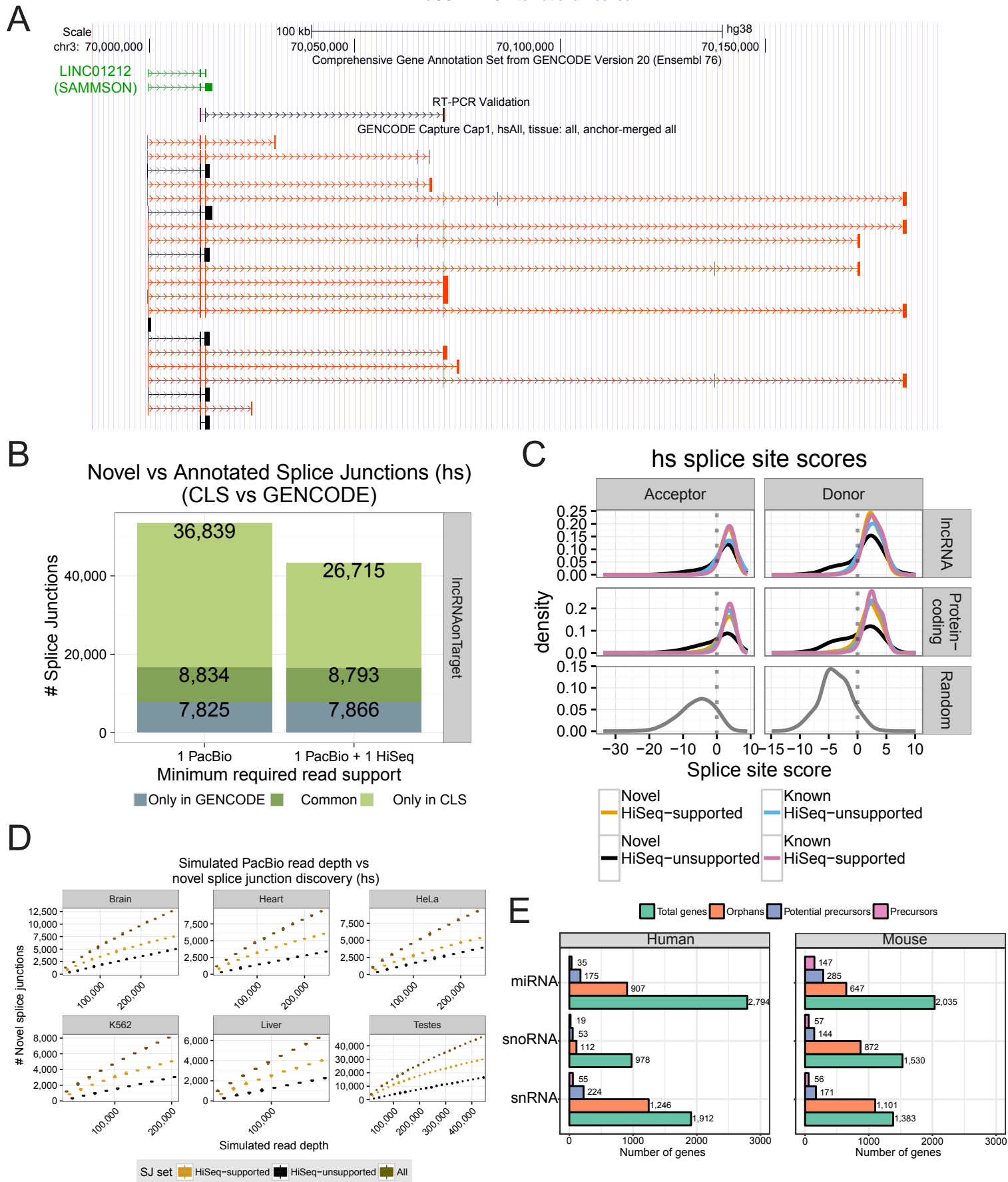


Figure 4 bioRxiv preprint doi: <https://doi.org/10.1101/105064>; this version posted June 16, 2017. The copyright holder for this preprint (which was not certified by peer review) is the author/funder, who has granted bioRxiv a license to display the preprint in perpetuity. It is made available under aCC-BY 4.0 International license.

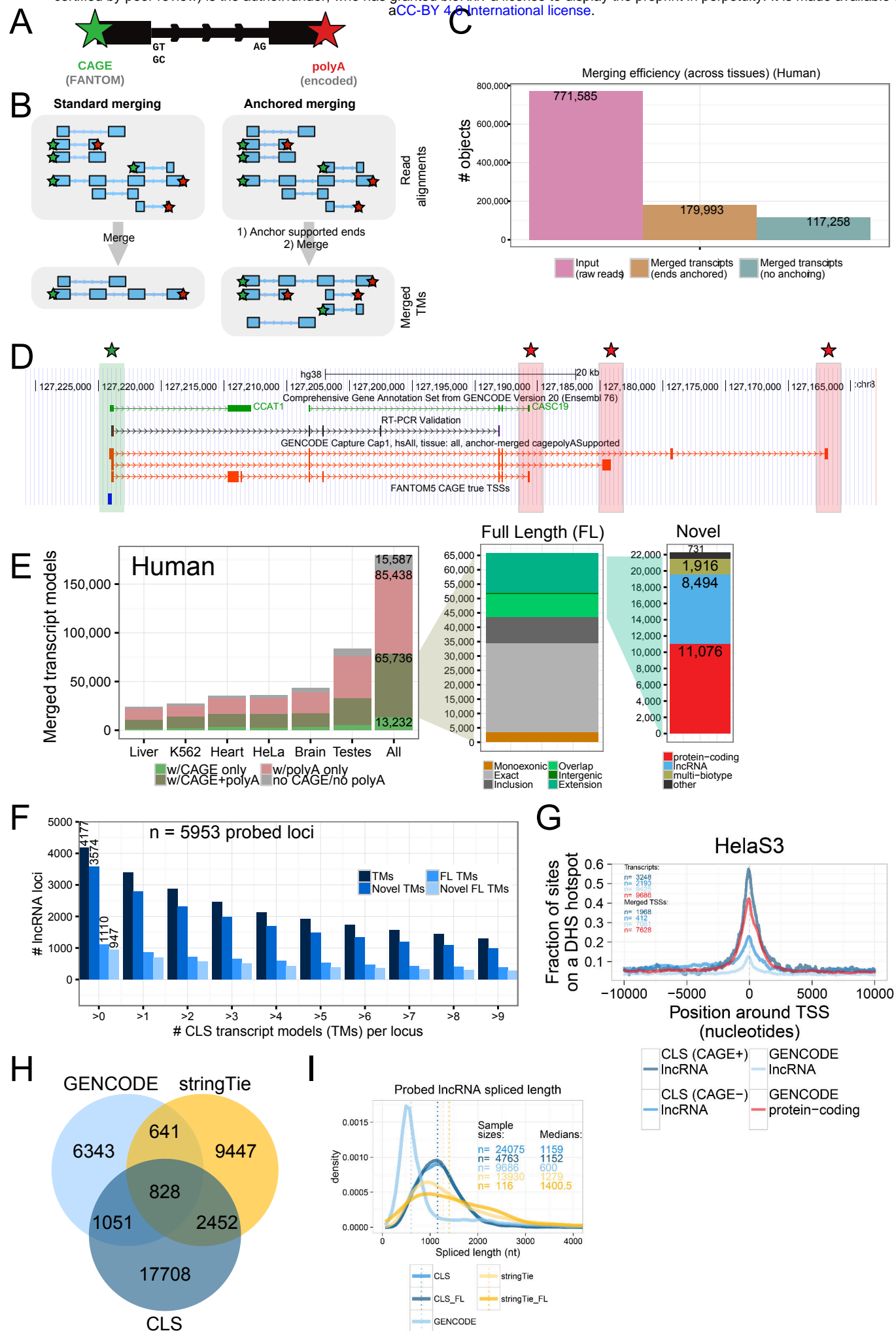


Figure 5 bioRxiv preprint doi: <https://doi.org/10.1101/105064>; this version posted June 16, 2017. The copyright holder for this preprint (which was not certified by peer review) is the author/funder, who has granted bioRxiv a license to display the preprint in perpetuity. It is made available under aCC-BY 4.0 International license.

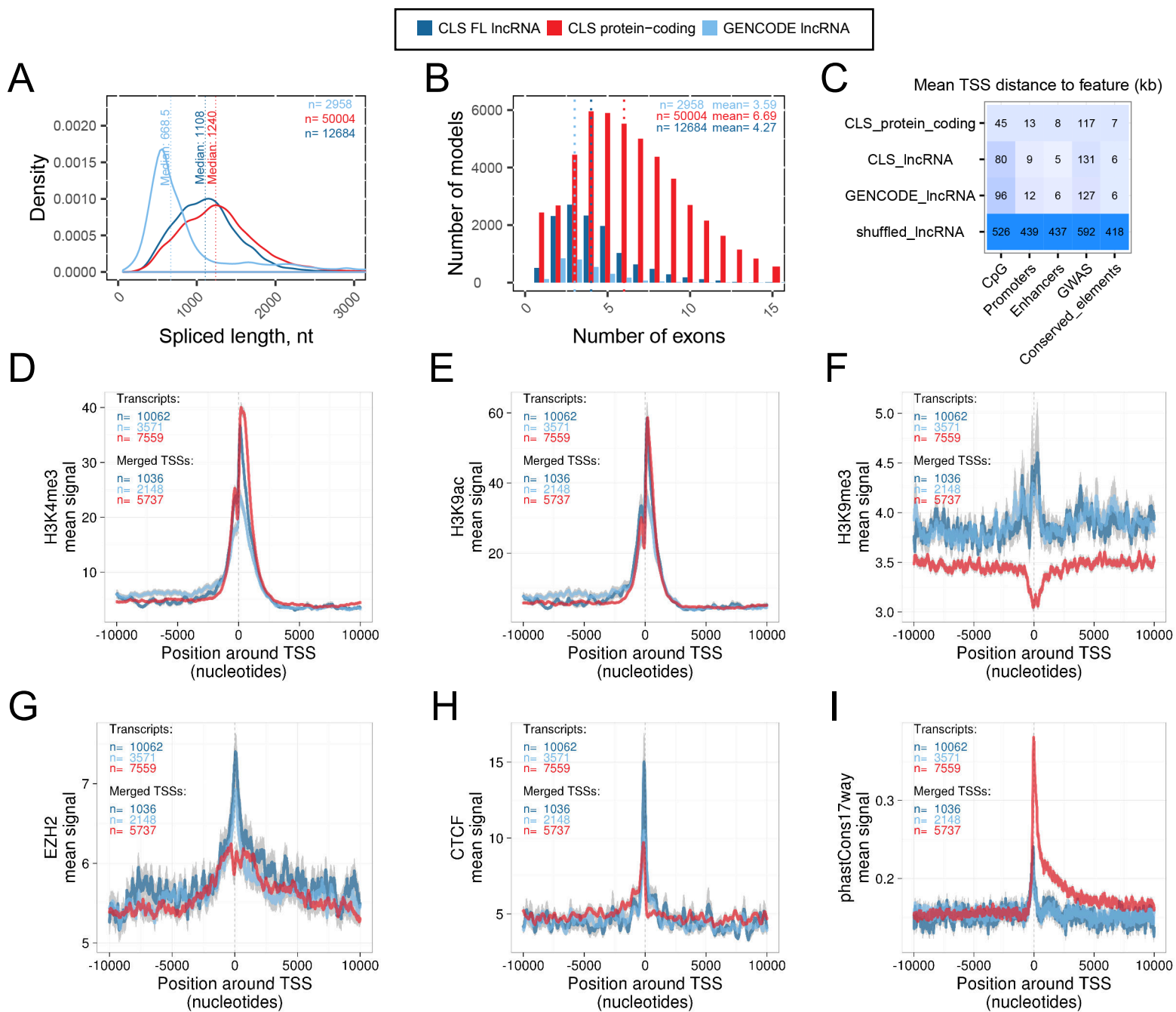
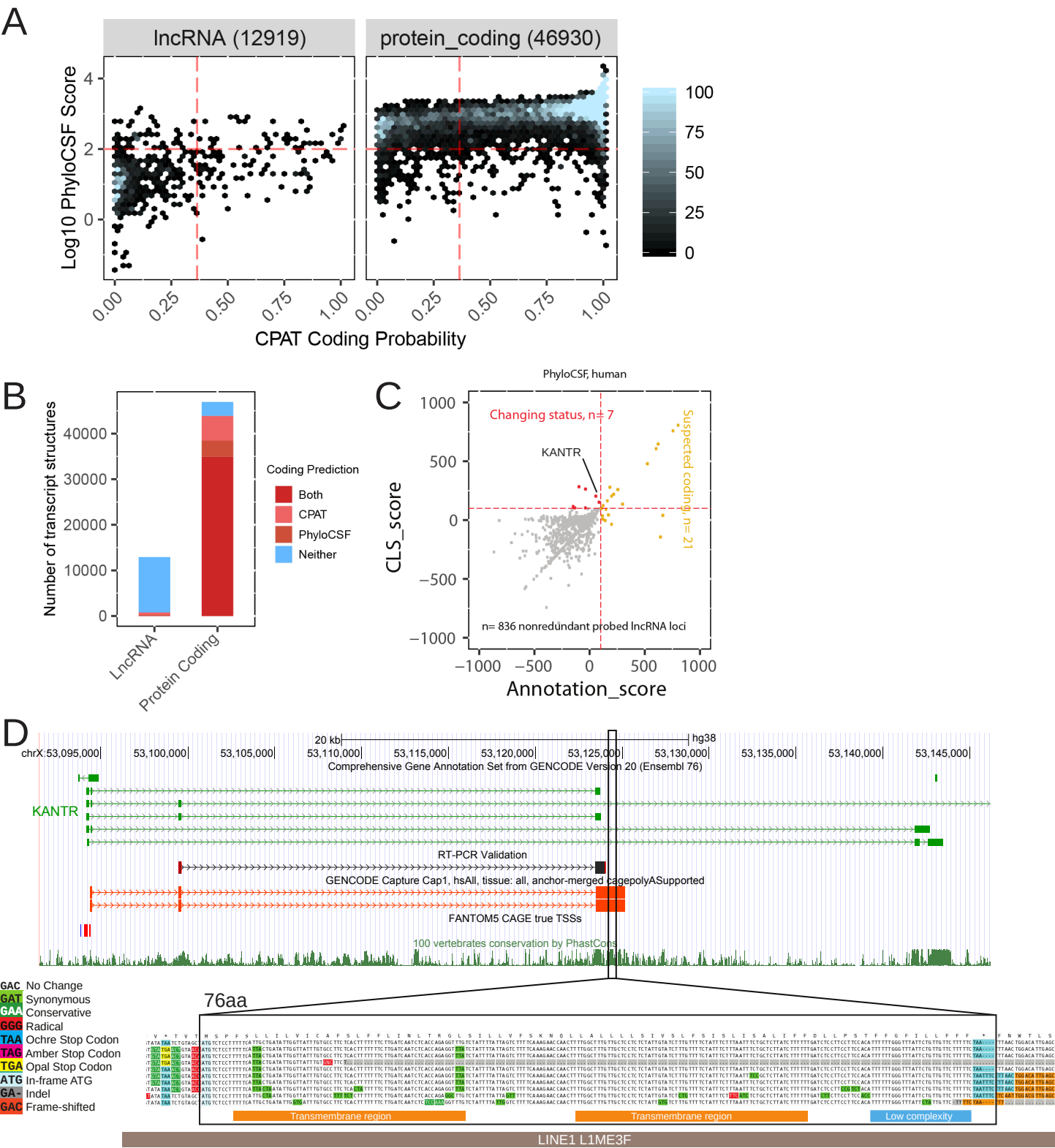
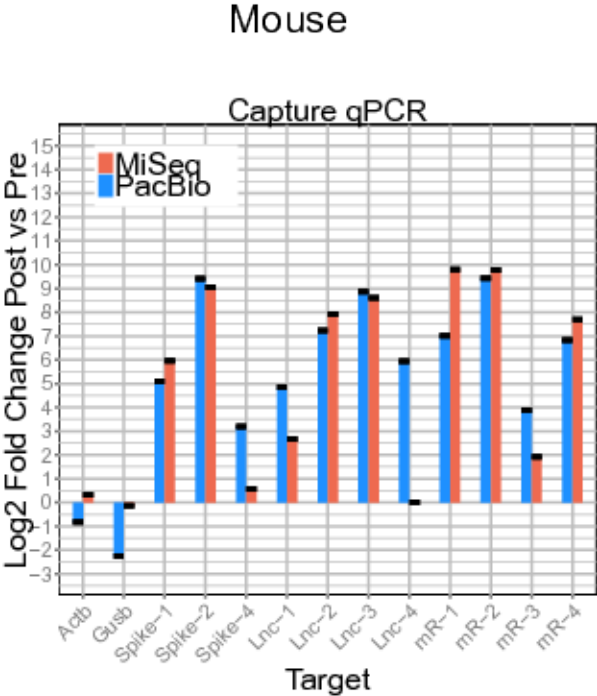
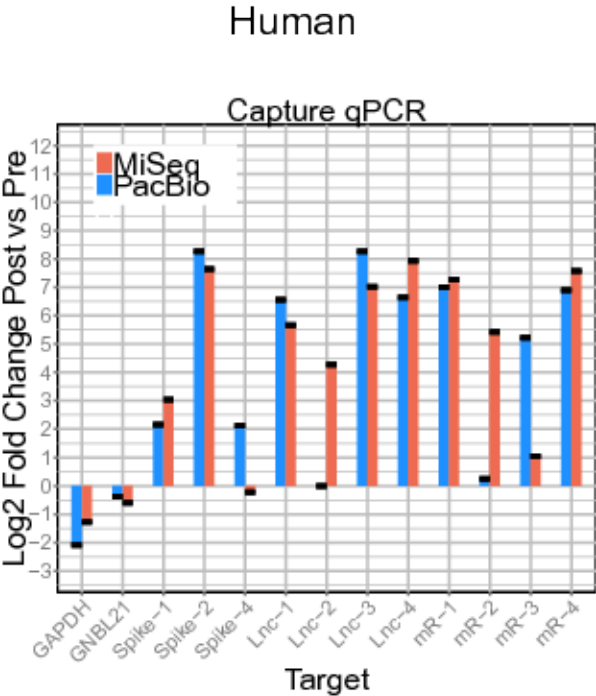


Figure 6 bioRxiv preprint doi: <https://doi.org/10.1101/105064>; this version posted June 16, 2017. The copyright holder for this preprint (which was not certified by peer review) is the author/funder, who has granted bioRxiv a license to display the preprint in perpetuity. It is made available under aCC-BY 4.0 International license.



Supplementary Figure S1

bioRxiv preprint doi: <https://doi.org/10.1101/105064>; this version posted June 16, 2017. The copyright holder for this preprint (which was not certified by peer review) is the author/funder, who has granted bioRxiv a license to display the preprint in perpetuity. It is made available under aCC-BY 4.0 International license.



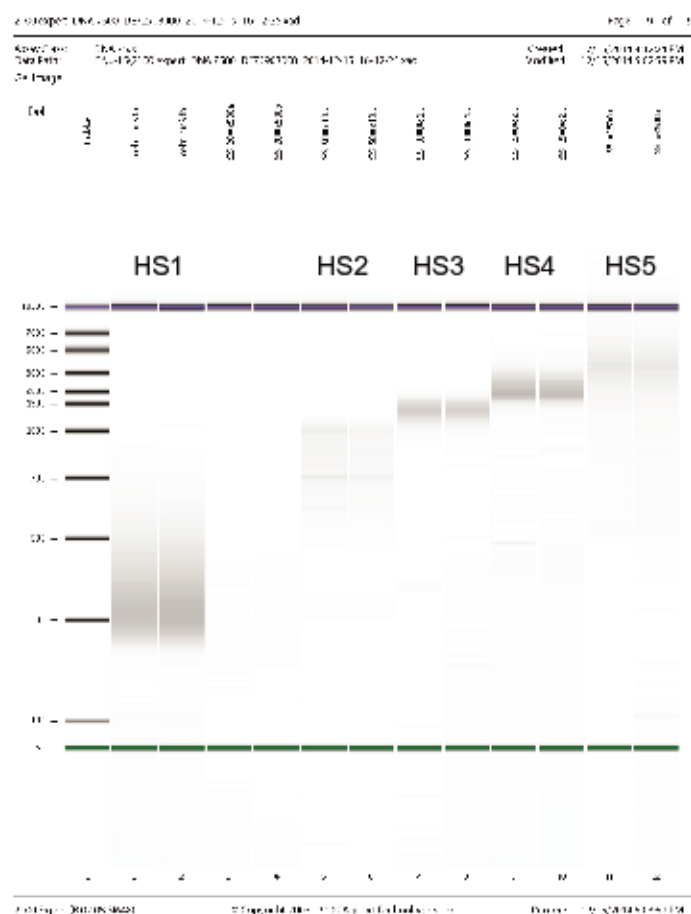
Supplementary Figure S2

bioRxiv preprint doi: <https://doi.org/10.1101/105064>; this version posted June 16, 2017. The copyright holder for this preprint (which was not certified by peer review) is the author/funder, who has granted bioRxiv a license to display the preprint in perpetuity. It is made available under aCC-BY 4.0 International license.

A

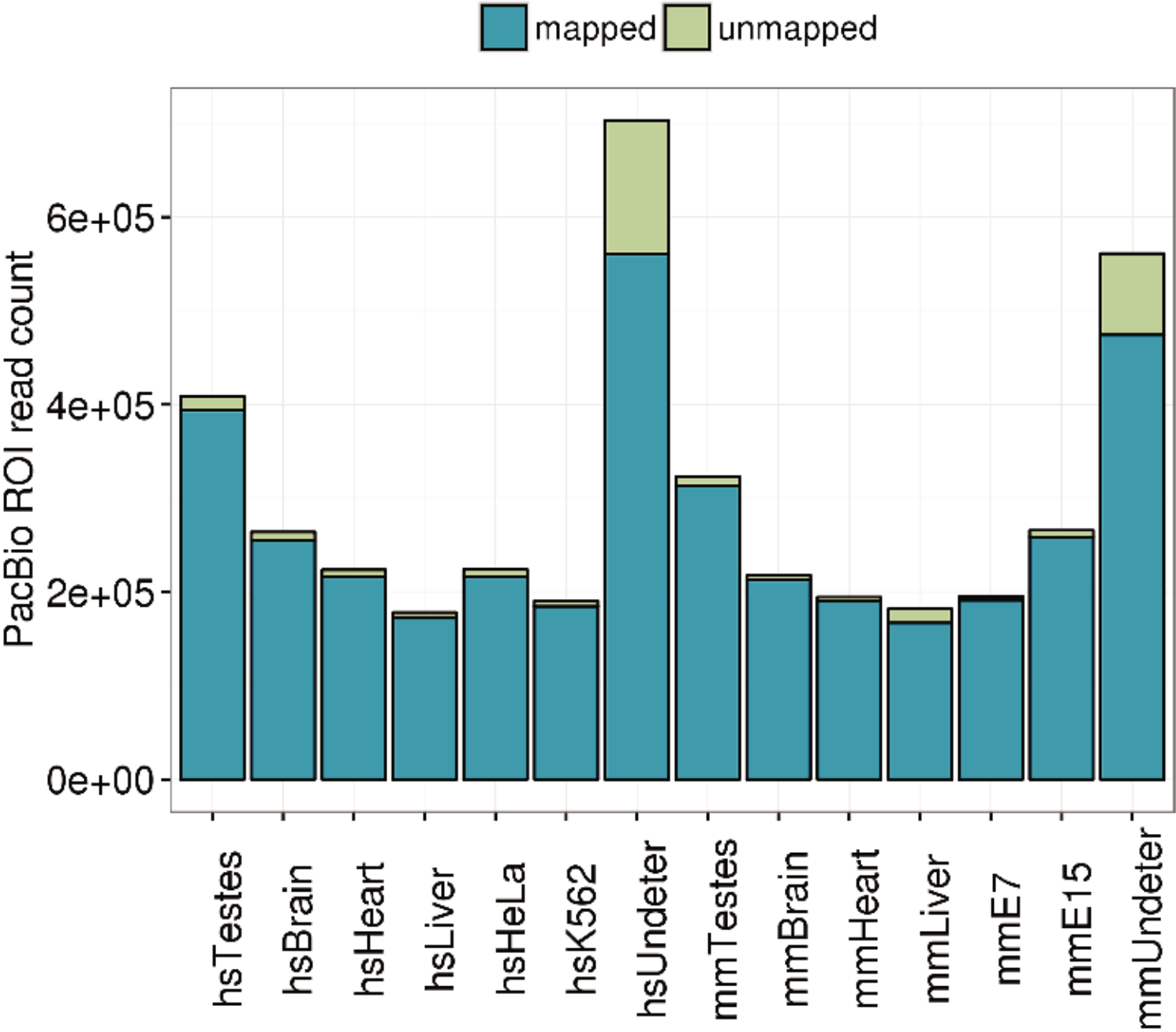
	Range (nt)	Human
1	200-500	HS1
2	500-1000	HS2
3	1000-1500	HS3
4	1500-2500	HS4
5	>2500	HS5

B



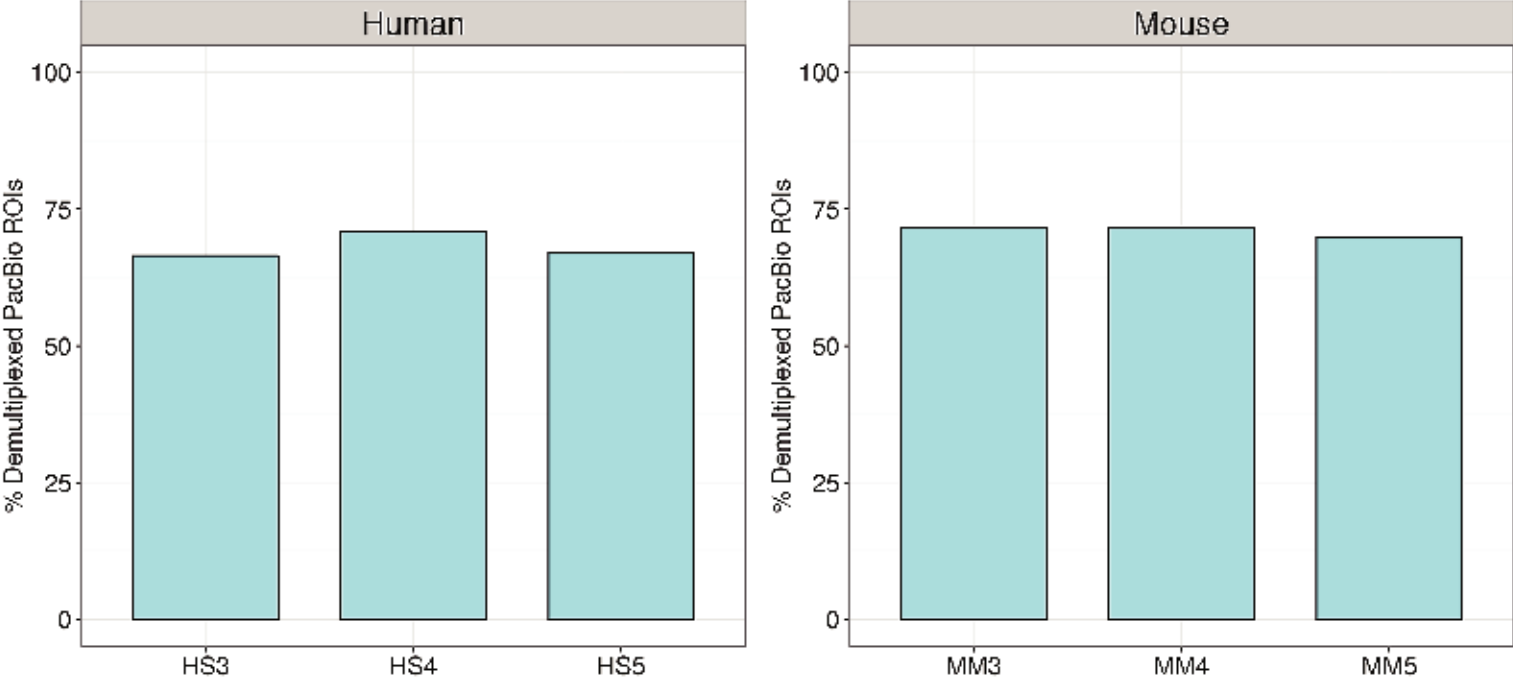
Supplementary Figure S3

bioRxiv preprint doi: <https://doi.org/10.1101/105064>; this version posted June 16, 2017. The copyright holder for this preprint (which was not certified by peer review) is the author/funder, who has granted bioRxiv a license to display the preprint in perpetuity. It is made available under aCC-BY 4.0 International license.



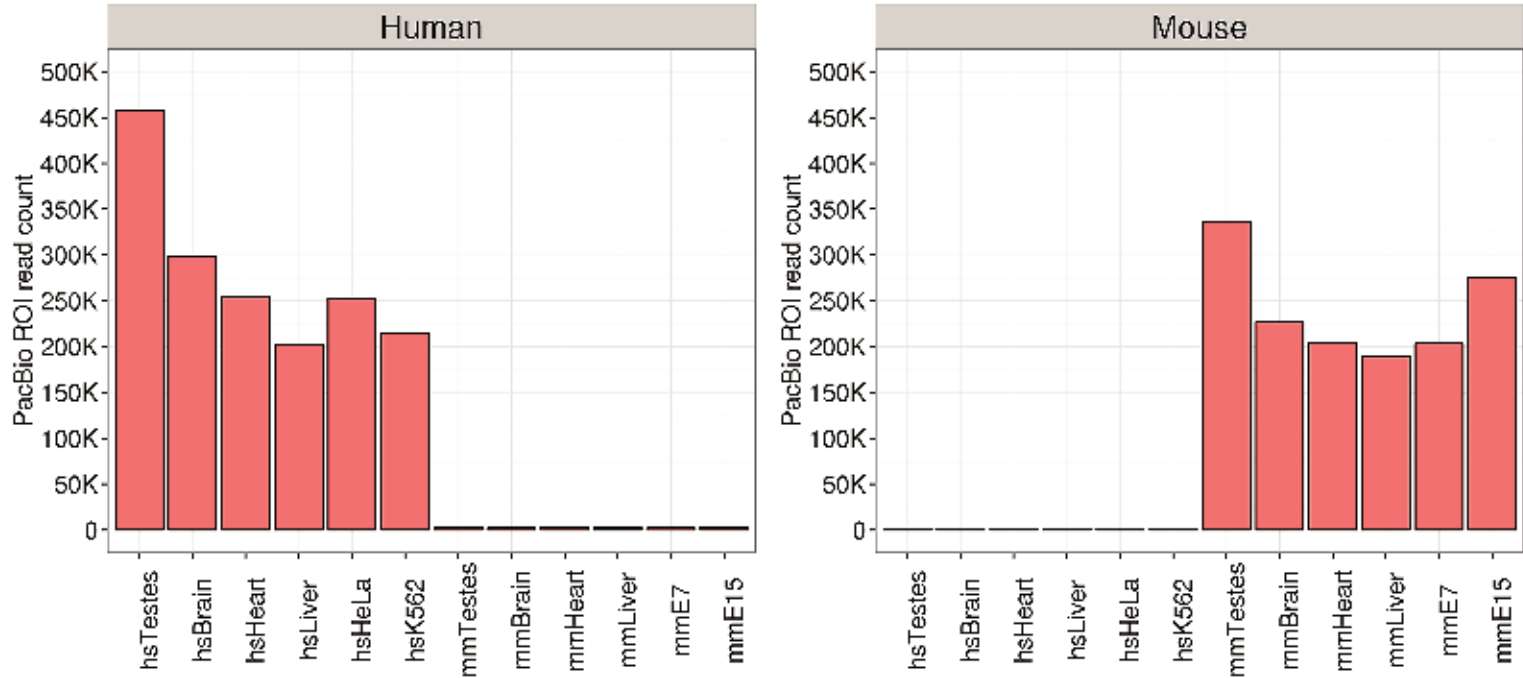
Supplementary Figure S4

bioRxiv preprint doi: <https://doi.org/10.1101/105064>; this version posted June 16, 2017. The copyright holder for this preprint (which was not certified by peer review) is the author/funder, who has granted bioRxiv a license to display the preprint in perpetuity. It is made available under aCC-BY 4.0 International license.



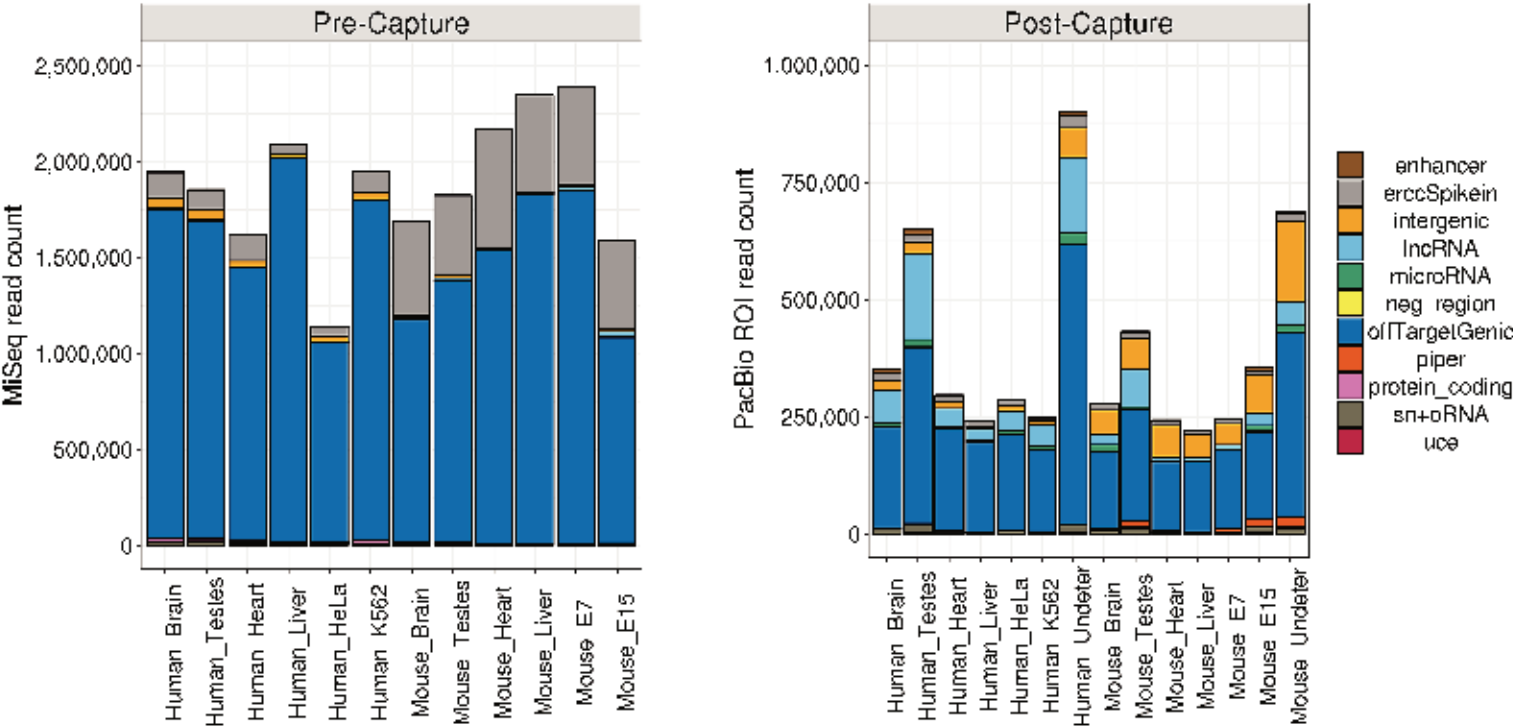
Supplementary Figure S5

bioRxiv preprint doi: <https://doi.org/10.1101/105064>; this version posted June 16, 2017. The copyright holder for this preprint (which was not certified by peer review) is the author/funder, who has granted bioRxiv a license to display the preprint in perpetuity. It is made available under aCC-BY 4.0 International license.



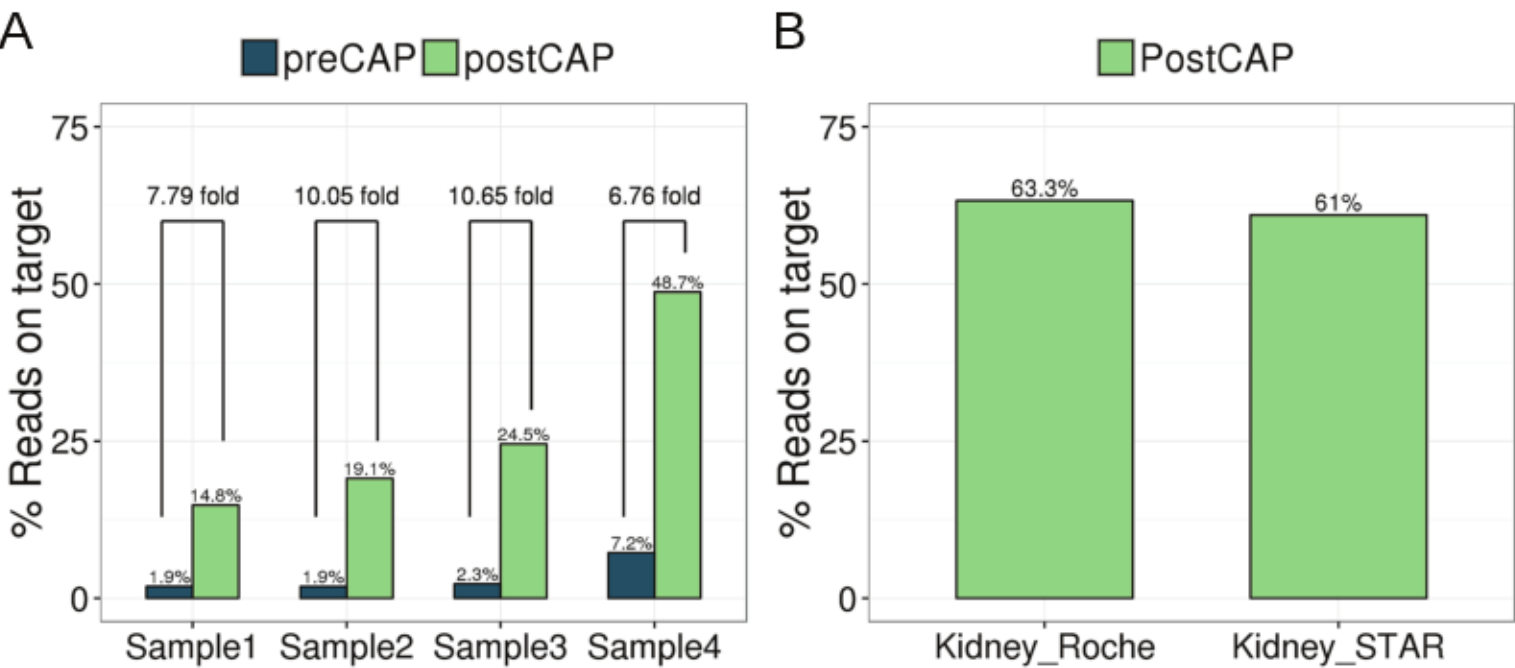
Supplementary Figure S6

bioRxiv preprint doi: <https://doi.org/10.1101/105064>; this version posted June 16, 2017. The copyright holder for this preprint (which was not certified by peer review) is the author/funder, who has granted bioRxiv a license to display the preprint in perpetuity. It is made available under aCC-BY 4.0 International license.



Supplementary Figure S7

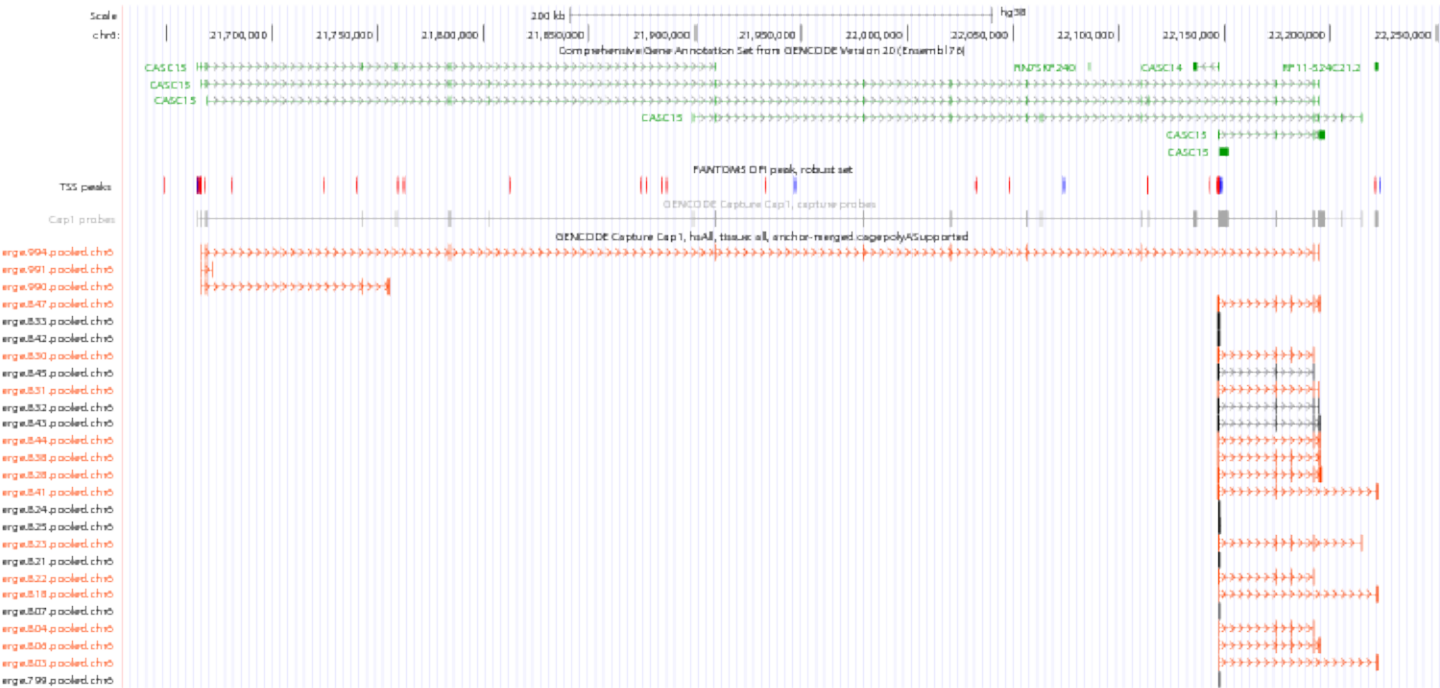
bioRxiv preprint doi: <https://doi.org/10.1101/105064>; this version posted June 16, 2017. The copyright holder for this preprint (which was not certified by peer review) is the author/funder, who has granted bioRxiv a license to display the preprint in perpetuity. It is made available under aCC-BY 4.0 International license.



Supplementary Figure S8

bioRxiv preprint doi: <https://doi.org/10.1101/105064>; this version posted June 16, 2017. The copyright holder for this preprint (which was not certified by peer review) is the author/funder, who has granted bioRxiv a license to display the preprint in perpetuity. It is made available under aCC-BY 4.0 International license.

CASC15 / ENSG00000272168



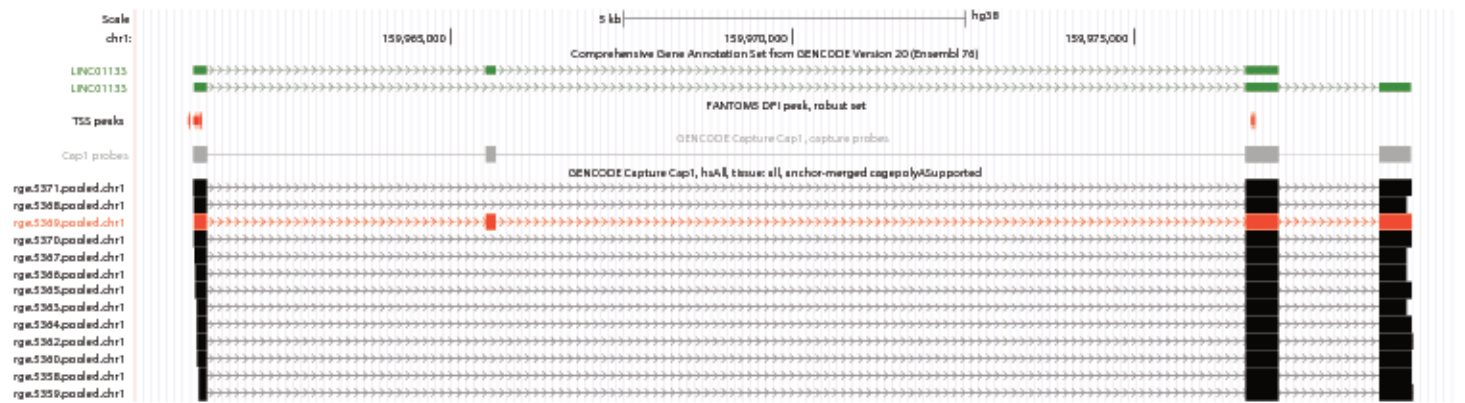
GAS5 / ENSG00000234741



Supplementary Figure S9

bioRxiv preprint doi: <https://doi.org/10.1101/105064>; this version posted June 16, 2017. The copyright holder for this preprint (which was not certified by peer review) is the author/funder, who has granted bioRxiv a license to display the preprint in perpetuity. It is made available under aCC-BY 4.0 International license.

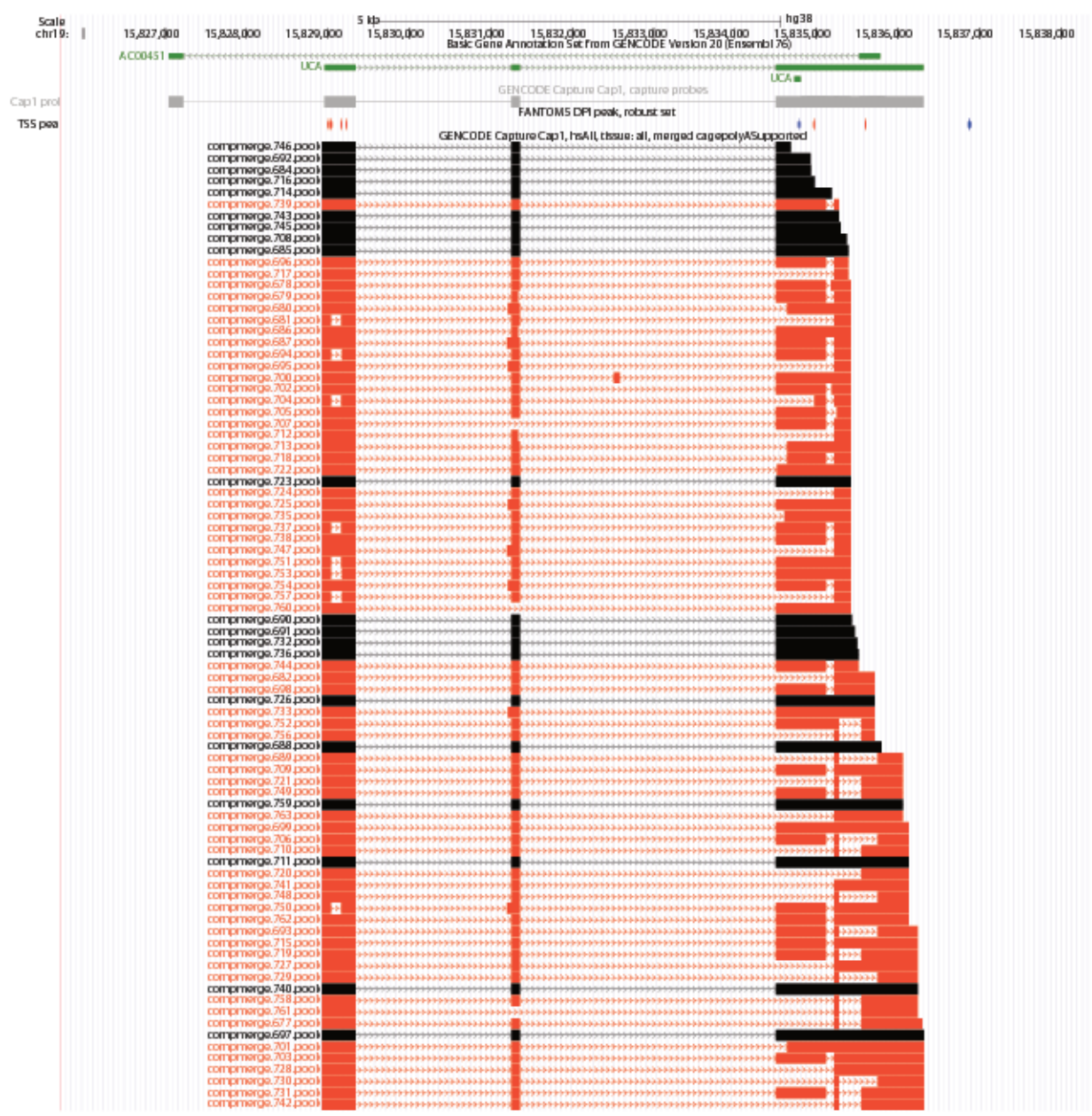
LINC01133 / ENSG00000224259



Supplementary Figure S10

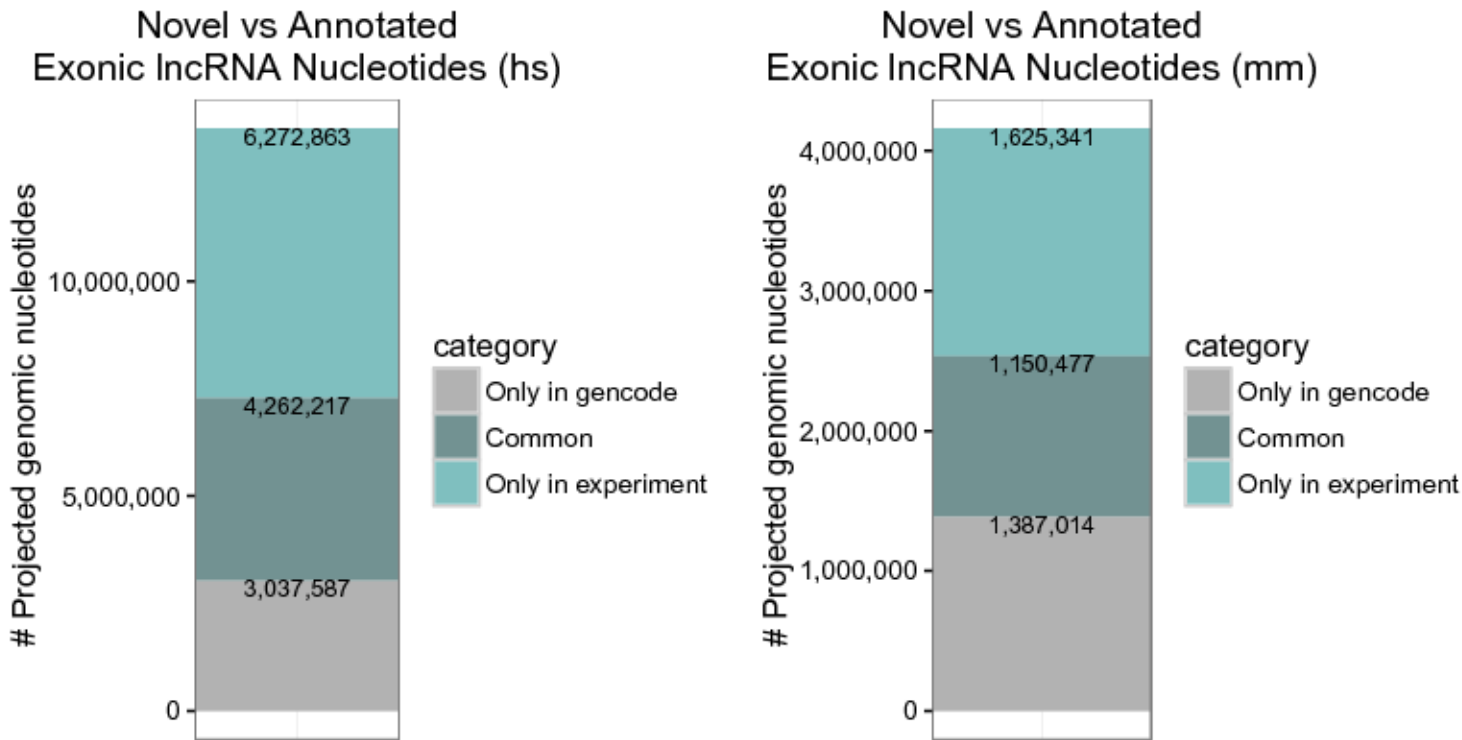
bioRxiv preprint doi: <https://doi.org/10.1101/105064>; this version posted June 16, 2017. The copyright holder for this preprint (which was not certified by peer review) is the author/funder, who has granted bioRxiv a license to display the preprint in perpetuity. It is made available under aCC-BY 4.0 International license.

UCAT / ENSG00000214049



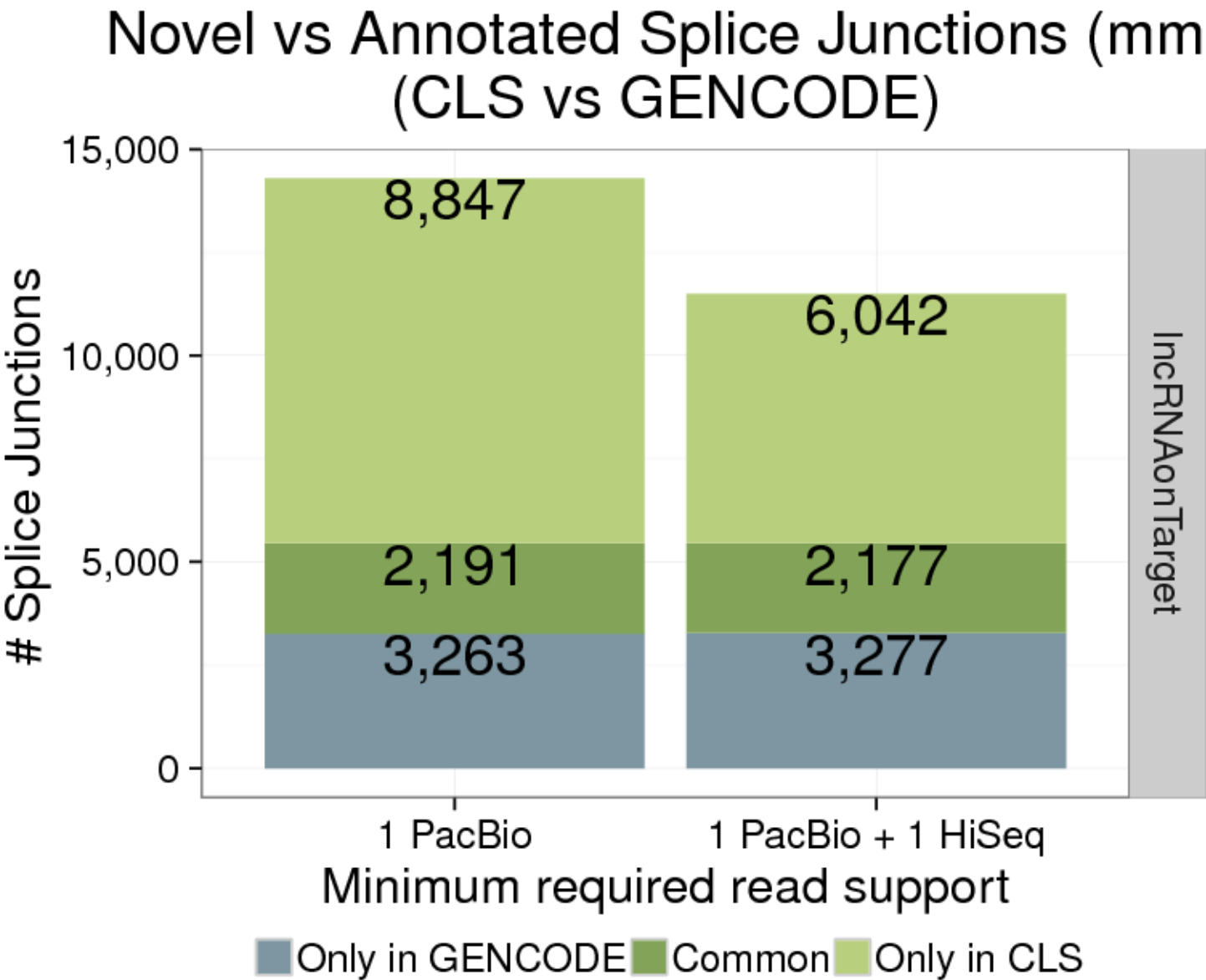
Supplementary Figure S11

bioRxiv preprint doi: <https://doi.org/10.1101/105064>; this version posted June 16, 2017. The copyright holder for this preprint (which was not certified by peer review) is the author/funder, who has granted bioRxiv a license to display the preprint in perpetuity. It is made available under aCC-BY 4.0 International license.



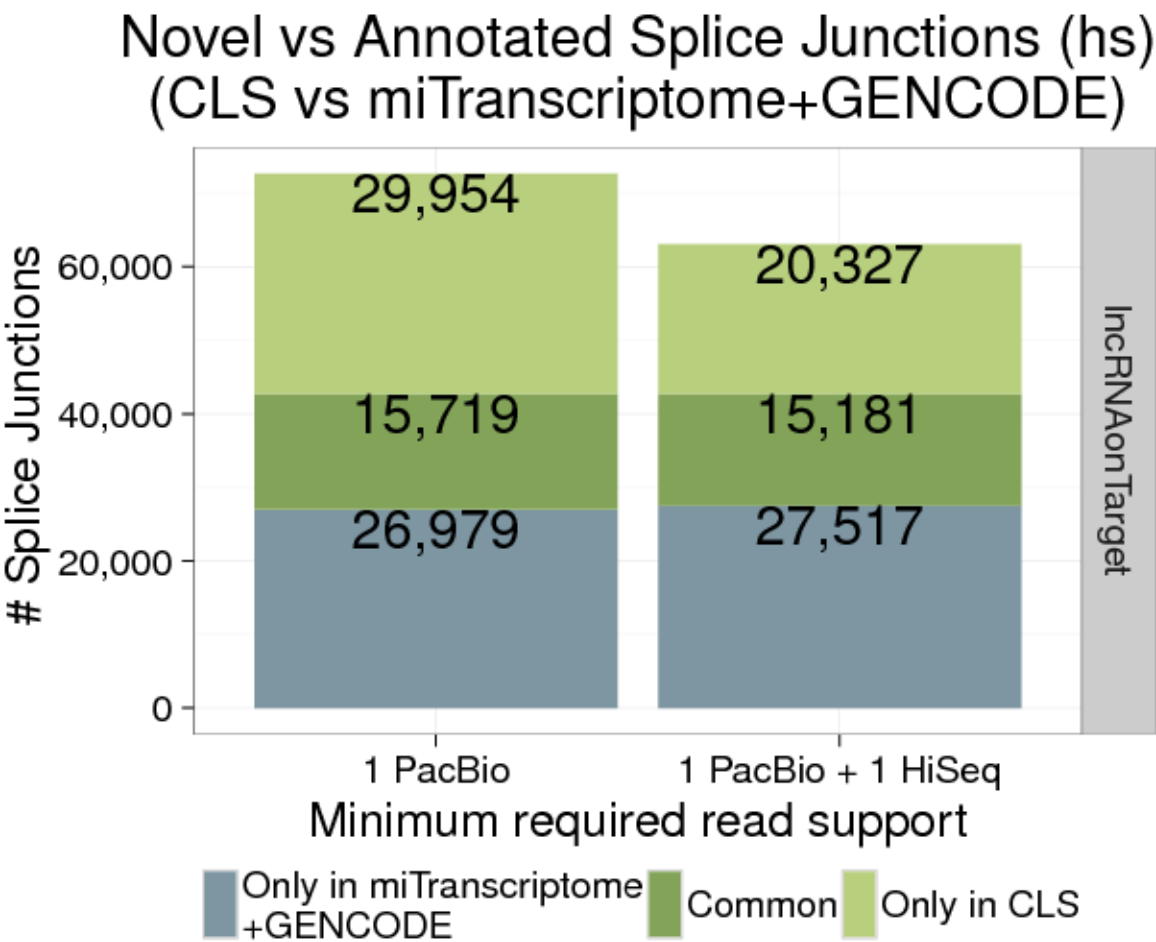
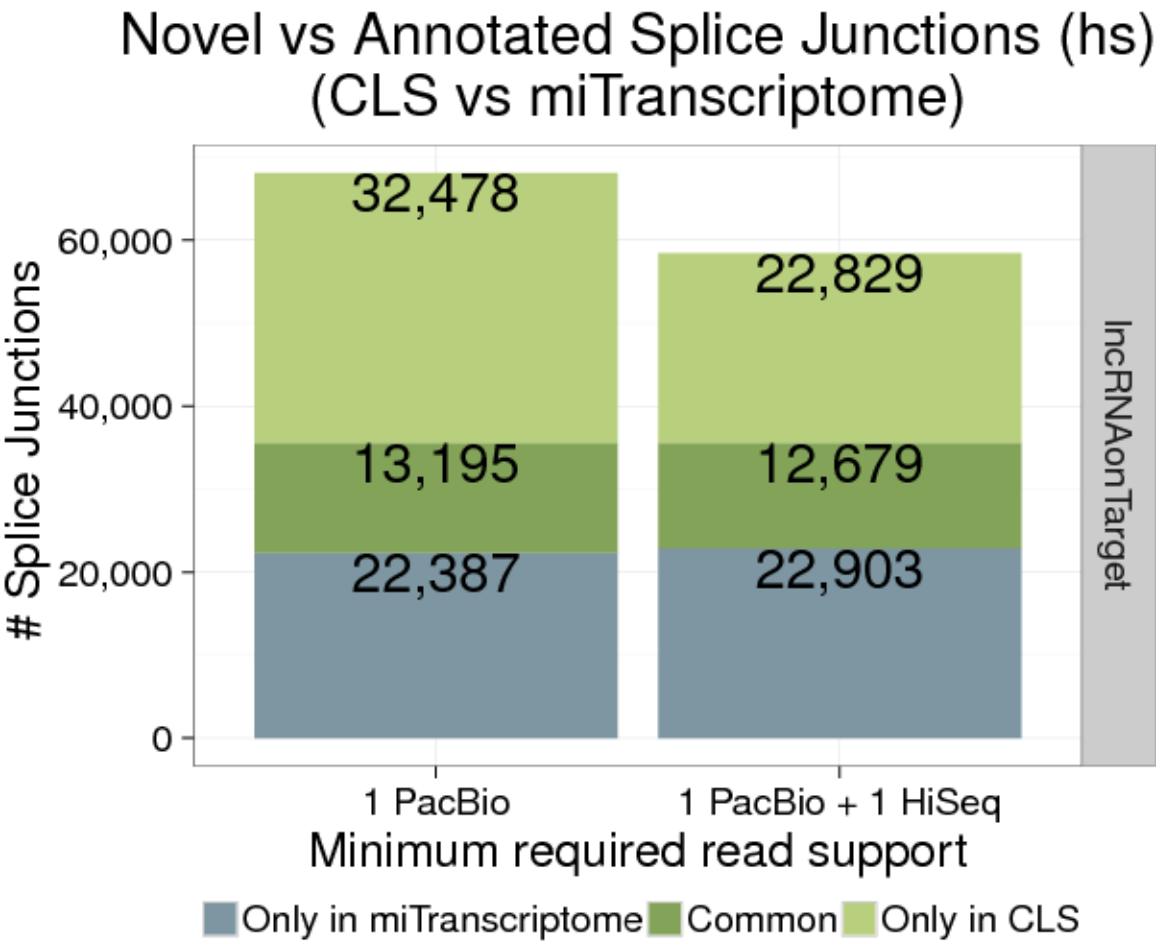
Supplementary Figure S12

bioRxiv preprint doi: <https://doi.org/10.1101/105064>; this version posted June 16, 2017. The copyright holder for this preprint (which was not certified by peer review) is the author/funder, who has granted bioRxiv a license to display the preprint in perpetuity. It is made available under aCC-BY 4.0 International license.



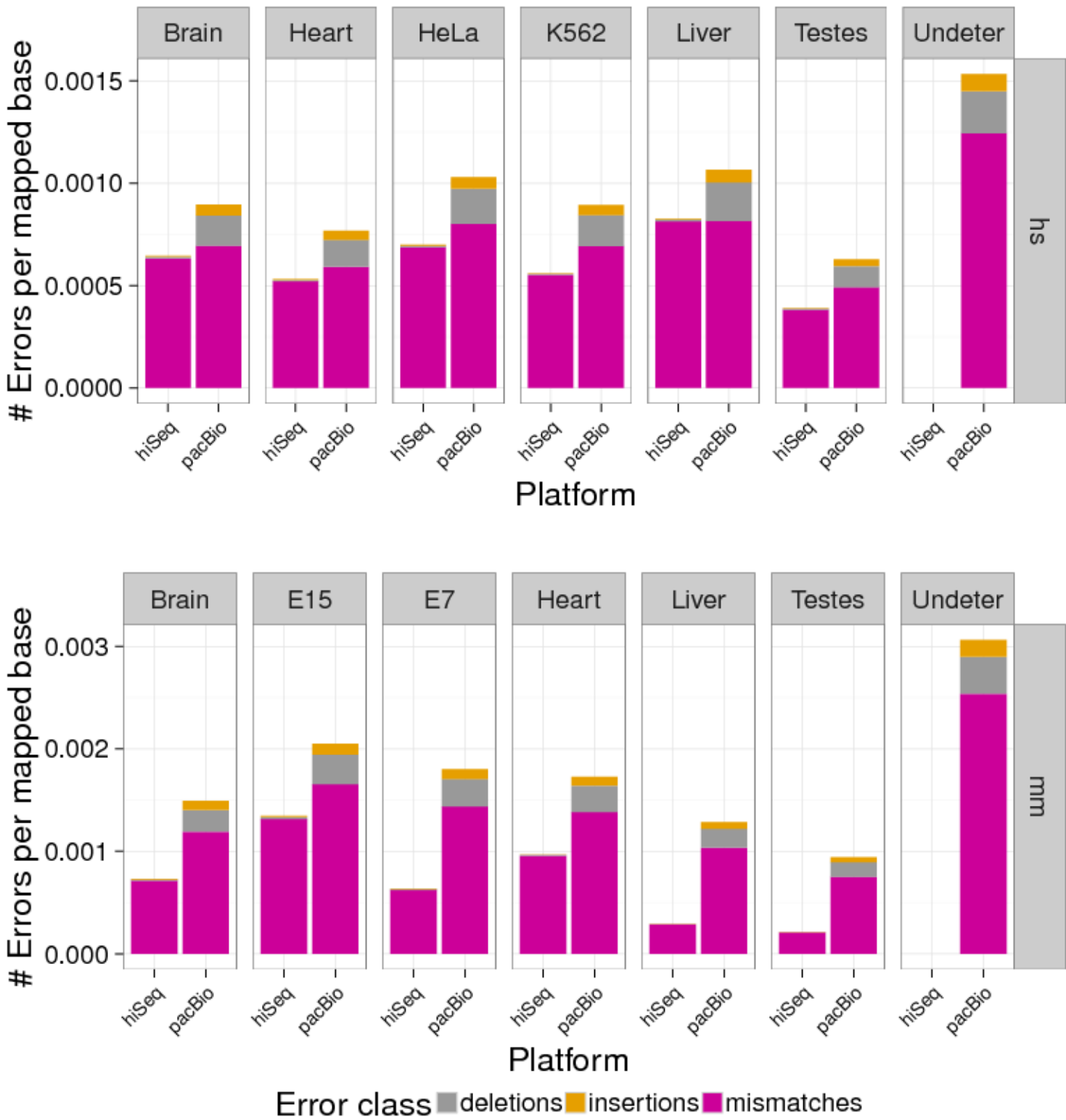
Supplementary Figure S13

bioRxiv preprint doi: <https://doi.org/10.1101/105064>; this version posted June 16, 2017. The copyright holder for this preprint (which was not certified by peer review) is the author/funder, who has granted bioRxiv a license to display the preprint in perpetuity. It is made available under aCC-BY 4.0 International license.



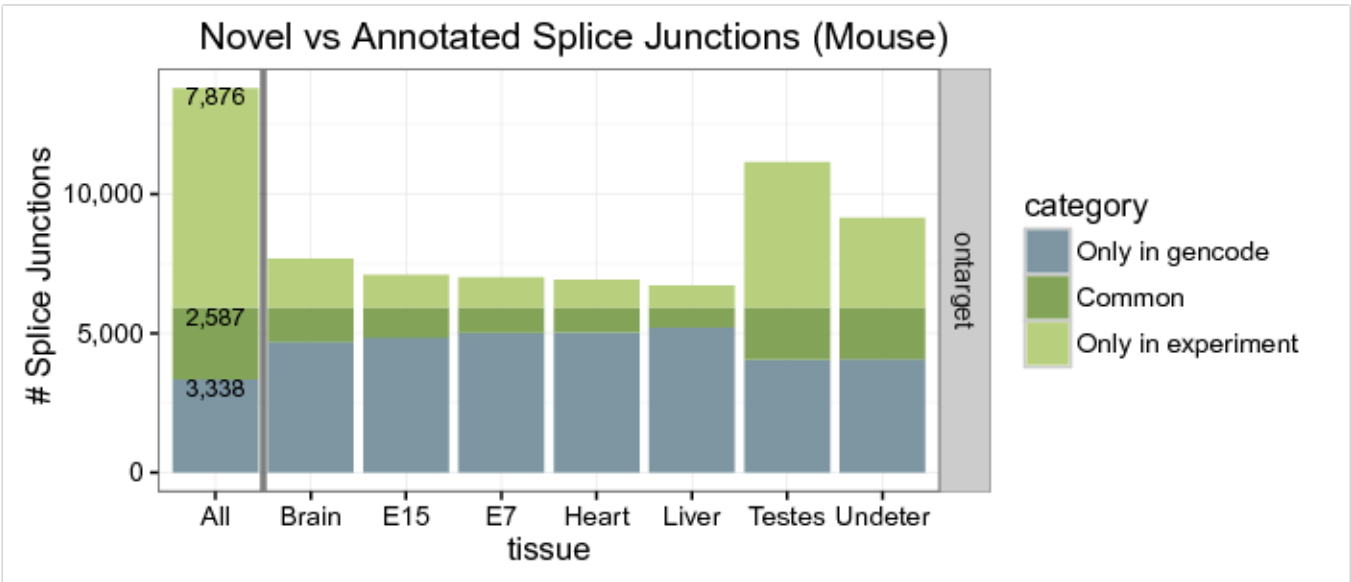
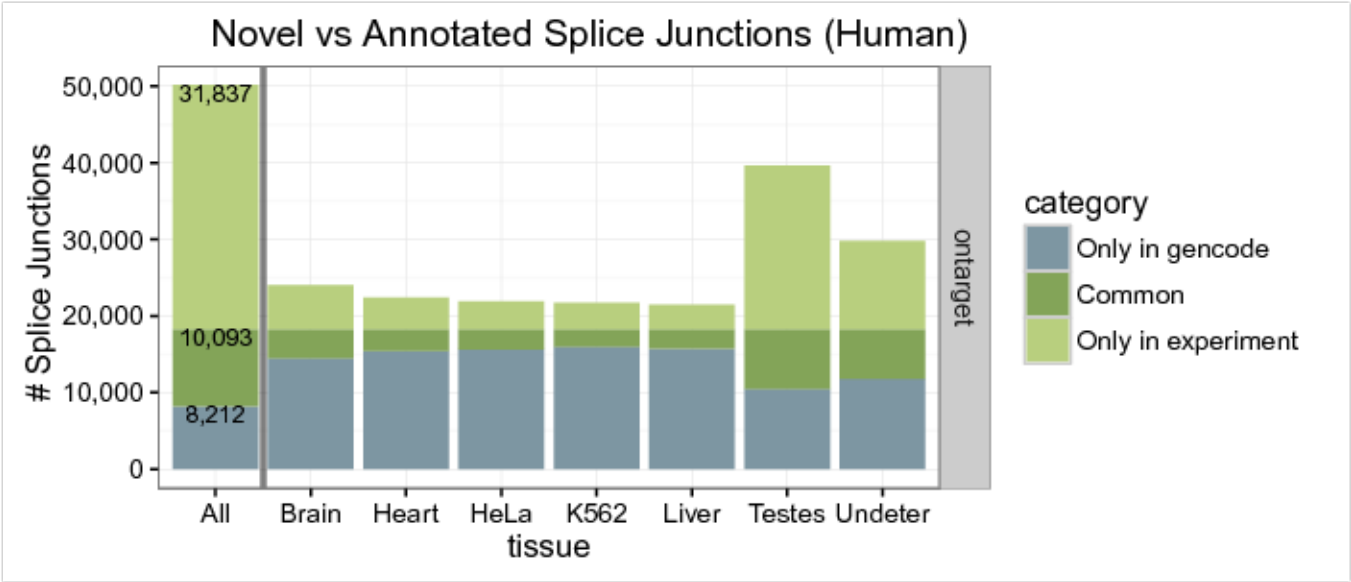
Supplementary Figure S14

bioRxiv preprint doi: <https://doi.org/10.1101/105064>; this version posted June 16, 2017. The copyright holder for this preprint (which was not certified by peer review) is the author/funder, who has granted bioRxiv a license to display the preprint in perpetuity. It is made available under aCC-BY 4.0 International license.



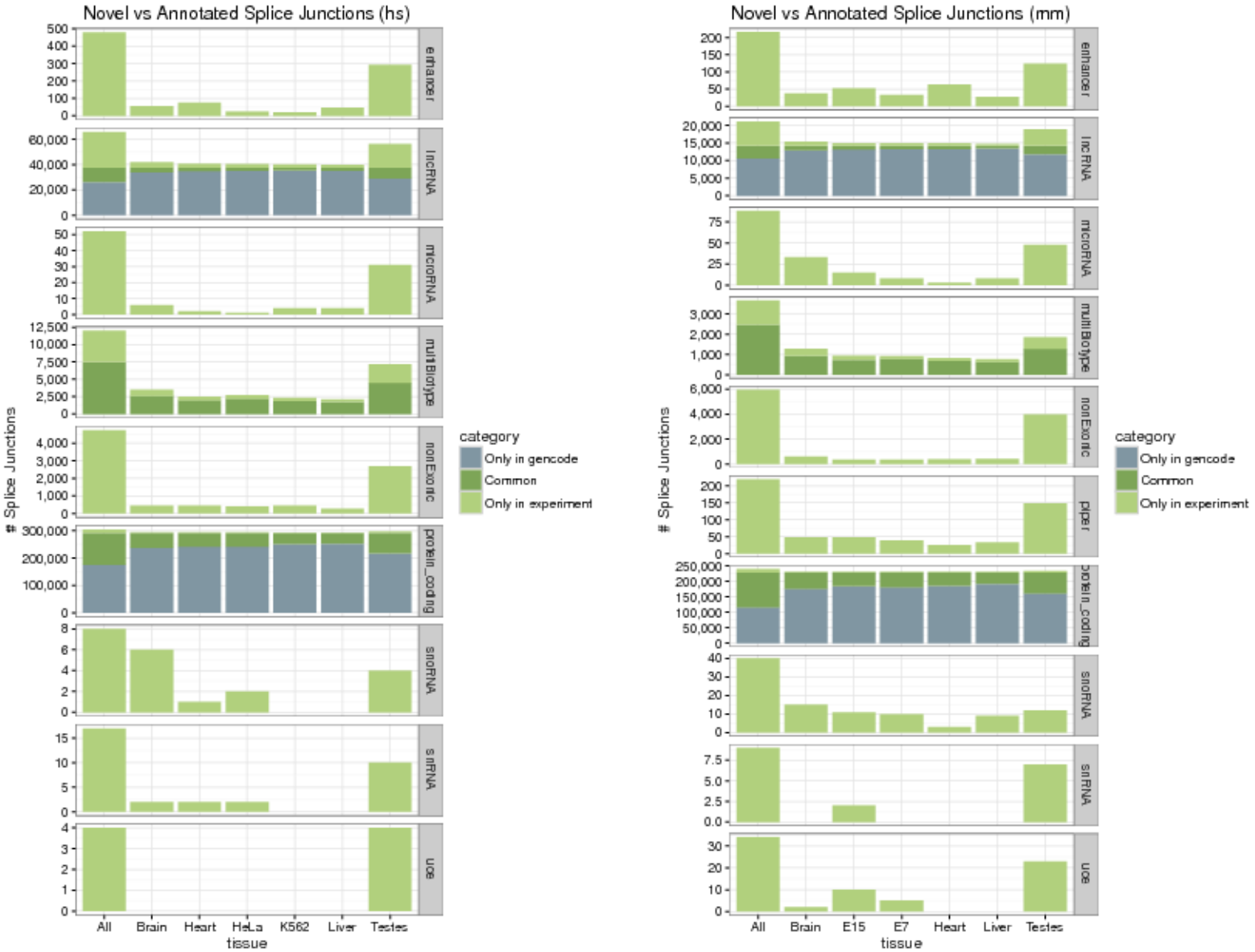
Supplementary Figure S15

bioRxiv preprint doi: <https://doi.org/10.1101/105064>; this version posted June 16, 2017. The copyright holder for this preprint (which was not certified by peer review) is the author/funder, who has granted bioRxiv a license to display the preprint in perpetuity. It is made available under aCC-BY 4.0 International license.



Supplementary Figure S16

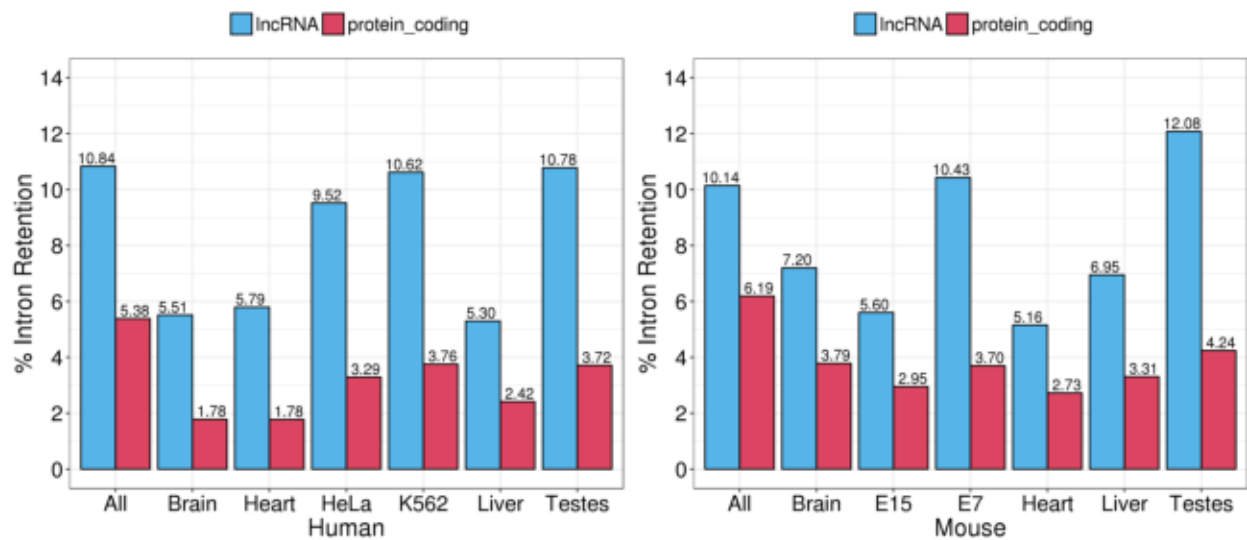
bioRxiv preprint doi: <https://doi.org/10.1101/105064>; this version posted June 16, 2017. The copyright holder for this preprint (which was not certified by peer review) is the author/funder, who has granted bioRxiv a license to display the preprint in perpetuity. It is made available under aCC-BY 4.0 International license.



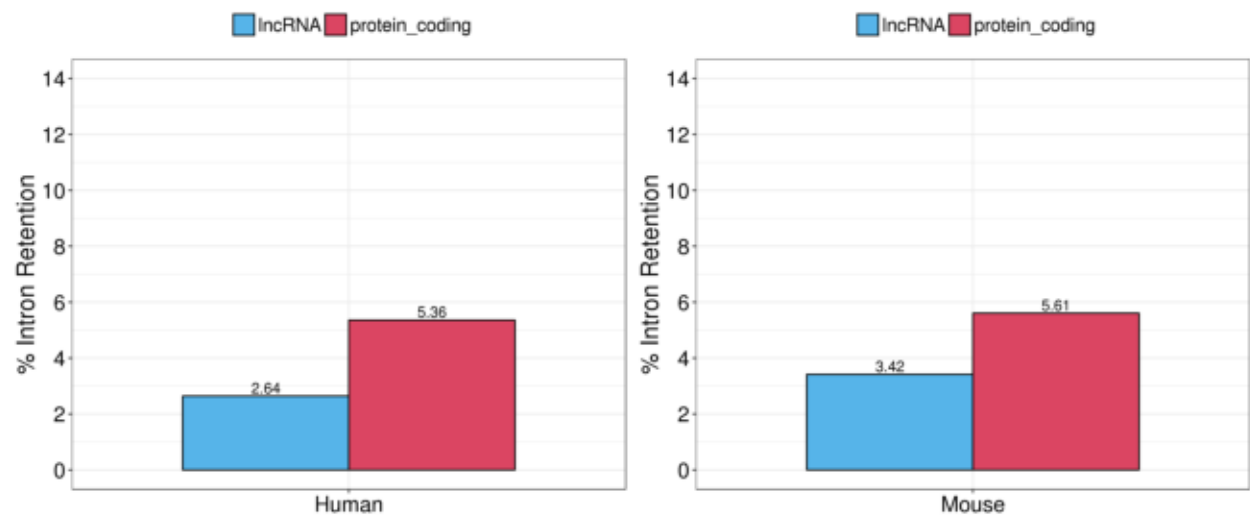
Supplementary Figure S17

bioRxiv preprint doi: <https://doi.org/10.1101/105064>; this version posted June 16, 2017. The copyright holder for this preprint (which was not certified by peer review) is the author/funder, who has granted bioRxiv a license to display the preprint in perpetuity. It is made available under aCC-BY 4.0 International license.

CLS

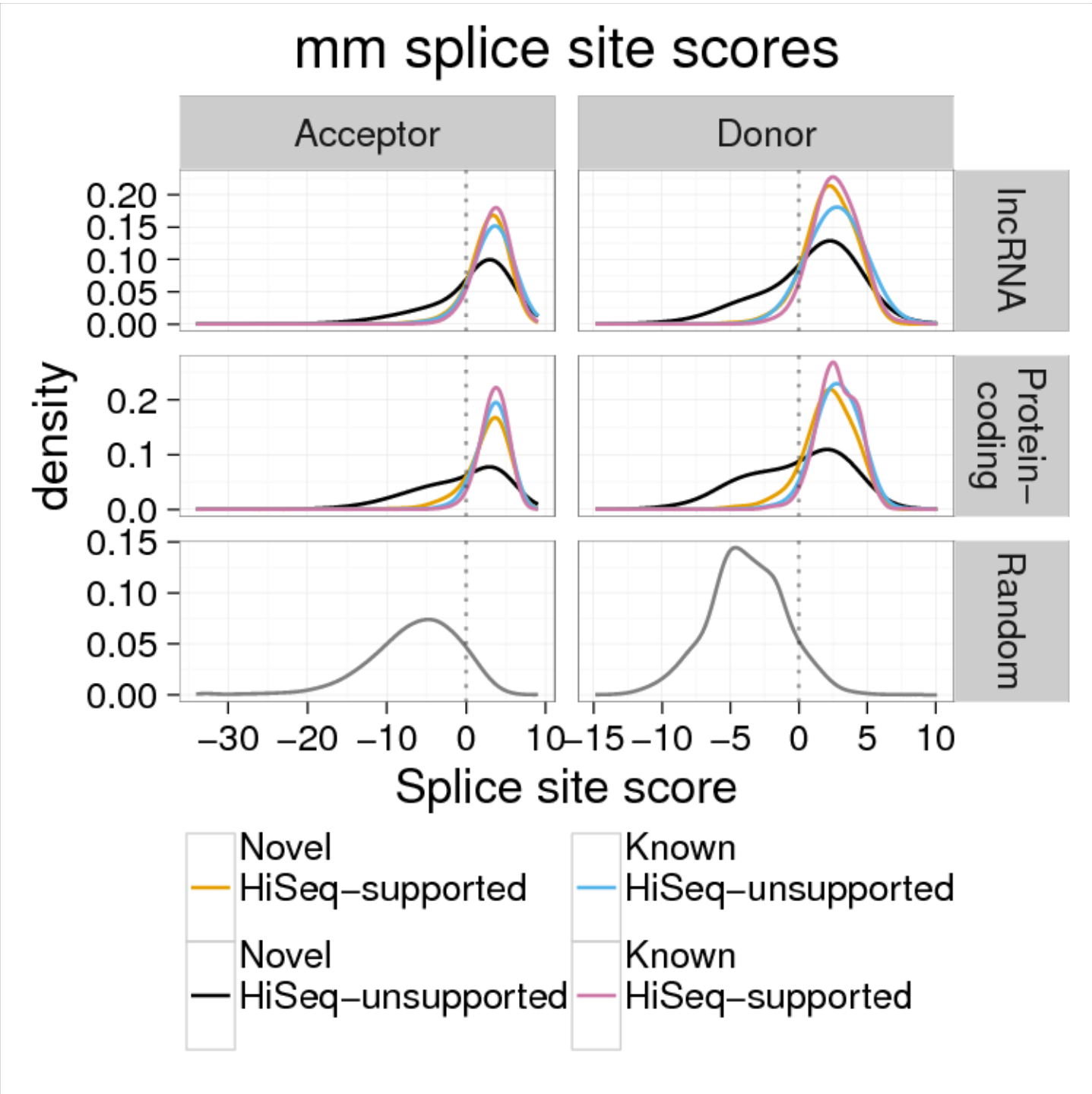


GENCODE



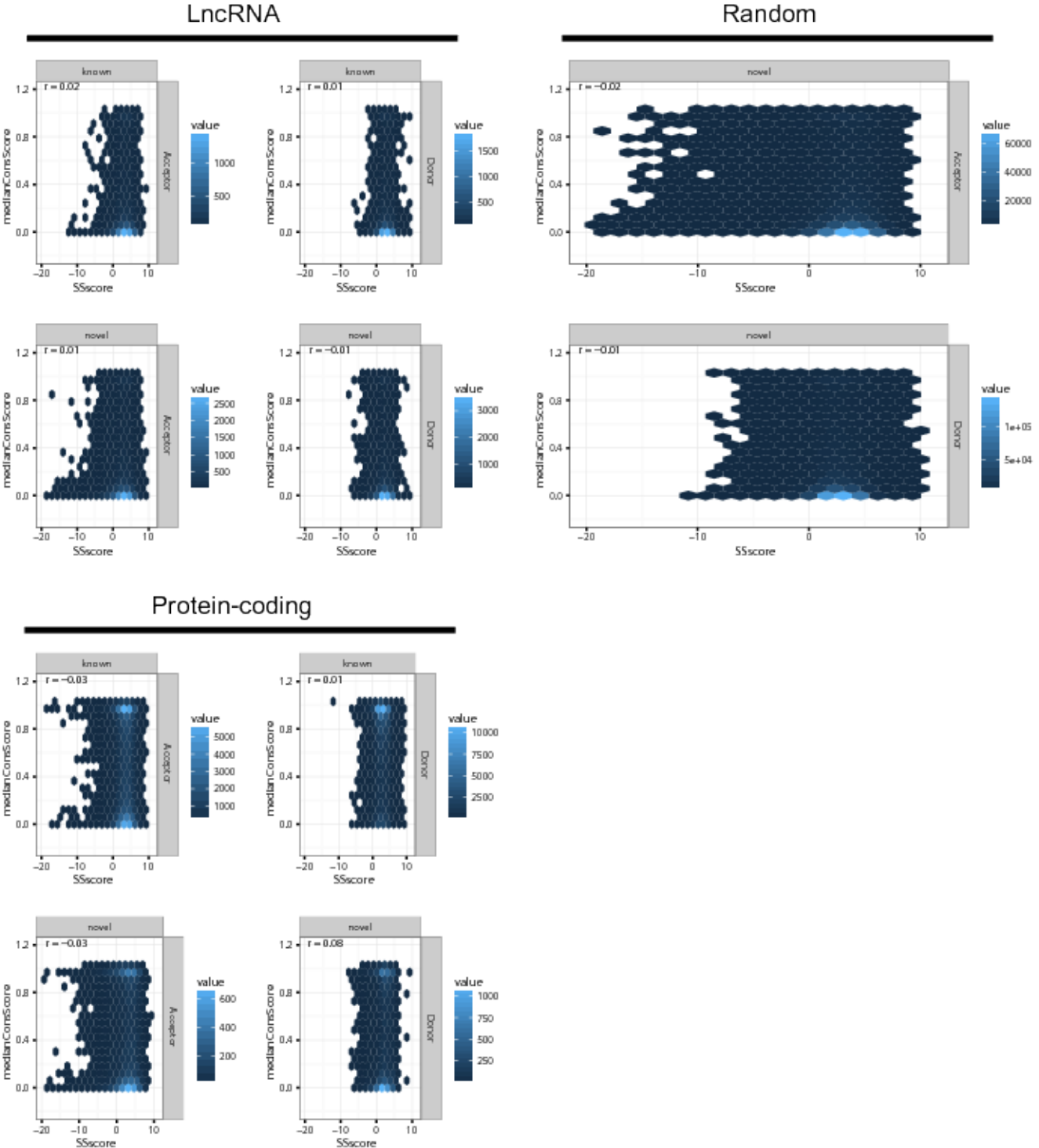
Supplementary Figure S18

bioRxiv preprint doi: <https://doi.org/10.1101/105064>; this version posted June 16, 2017. The copyright holder for this preprint (which was not certified by peer review) is the author/funder, who has granted bioRxiv a license to display the preprint in perpetuity. It is made available under aCC-BY 4.0 International license.



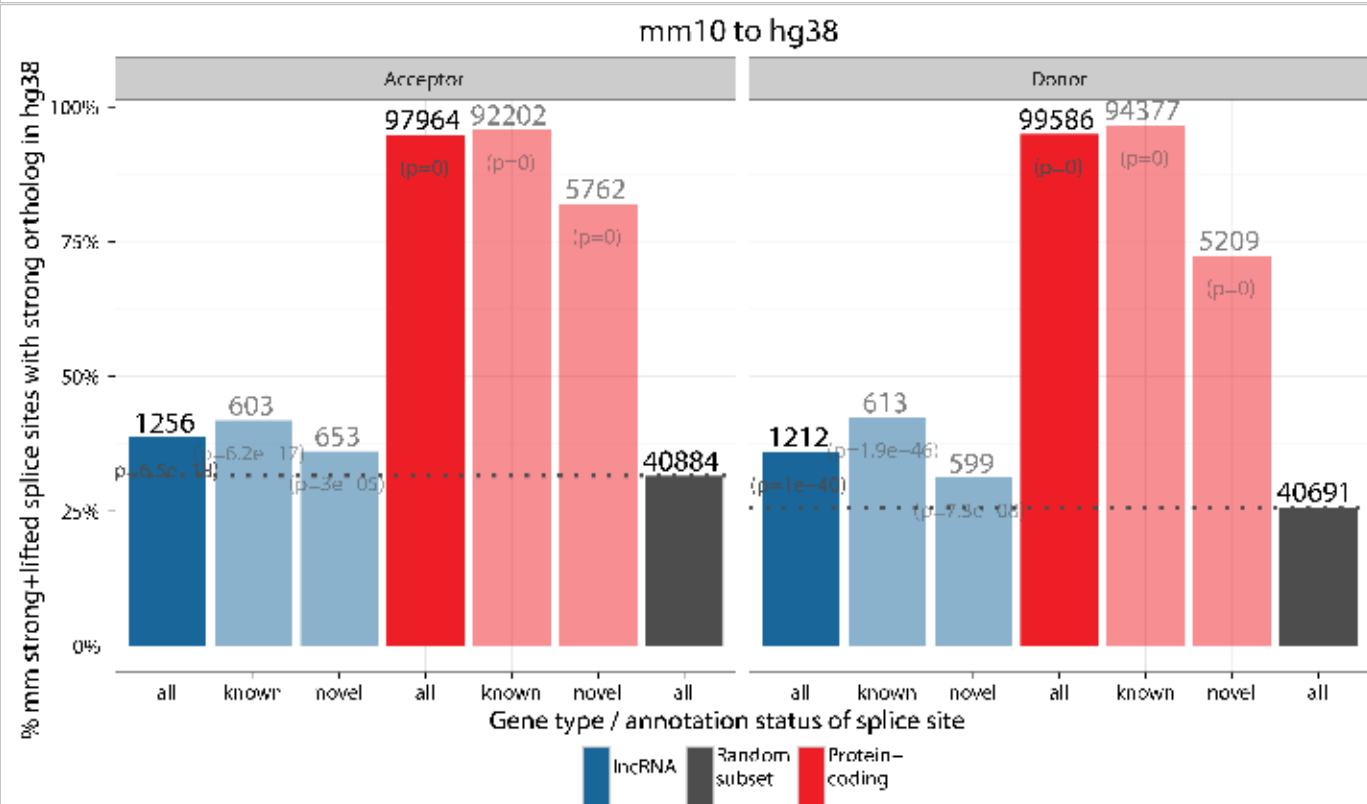
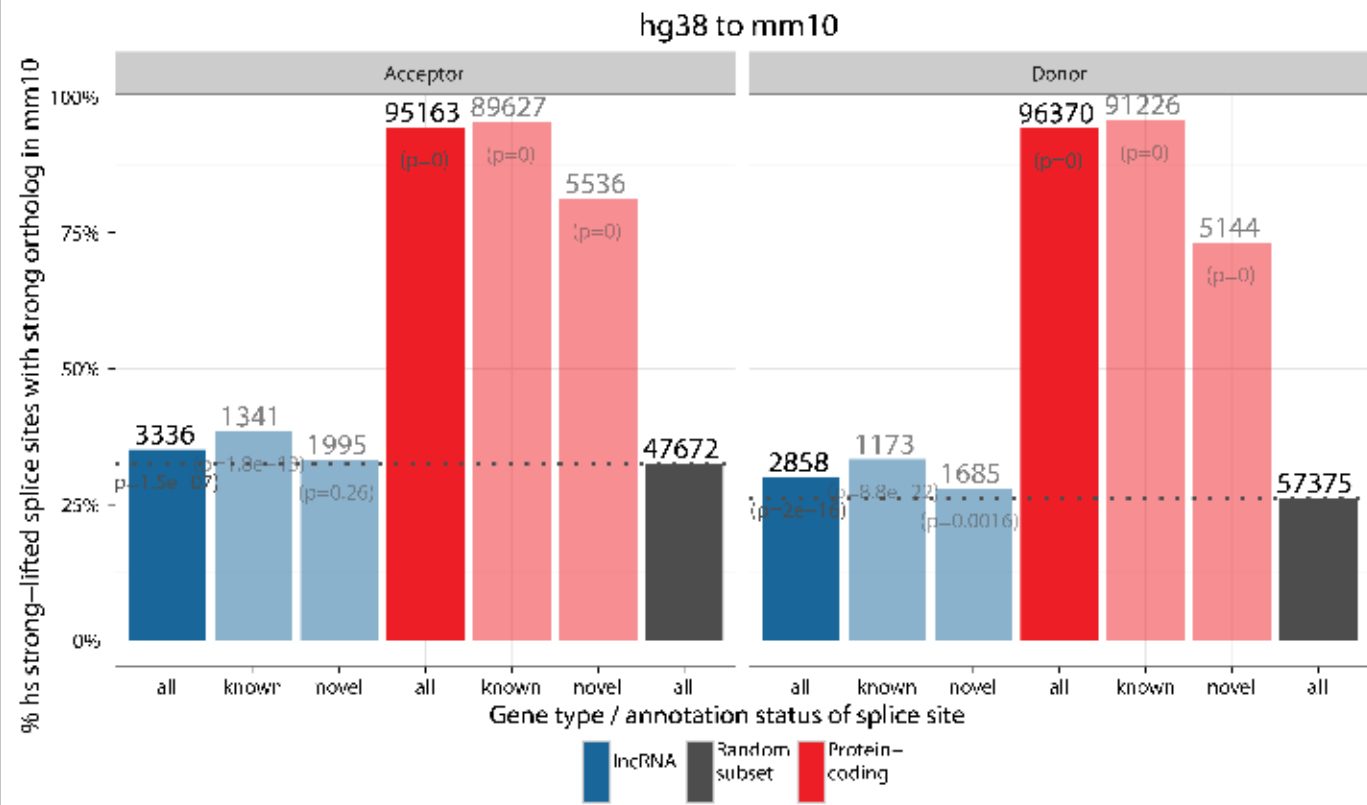
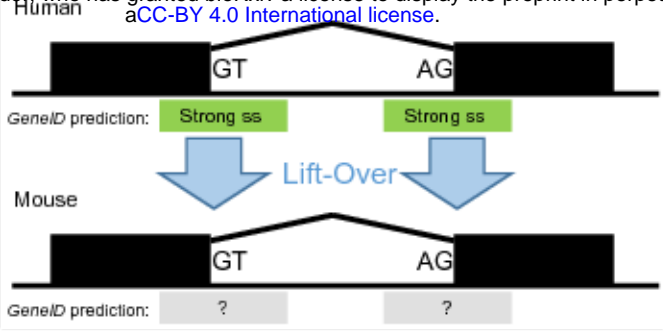
Supplementary Figure S19

bioRxiv preprint doi: <https://doi.org/10.1101/105064>; this version posted June 16, 2017. The copyright holder for this preprint (which was not certified by peer review) is the author/funder, who has granted bioRxiv a license to display the preprint in perpetuity. It is made available under aCC-BY 4.0 International license.



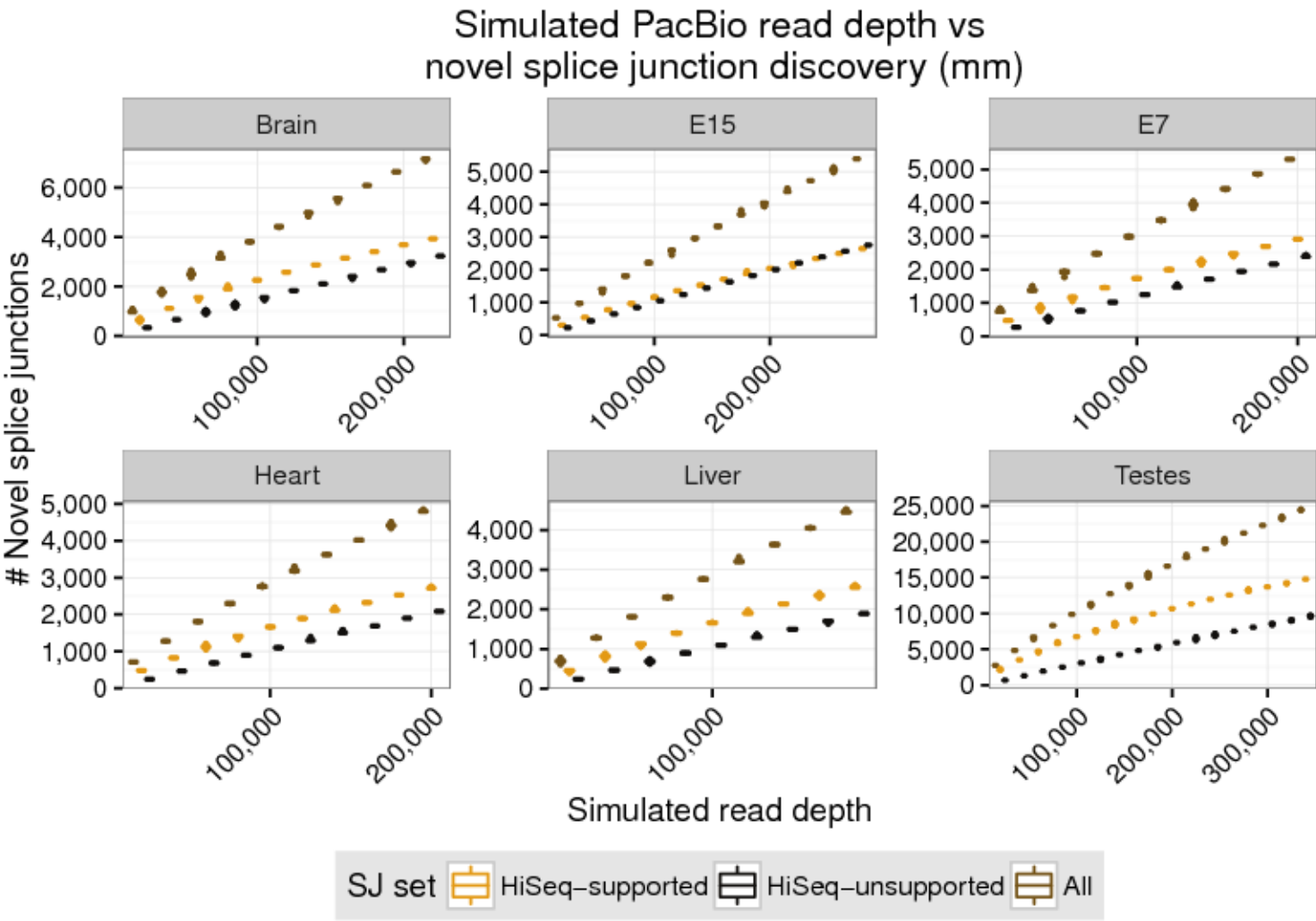
Supplementary Figure S20

bioRxiv preprint doi: <https://doi.org/10.1101/105064>; this version posted June 16, 2017. The copyright holder for this preprint (which was not certified by peer review) is the author/funder, who has granted bioRxiv a license to display the preprint in perpetuity. It is made available under aCC-BY 4.0 International license.



Supplementary Figure S21

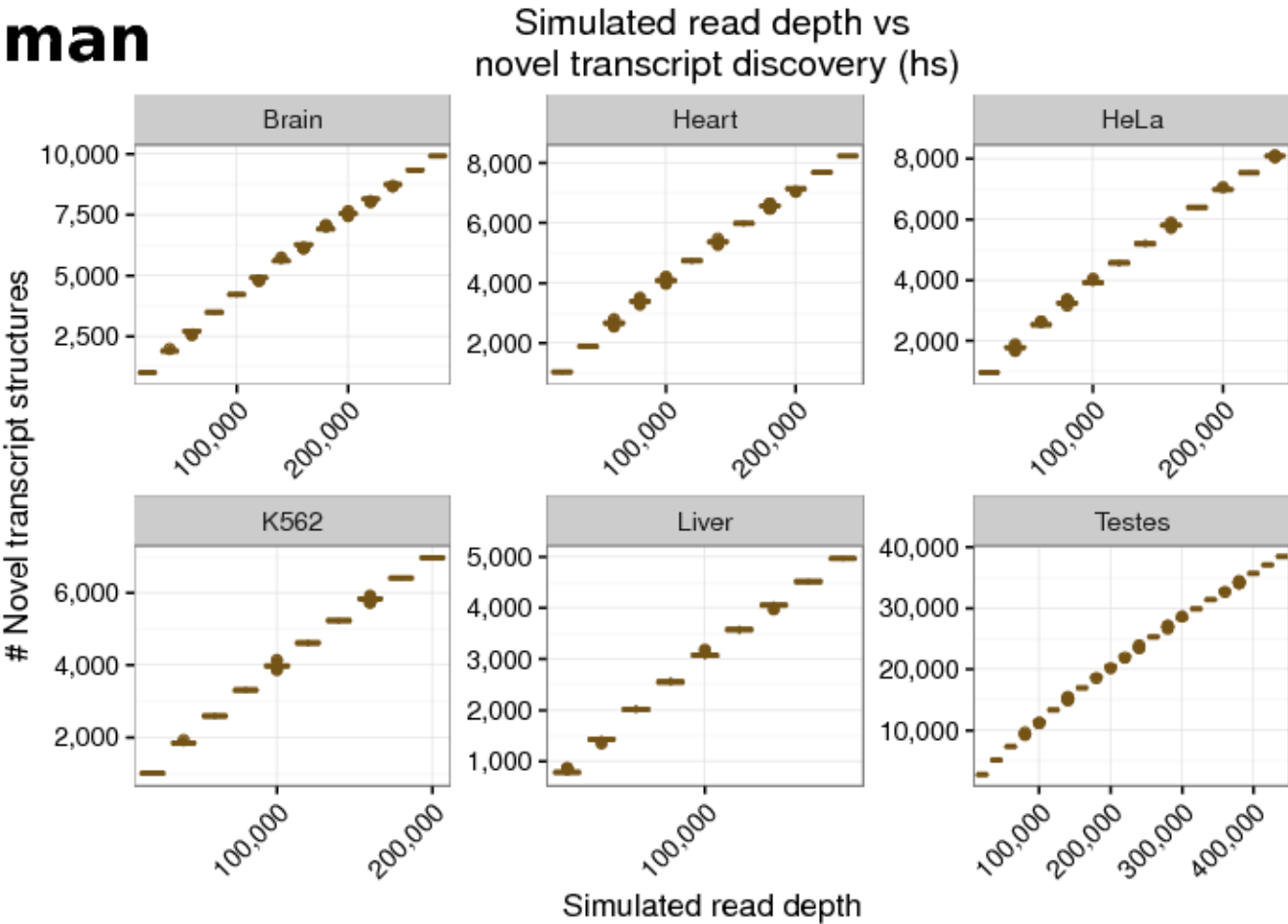
bioRxiv preprint doi: <https://doi.org/10.1101/105064>; this version posted June 16, 2017. The copyright holder for this preprint (which was not certified by peer review) is the author/funder, who has granted bioRxiv a license to display the preprint in perpetuity. It is made available under aCC-BY 4.0 International license.



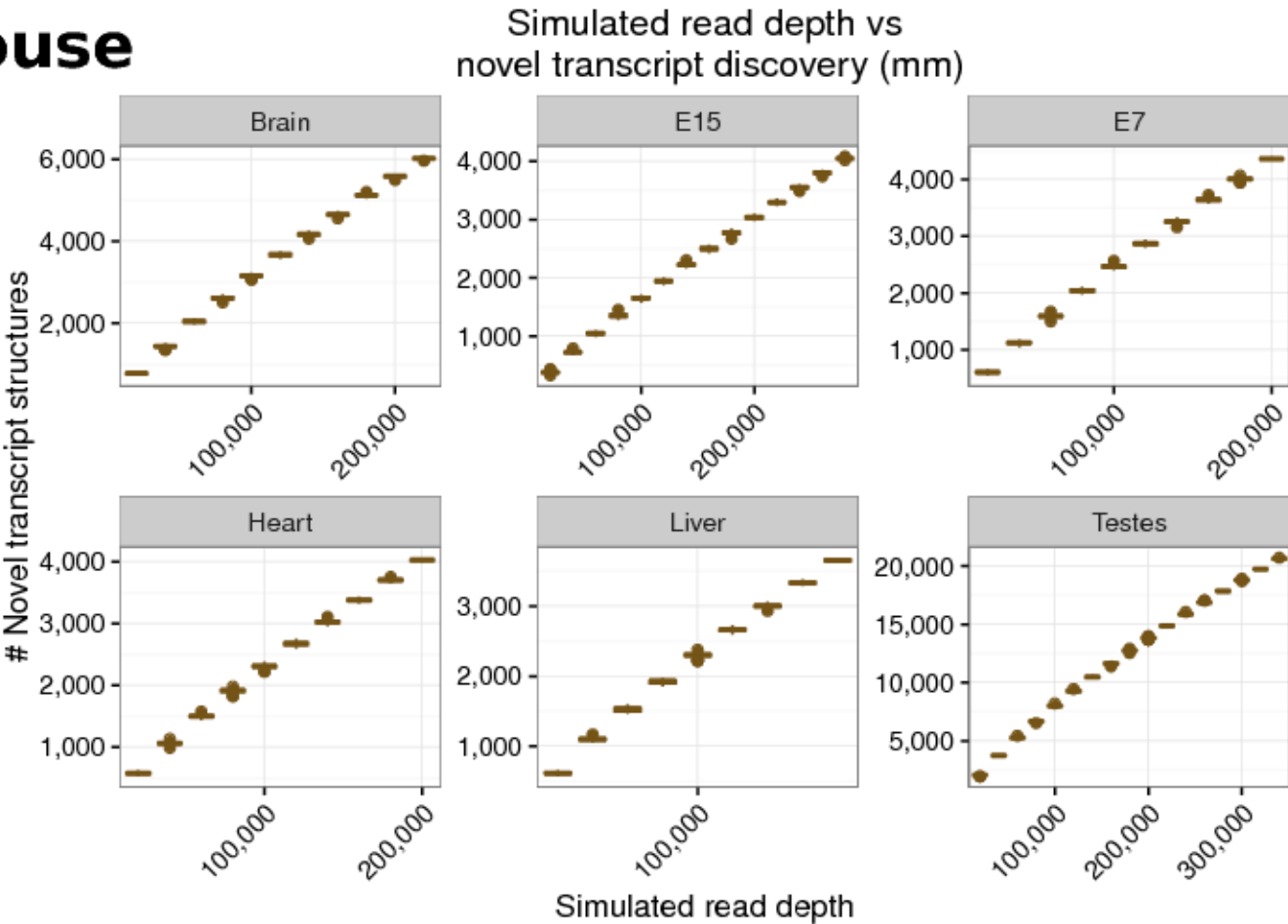
Supplementary Figure S22

bioRxiv preprint doi: <https://doi.org/10.1101/105064>; this version posted June 16, 2017. The copyright holder for this preprint (which was not certified by peer review) is the author/funder, who has granted bioRxiv a license to display the preprint in perpetuity. It is made available under aCC-BY 4.0 International license.

Human



Mouse

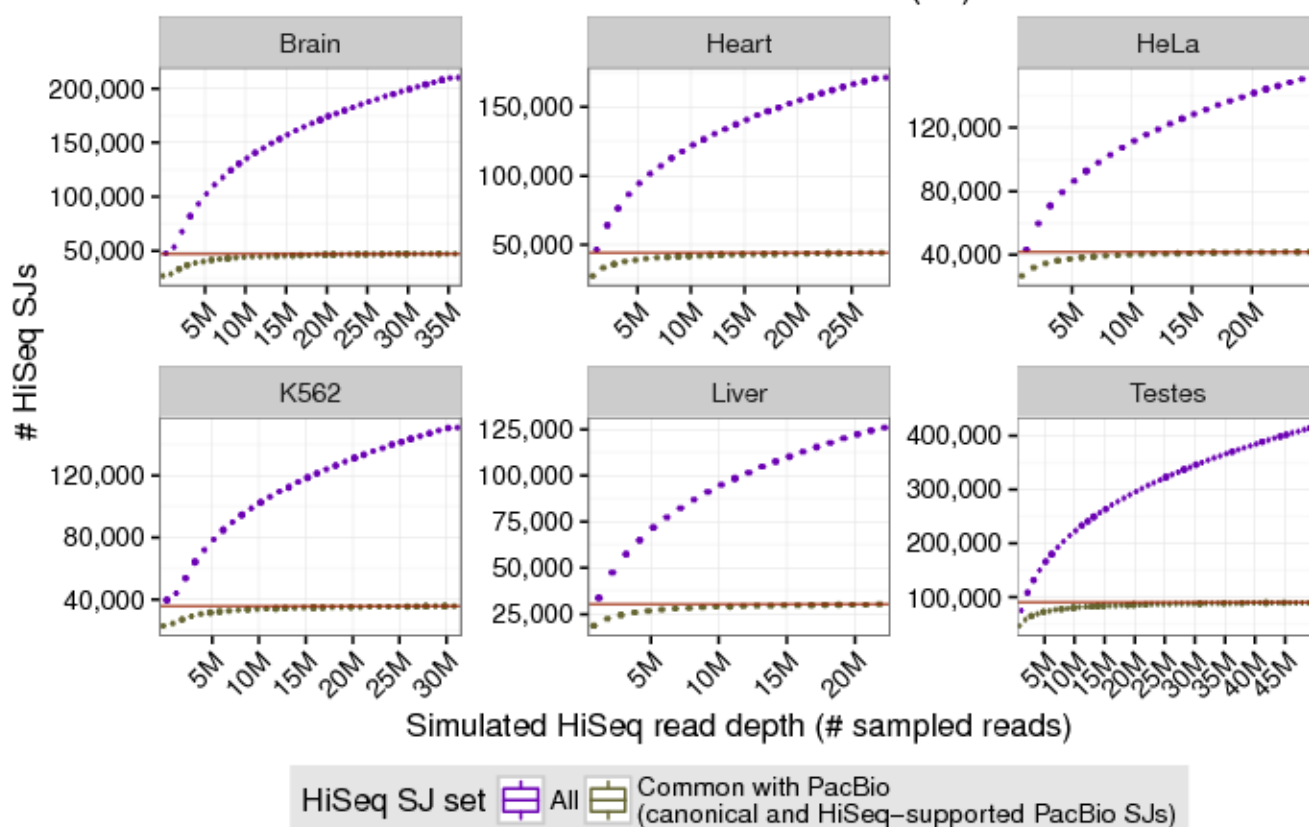


Supplementary Figure S23

bioRxiv preprint doi: <https://doi.org/10.1101/105064>; this version posted June 16, 2017. The copyright holder for this preprint (which was not certified by peer review) is the author/funder, who has granted bioRxiv a license to display the preprint in perpetuity. It is made available under aCC-BY 4.0 International license.

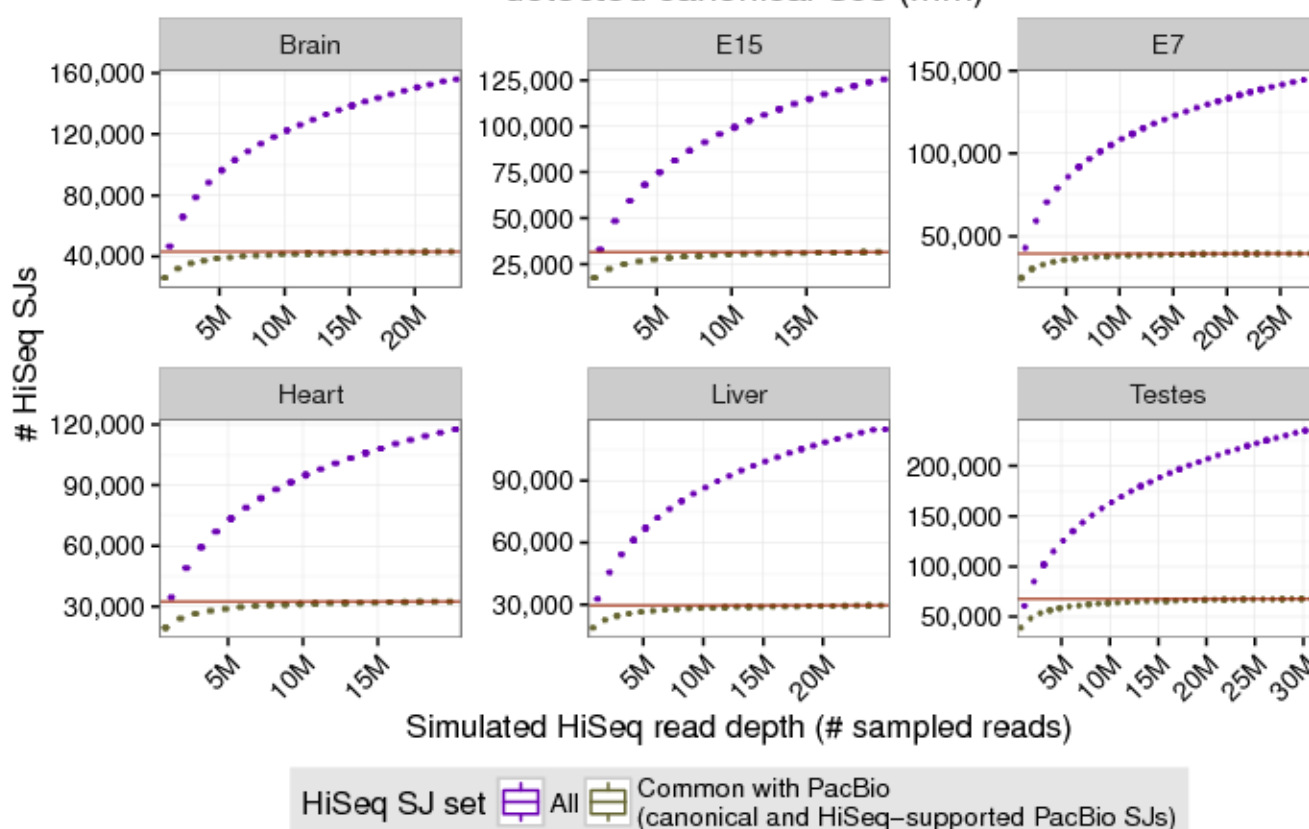
Human

Simulated HiSeq read depth vs detected canonical SJs (hs)



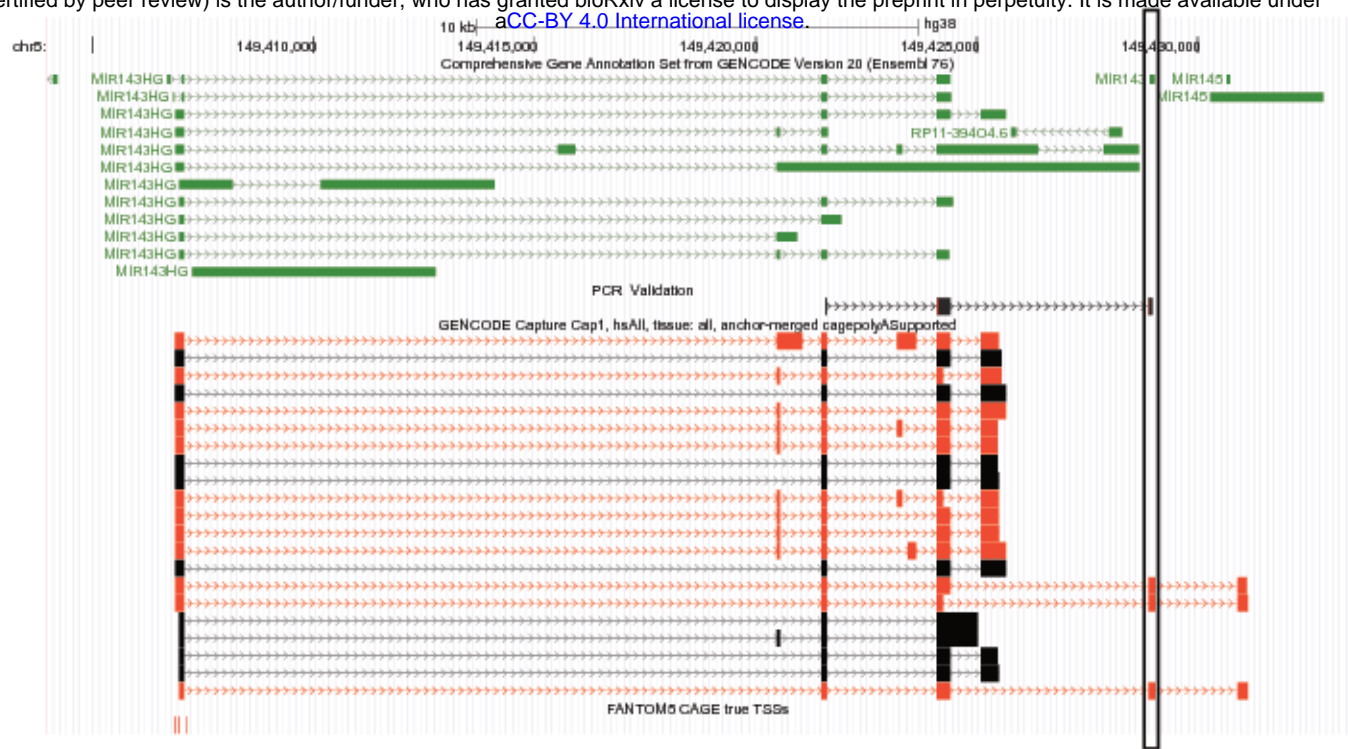
Mouse

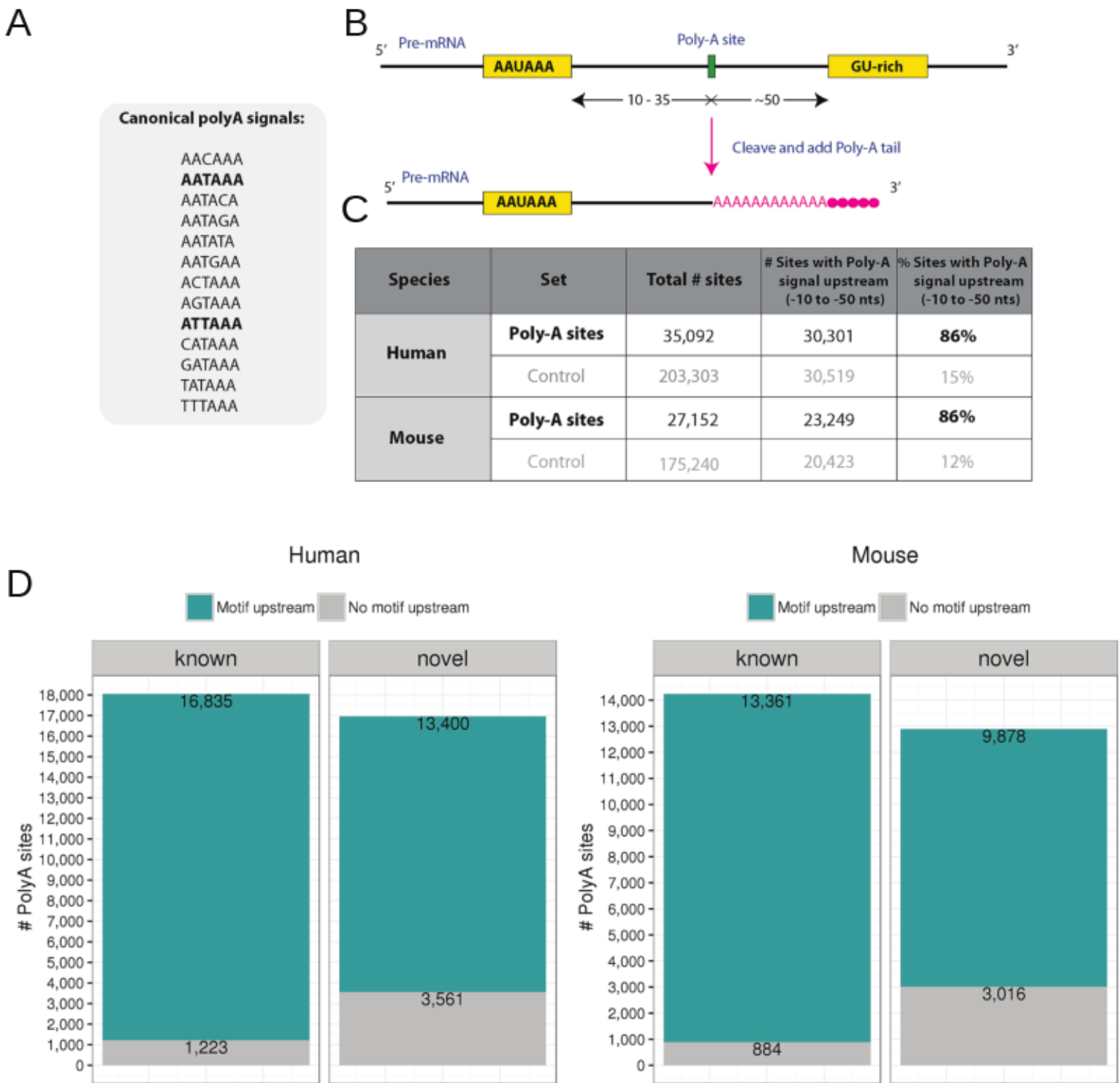
Simulated HiSeq read depth vs detected canonical SJs (mm)



Supplementary Figure S24

bioRxiv preprint doi: <https://doi.org/10.1101/105064>; this version posted June 16, 2017. The copyright holder for this preprint (which was not certified by peer review) is the author/funder, who has granted bioRxiv a license to display the preprint in perpetuity. It is made available under aCC-BY 4.0 International license.

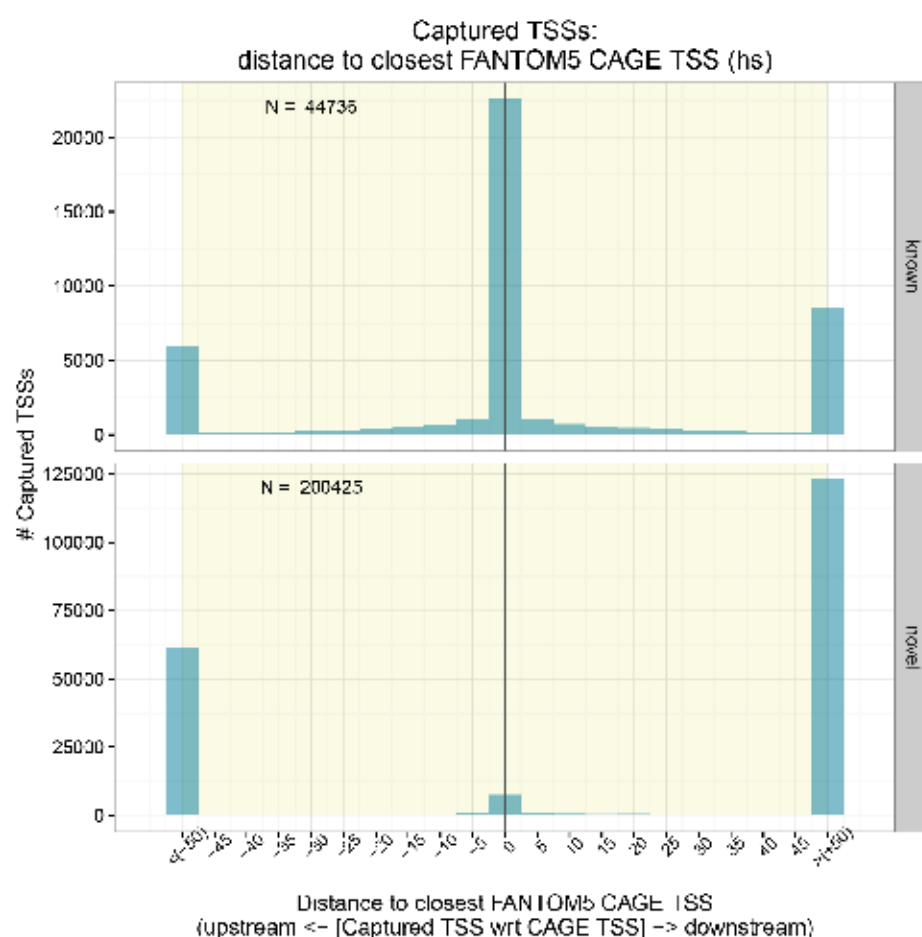




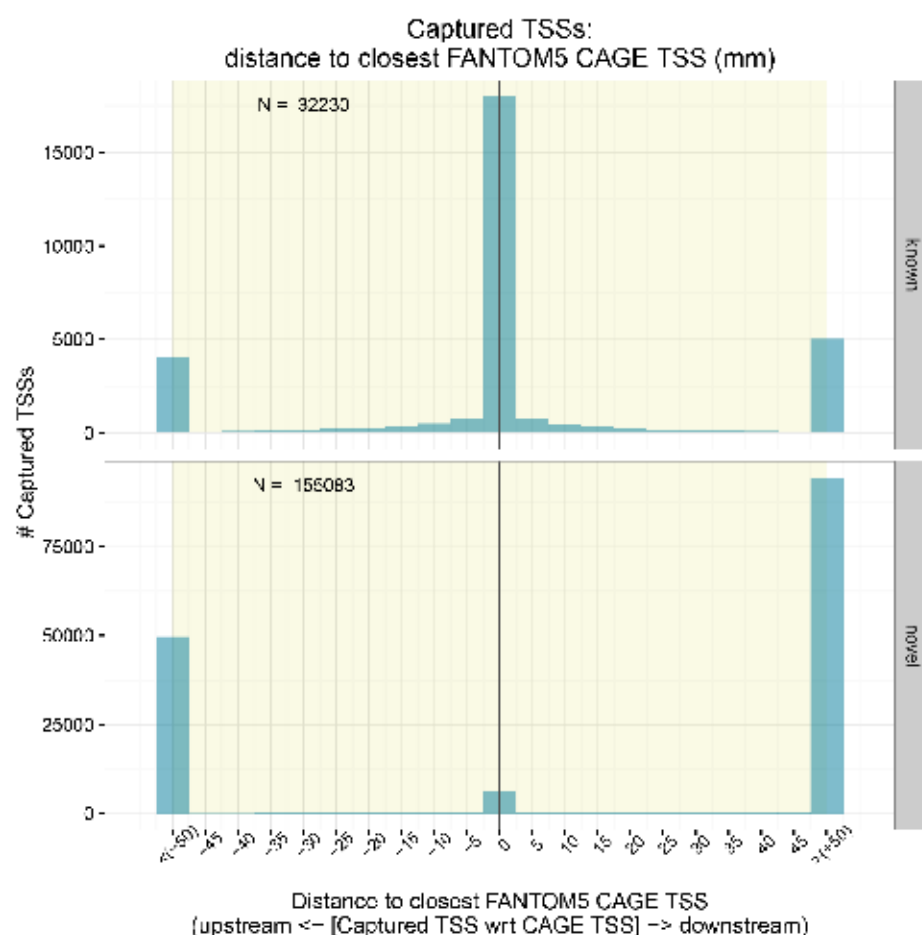
Supplementary Figure S26

bioRxiv preprint doi: <https://doi.org/10.1101/105064>; this version posted June 16, 2017. The copyright holder for this preprint (which was not certified by peer review) is the author/funder, who has granted bioRxiv a license to display the preprint in perpetuity. It is made available under aCC-BY 4.0 International license.

Human



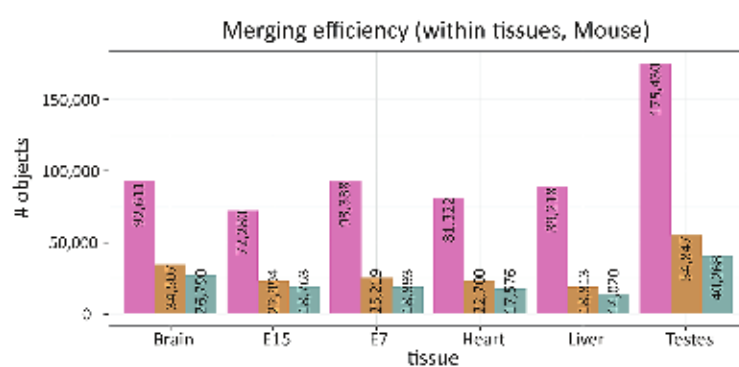
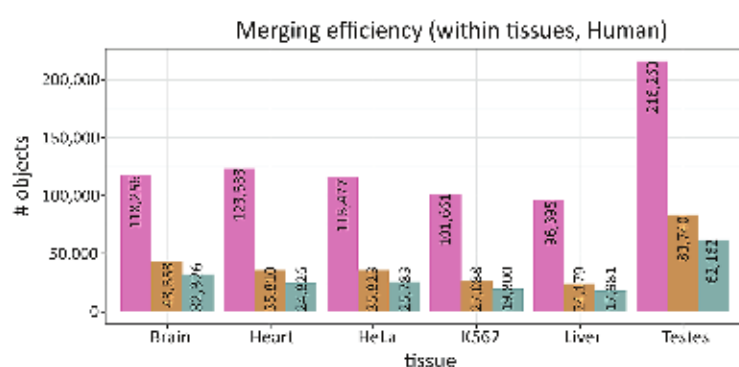
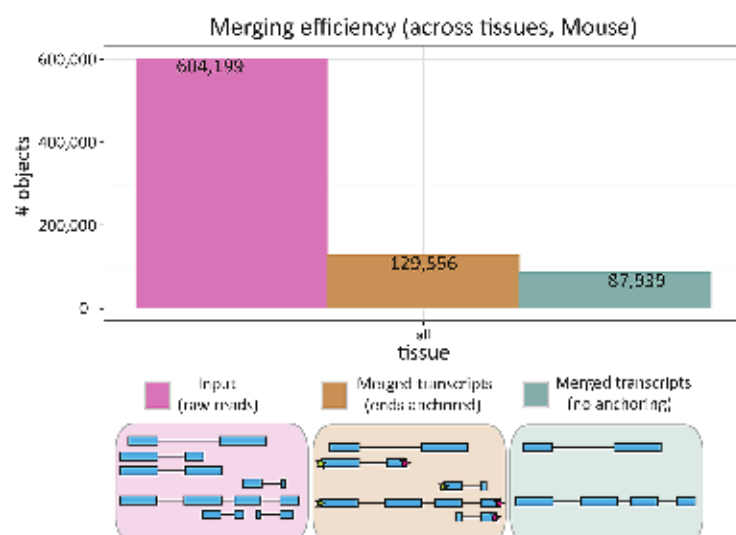
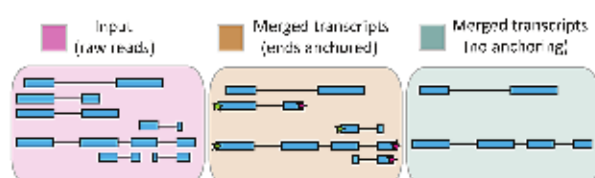
Mouse



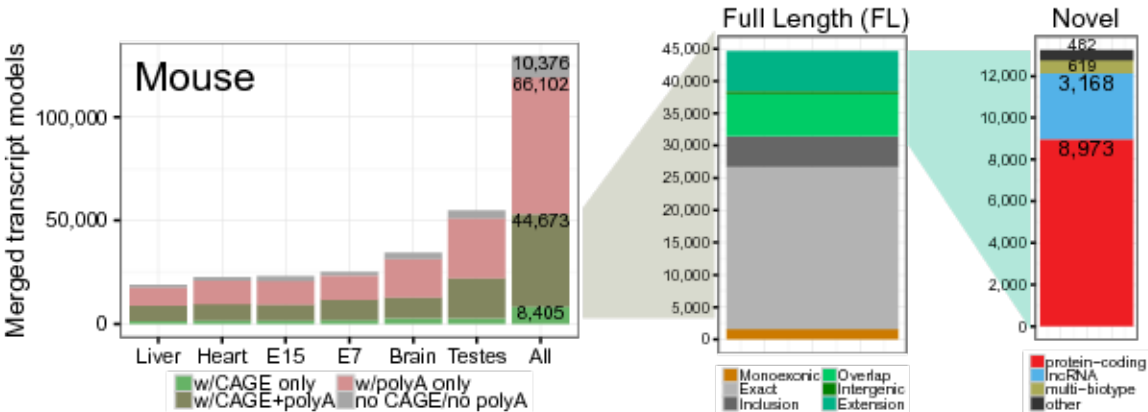
Supplementary Figure S27

bioRxiv preprint doi: <https://doi.org/10.1101/105064>; this version posted June 16, 2017. The copyright holder for this preprint (which was not certified by peer review) is the author/funder, who has granted bioRxiv a license to display the preprint in perpetuity. It is made available under aCC-BY 4.0 International license.

See Figure 4C

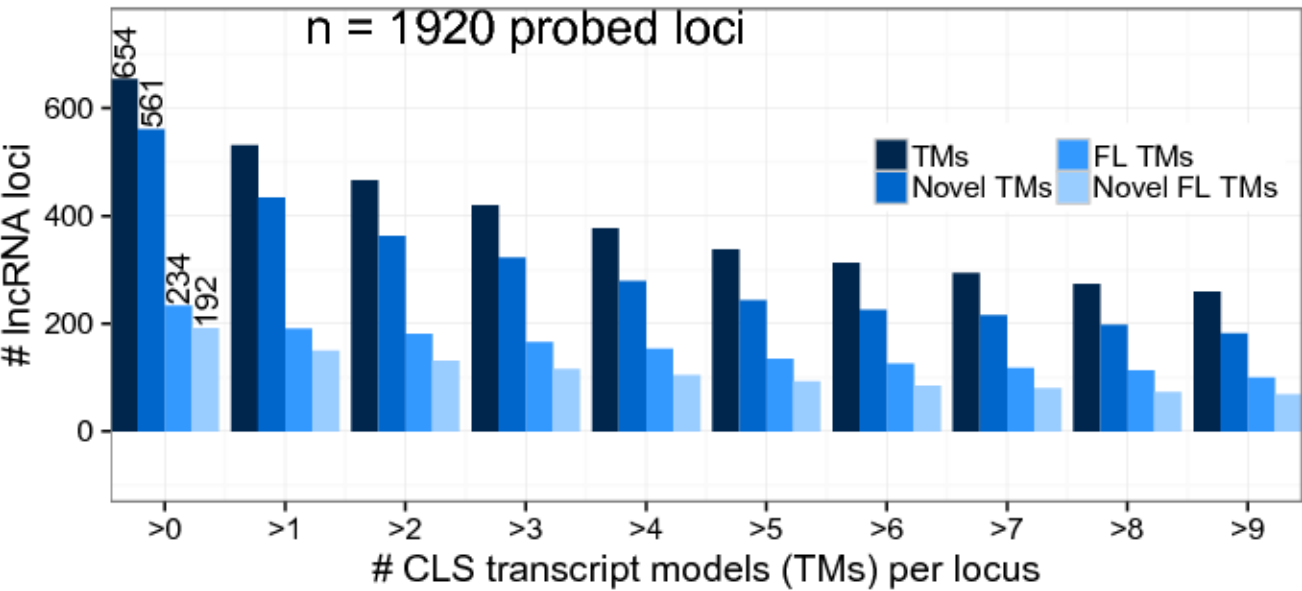


Supplementary Figure S28



Supplementary Figure S29

bioRxiv preprint doi: <https://doi.org/10.1101/105064>; this version posted June 16, 2017. The copyright holder for this preprint (which was not certified by peer review) is the author/funder, who has granted bioRxiv a license to display the preprint in perpetuity. It is made available under aCC-BY 4.0 International license.



Supplementary Figure S30

A

Human, full-length reads: $P=0.0014$, Fisher two-tail

	Conserved	Not_conserved
Detected	34	1076
Not_detected	23	1753

Human, all reads: $P=NS$, Fisher two-tail

	Conserved	Not_conserved
Detected	78	4101
Not_detected	23	1753

B

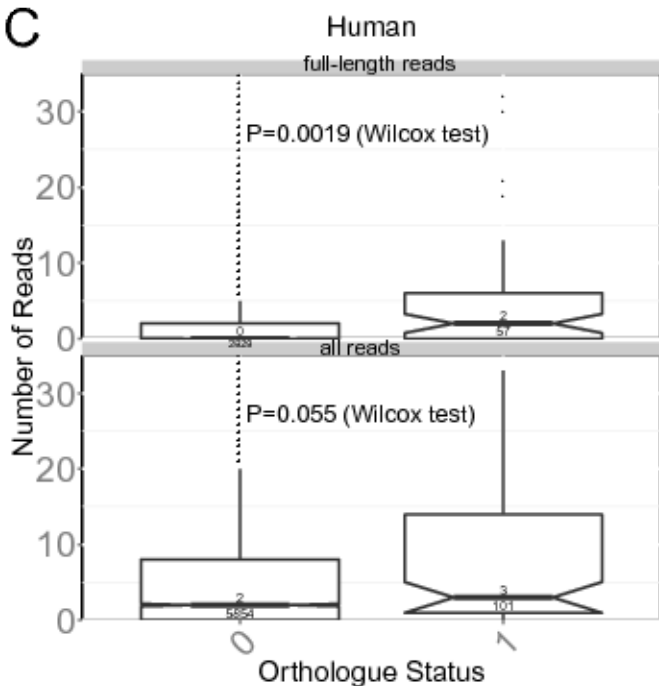
Mouse, full-length reads: $P=NS$, Fisher two-tail

	Conserved	Not_conserved
Detected	18	318
Not_detected	45	859

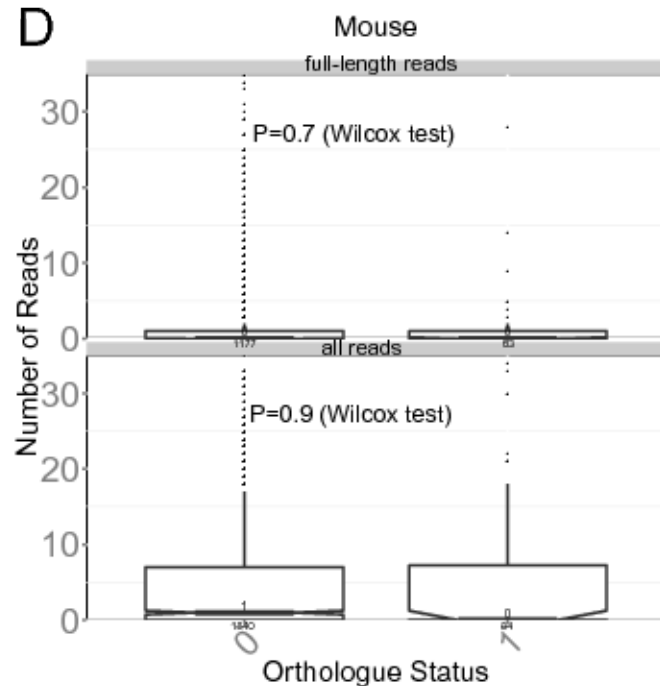
Mouse, all reads: $P=NS$, Fisher two-tail

	Conserved	Not_conserved
Detected	39	981
Not_detected	45	859

C

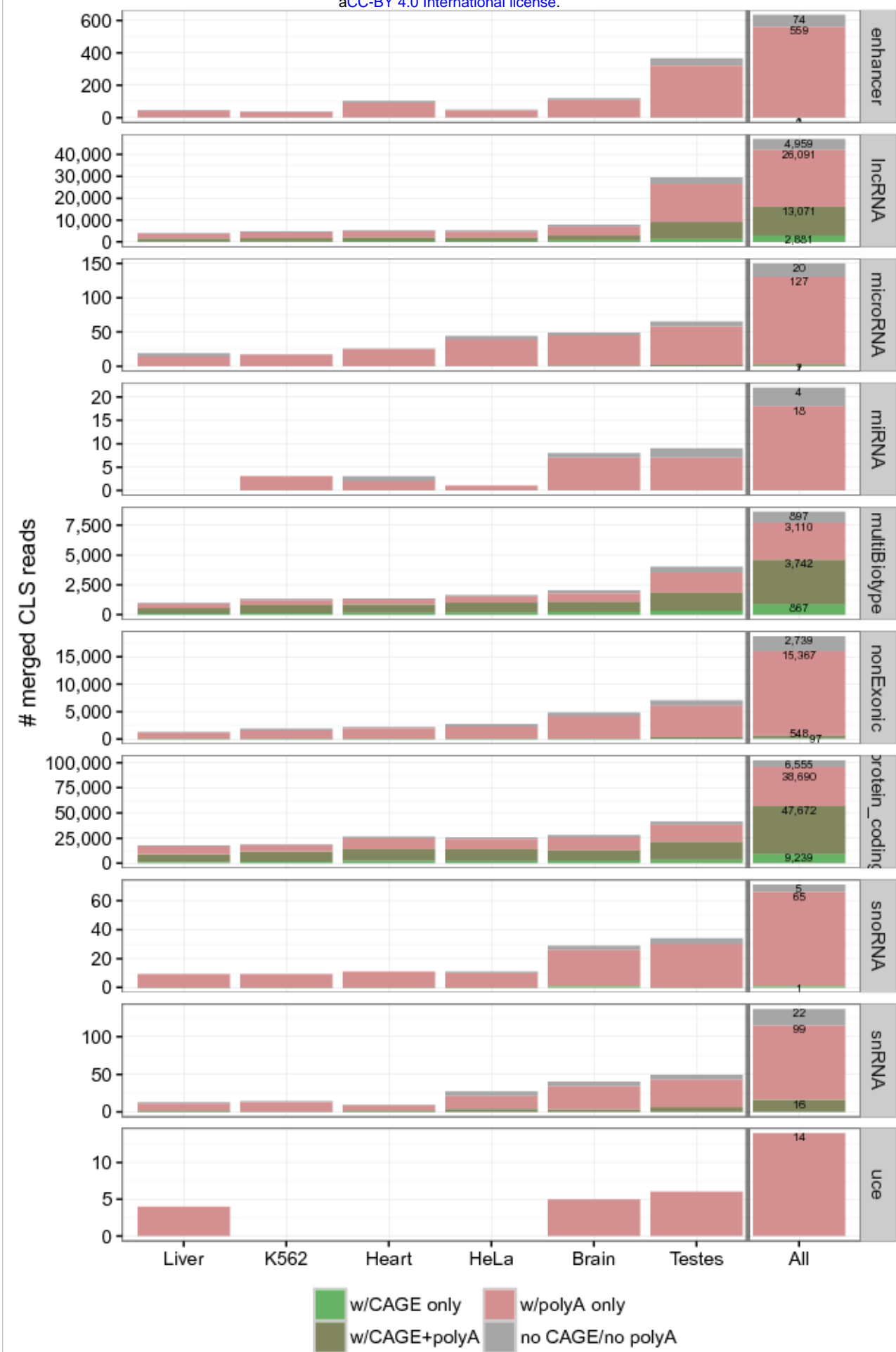


D



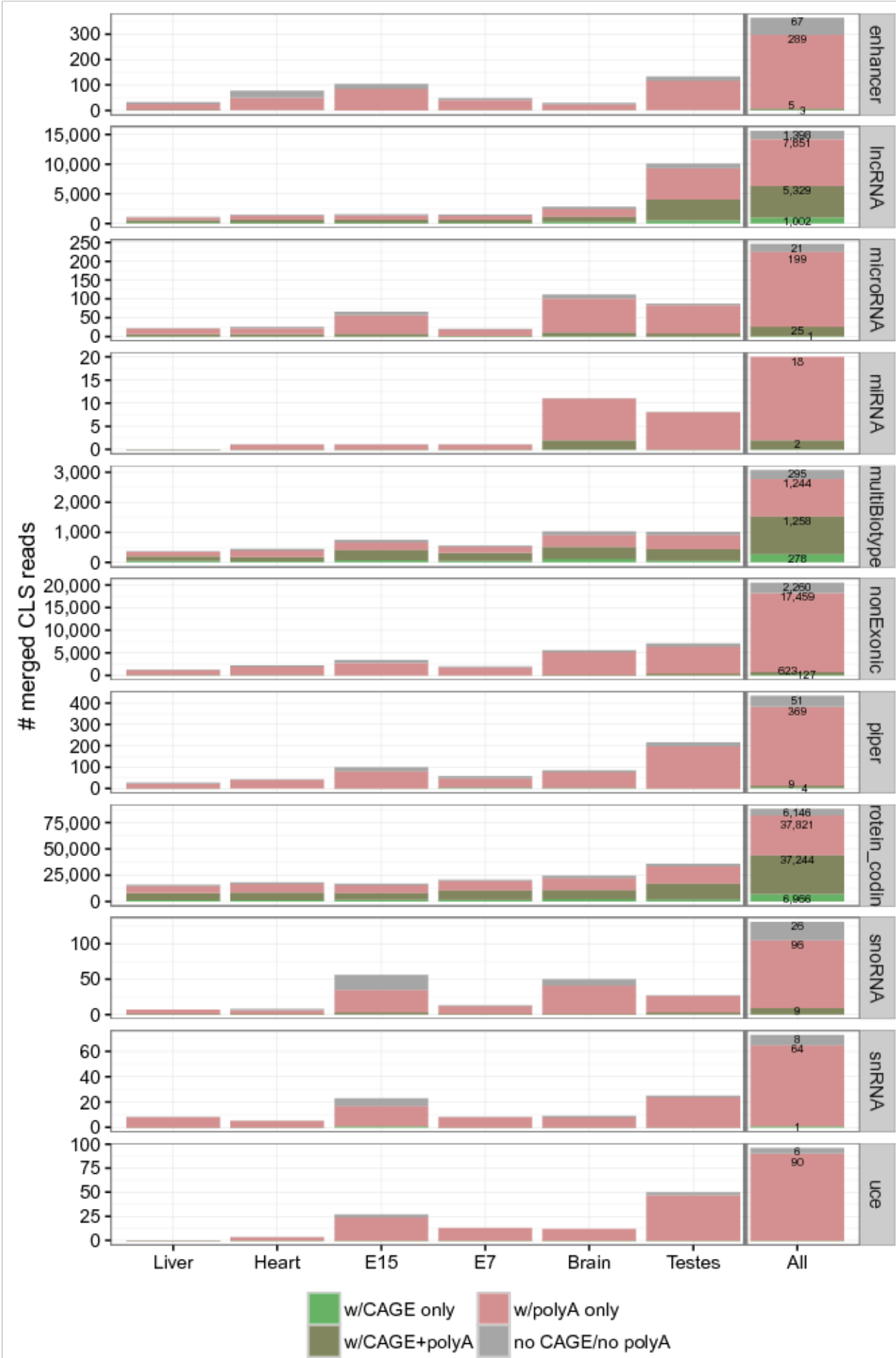
Supplementary Figure S31

bioRxiv preprint doi: <https://doi.org/10.1101/105064>; this version posted June 16, 2017. The copyright holder for this preprint (which was not certified by peer review) is the author/funder, who has granted bioRxiv a license to display the preprint in perpetuity. It is made available under aCC-BY 4.0 International license.



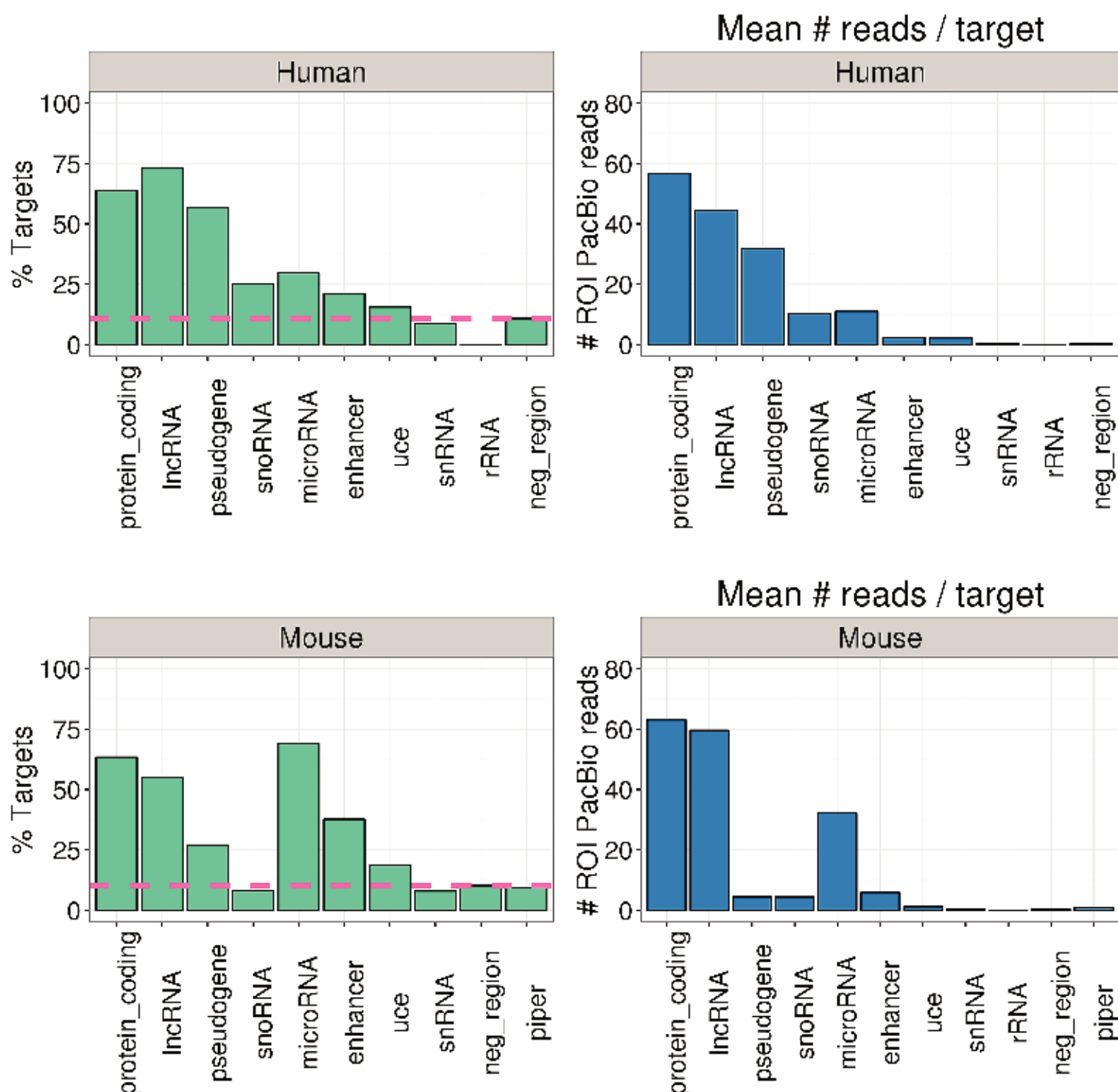
Supplementary Figure S32

bioRxiv preprint doi: <https://doi.org/10.1101/105064>; this version posted June 16, 2017. The copyright holder for this preprint (which was not certified by peer review) is the author/funder, who has granted bioRxiv a license to display the preprint in perpetuity. It is made available under aCC-BY 4.0 International license.



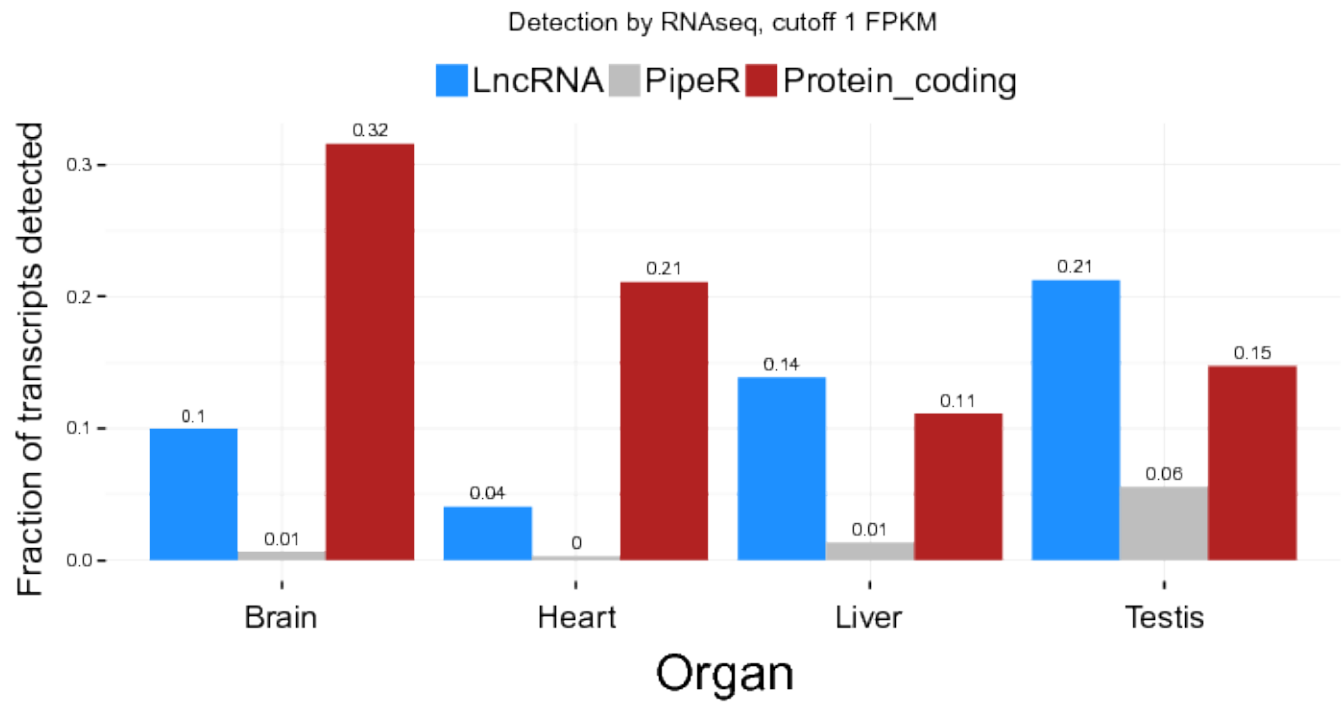
Supplementary Figure S33

bioRxiv preprint doi: <https://doi.org/10.1101/105064>; this version posted June 16, 2017. The copyright holder for this preprint (which was not certified by peer review) is the author/funder, who has granted bioRxiv a license to display the preprint in perpetuity. It is made available under aCC-BY 4.0 International license.



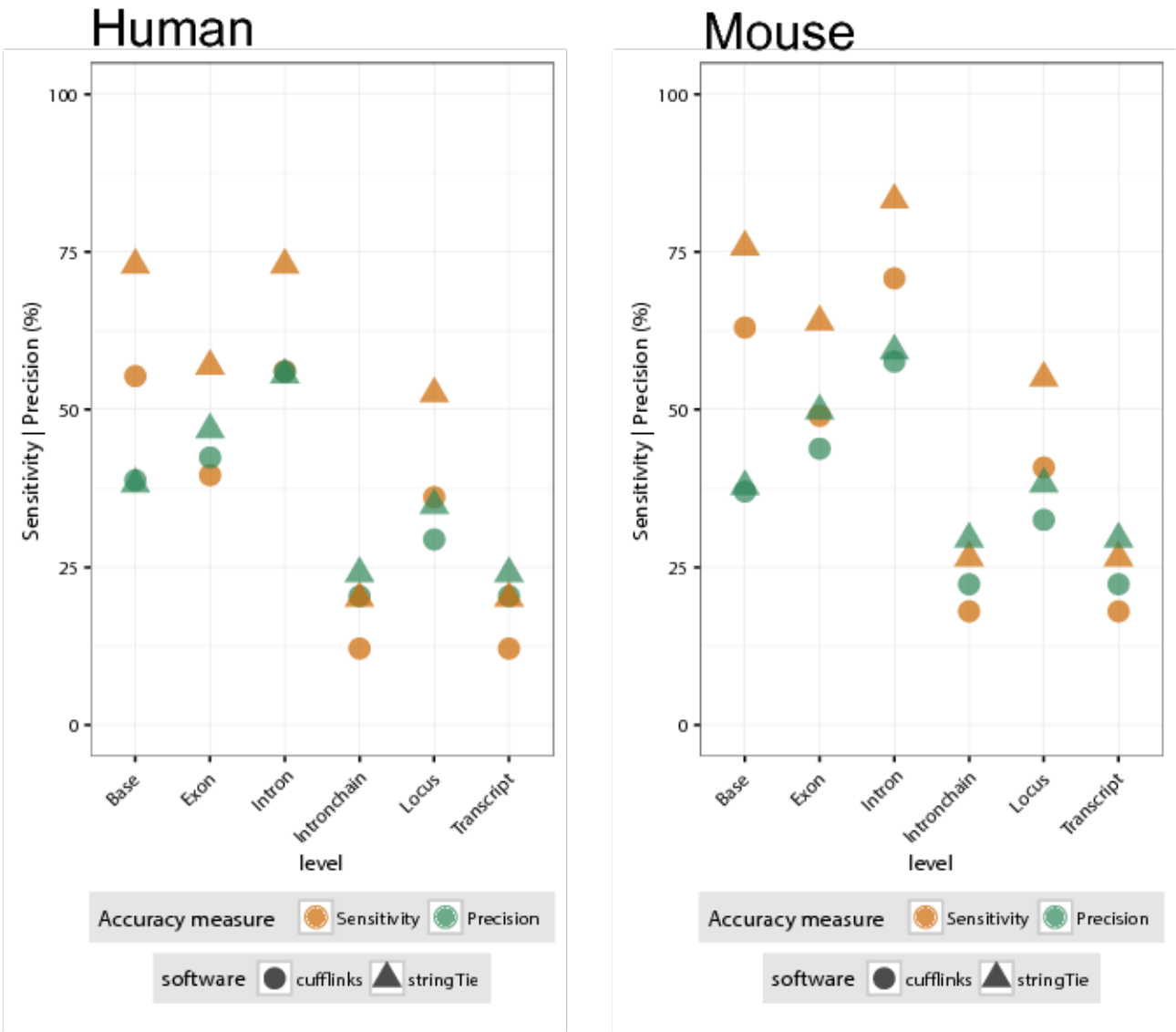
Supplementary Figure S34

bioRxiv preprint doi: <https://doi.org/10.1101/105064>; this version posted June 16, 2017. The copyright holder for this preprint (which was not certified by peer review) is the author/funder, who has granted bioRxiv a license to display the preprint in perpetuity. It is made available under aCC-BY 4.0 International license.



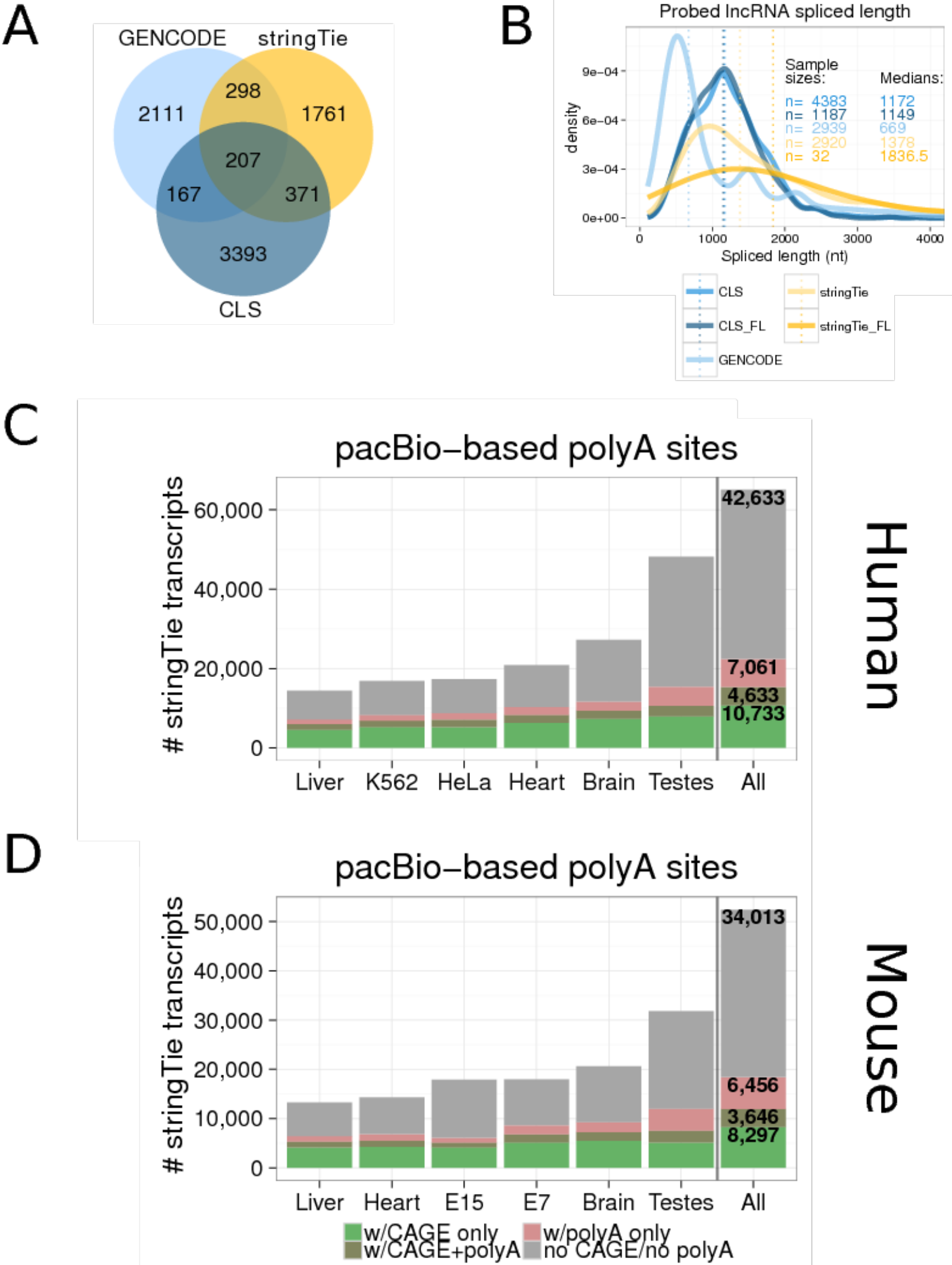
Supplementary Figure S35

bioRxiv preprint doi: <https://doi.org/10.1101/105064>; this version posted June 16, 2017. The copyright holder for this preprint (which was not certified by peer review) is the author/funder, who has granted bioRxiv a license to display the preprint in perpetuity. It is made available under aCC-BY 4.0 International license.



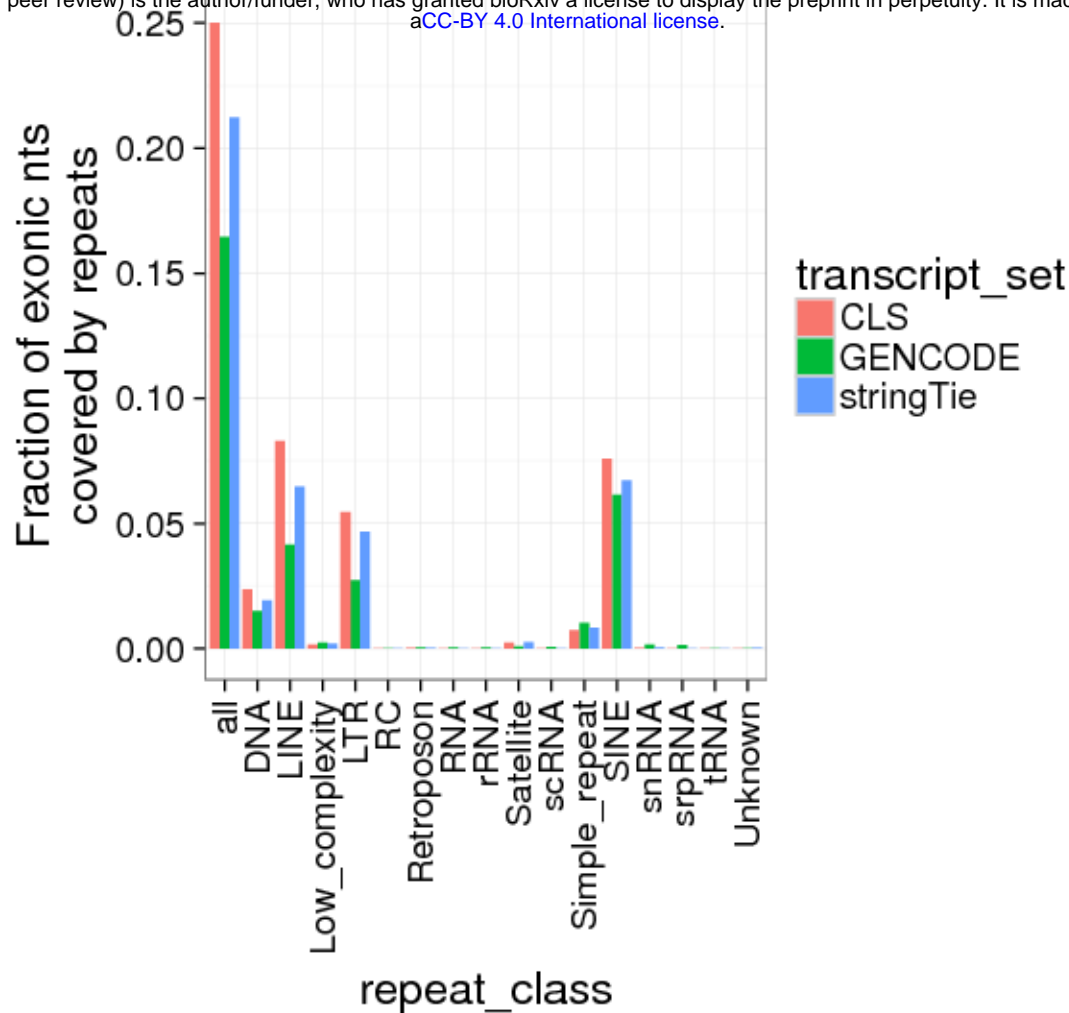
Supplementary Figure S36

bioRxiv preprint doi: <https://doi.org/10.1101/105064>; this version posted June 16, 2017. The copyright holder for this preprint (which was not certified by peer review) is the author/funder, who has granted bioRxiv a license to display the preprint in perpetuity. It is made available under aCC-BY 4.0 International license.

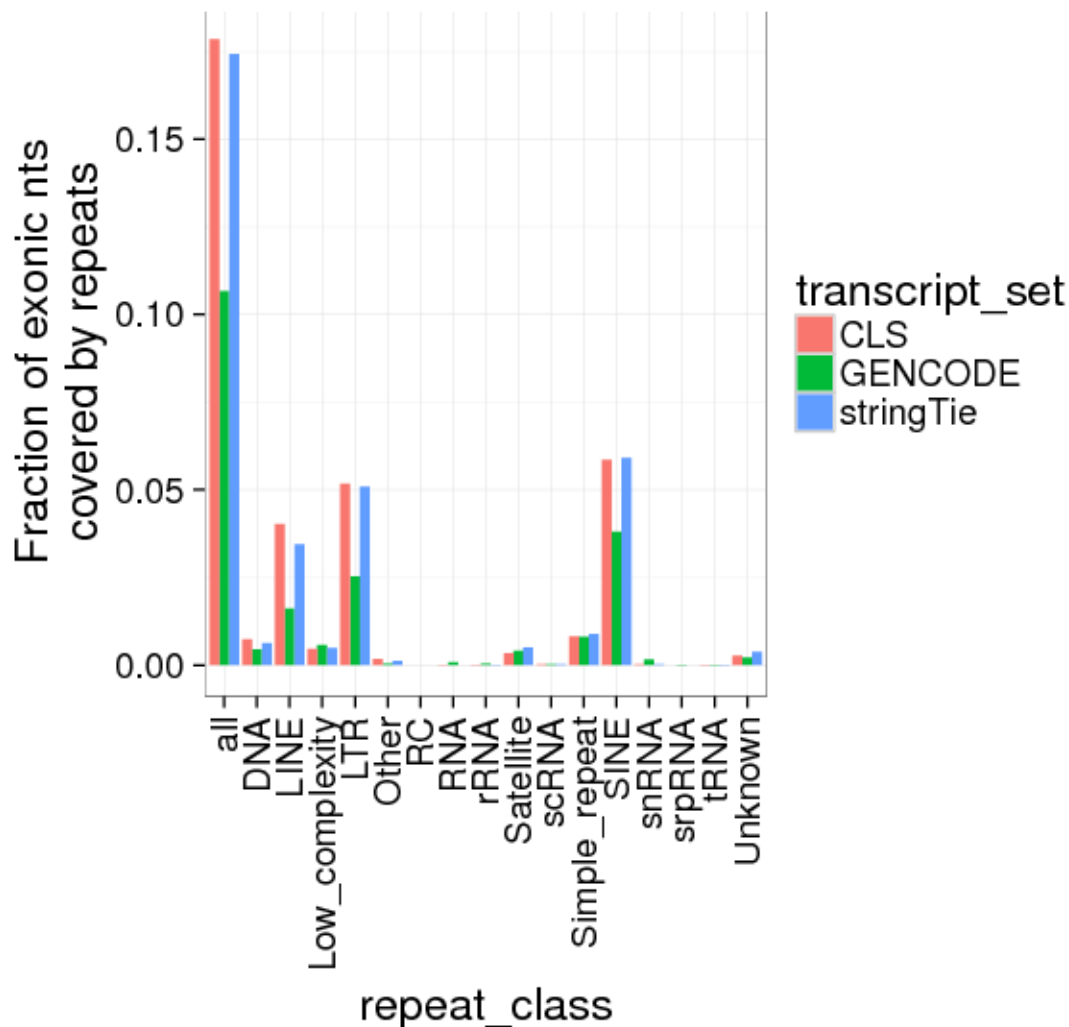


Supplementary Figure S37

bioRxiv preprint doi: <https://doi.org/10.1101/105064>; this version posted June 16, 2017. The copyright holder for this preprint (which was not certified by peer review) is the author/funder, who has granted bioRxiv a license to display the preprint in perpetuity. It is made available under aCC-BY 4.0 International license.



Human

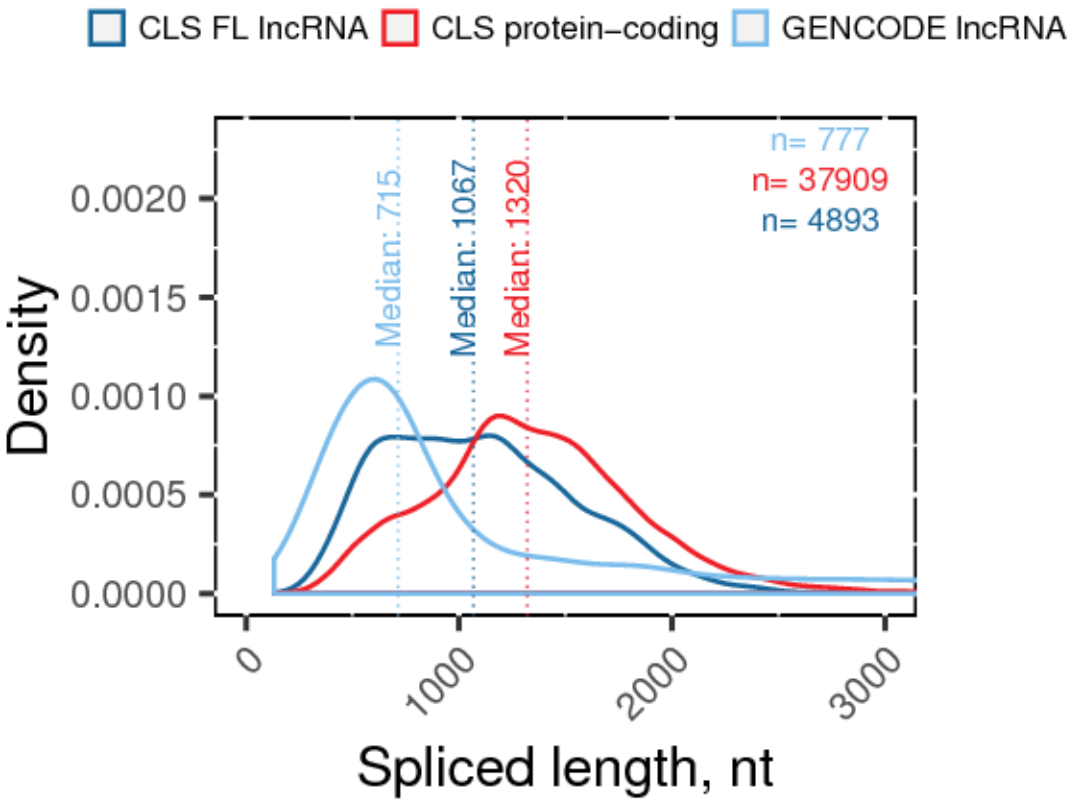


Mouse

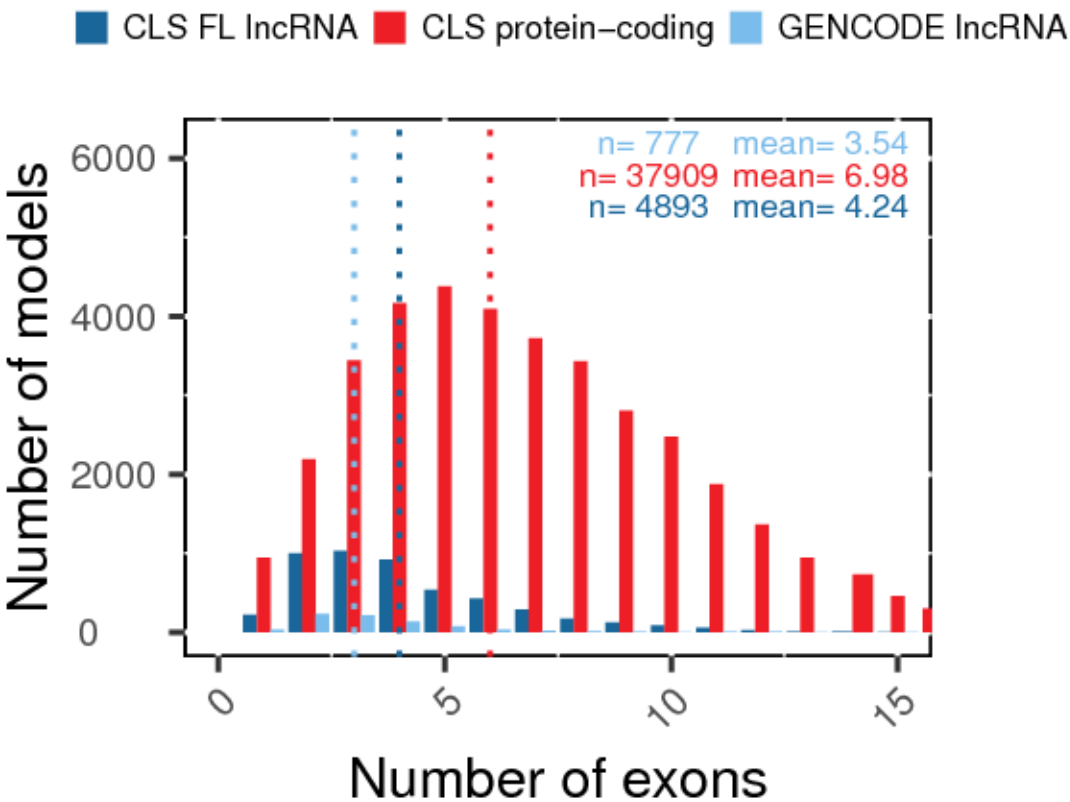
Supplementary Figure S38

bioRxiv preprint doi: <https://doi.org/10.1101/105064>; this version posted June 16, 2017. The copyright holder for this preprint (which was not certified by peer review) is the author/funder, who has granted bioRxiv a license to display the preprint in perpetuity. It is made available under aCC-BY 4.0 International license.

A

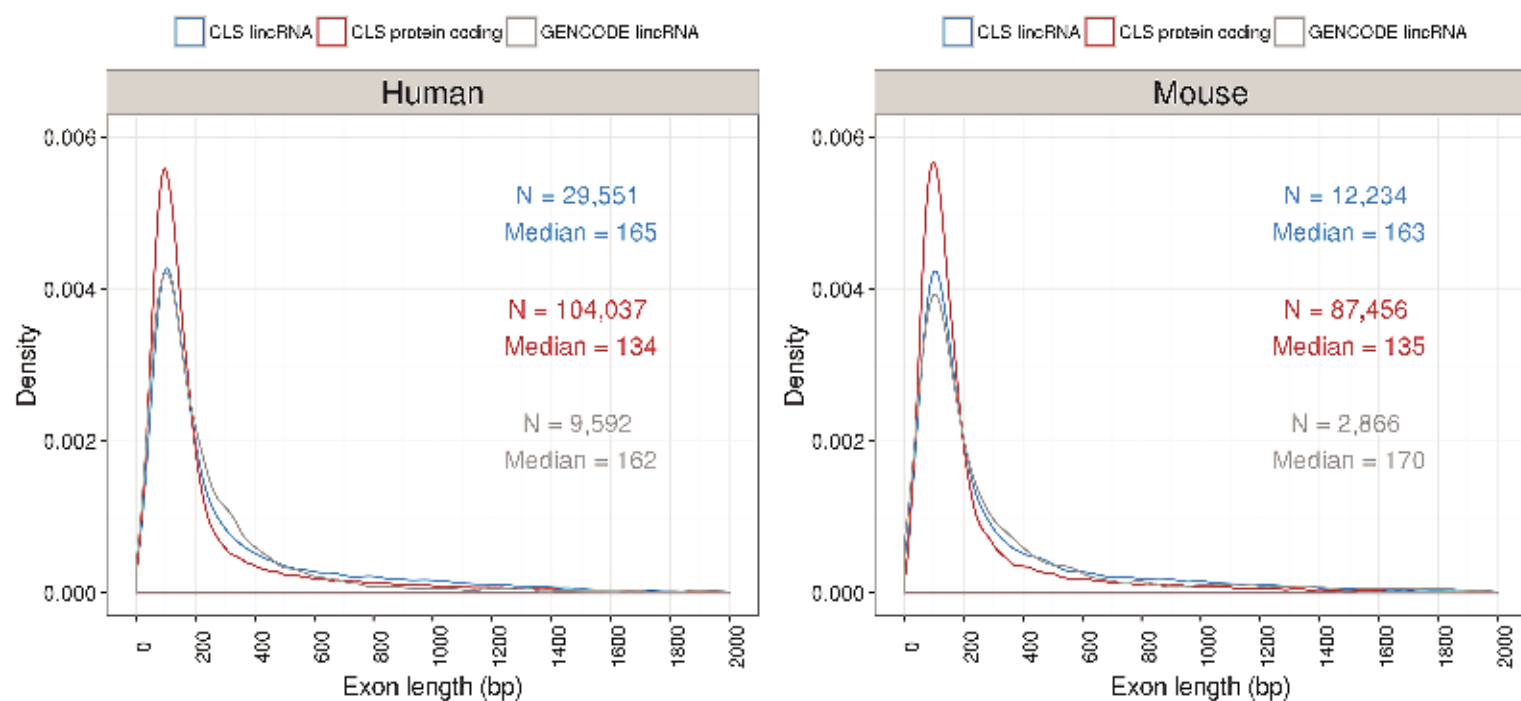


B



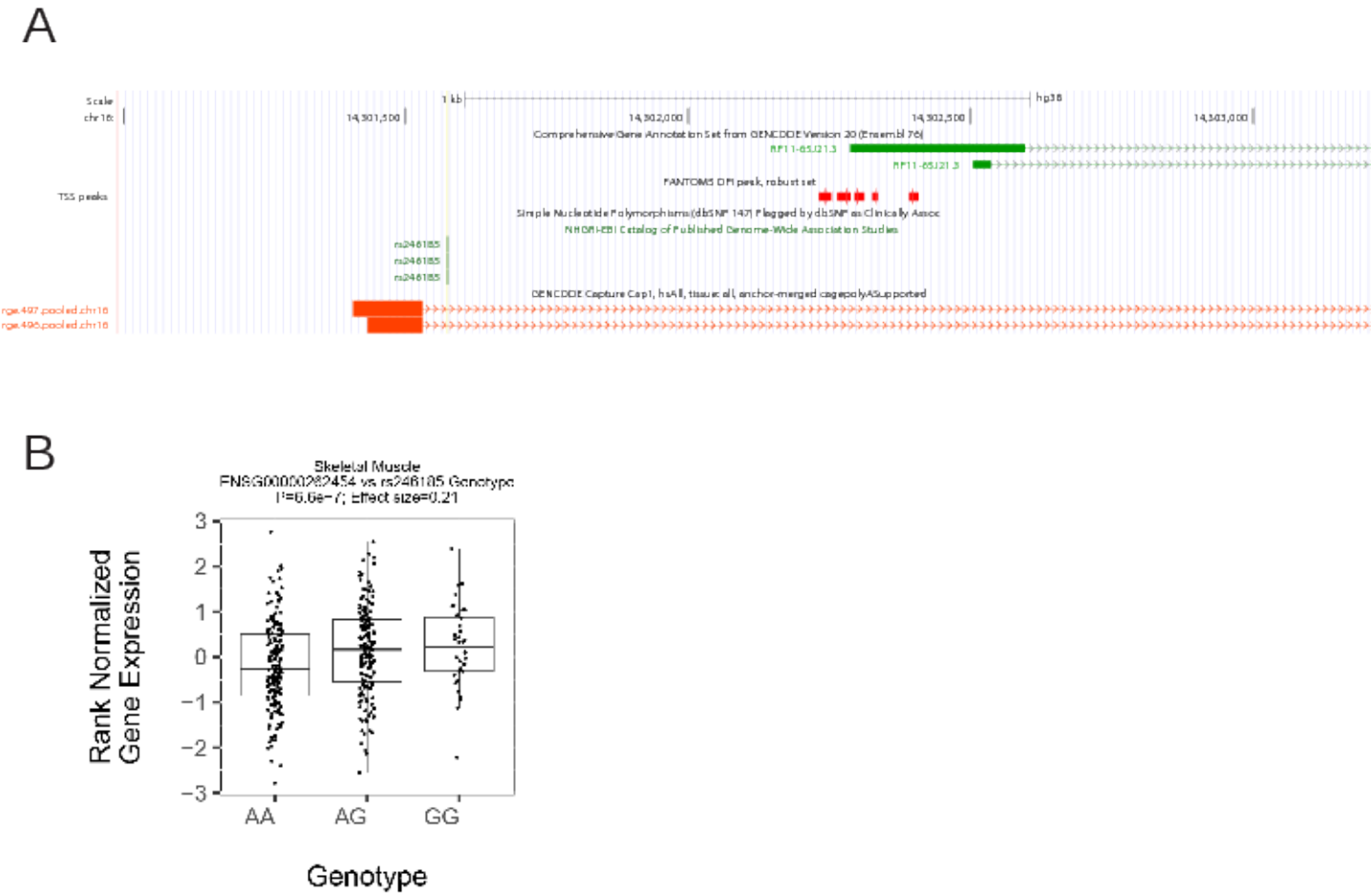
Supplementary Figure S39

bioRxiv preprint doi: <https://doi.org/10.1101/105064>; this version posted June 16, 2017. The copyright holder for this preprint (which was not certified by peer review) is the author/funder, who has granted bioRxiv a license to display the preprint in perpetuity. It is made available under aCC-BY 4.0 International license.



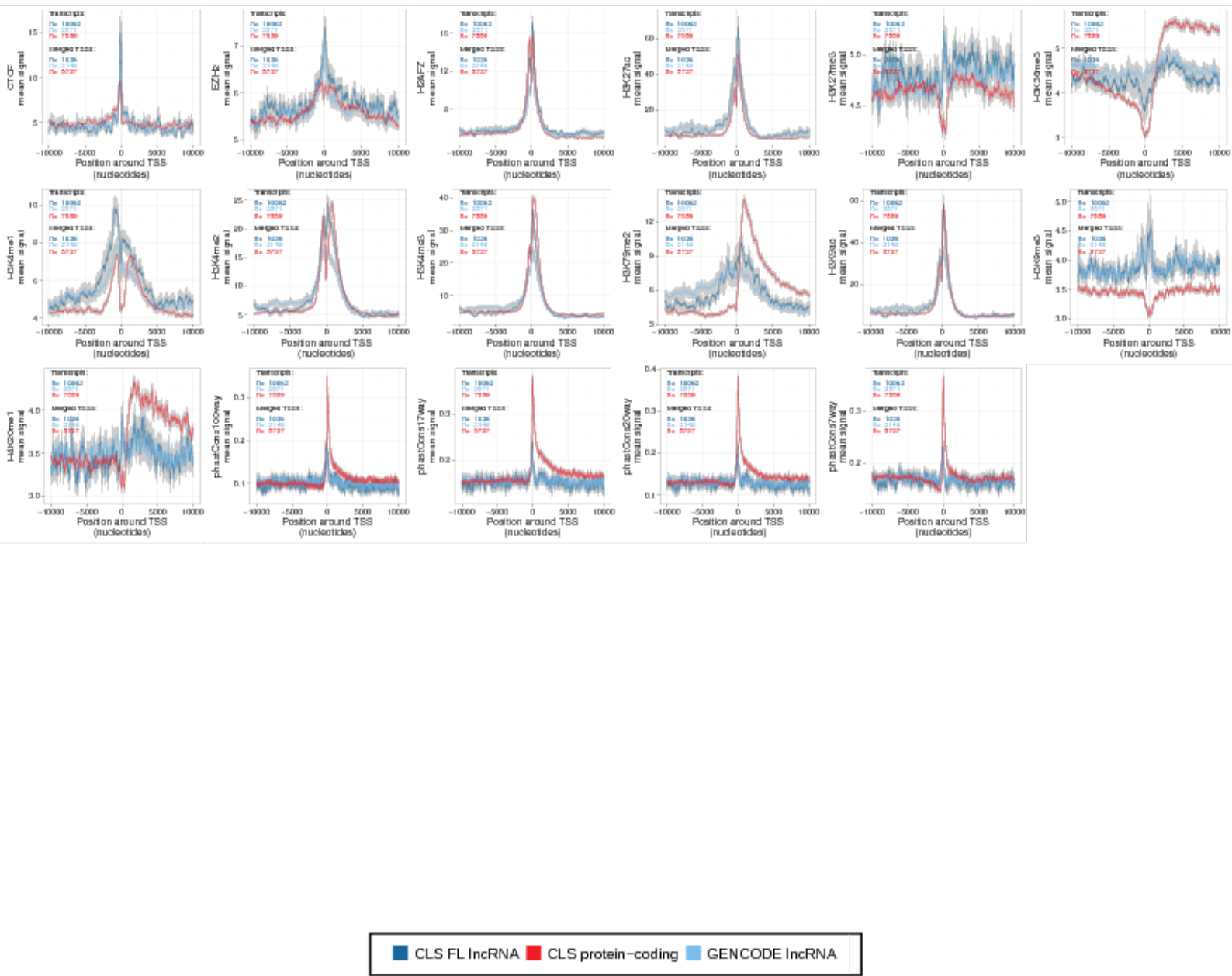
Supplementary Figure S40

bioRxiv preprint doi: <https://doi.org/10.1101/105064>; this version posted June 16, 2017. The copyright holder for this preprint (which was not certified by peer review) is the author/funder, who has granted bioRxiv a license to display the preprint in perpetuity. It is made available under aCC-BY 4.0 International license.



Supplementary Figure S41

bioRxiv preprint doi: <https://doi.org/10.1101/105064>; this version posted June 16, 2017. The copyright holder for this preprint (which was not certified by peer review) is the author/funder, who has granted bioRxiv a license to display the preprint in perpetuity. It is made available under aCC-BY 4.0 International license.

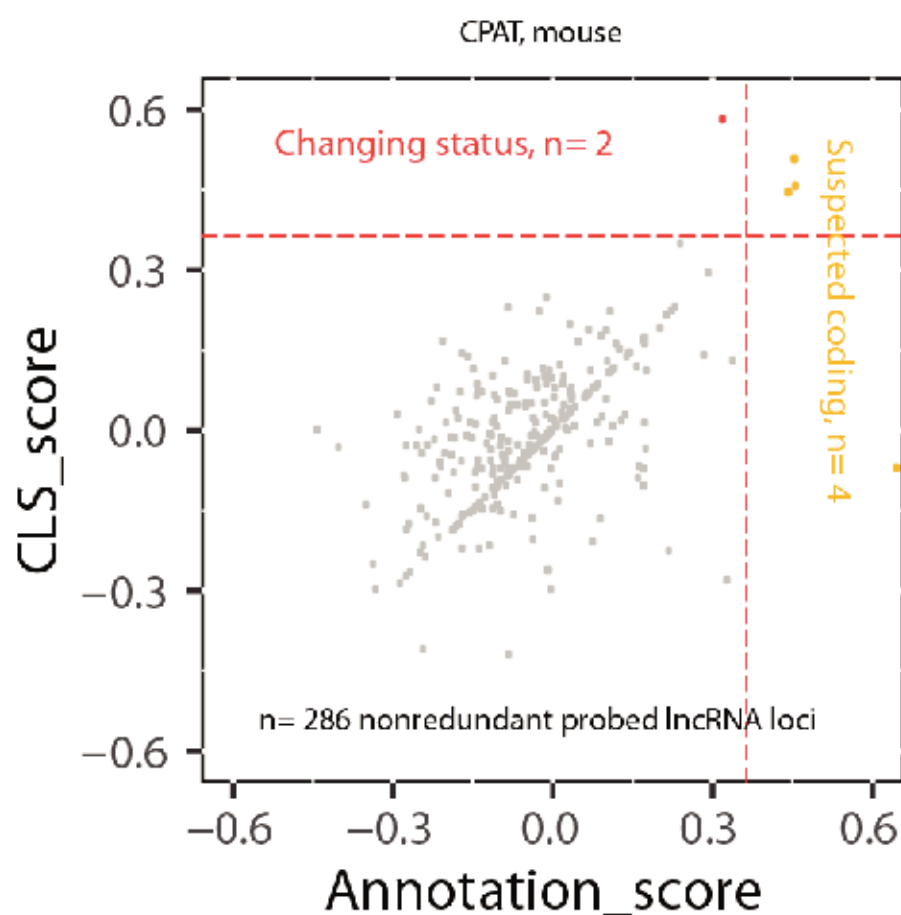
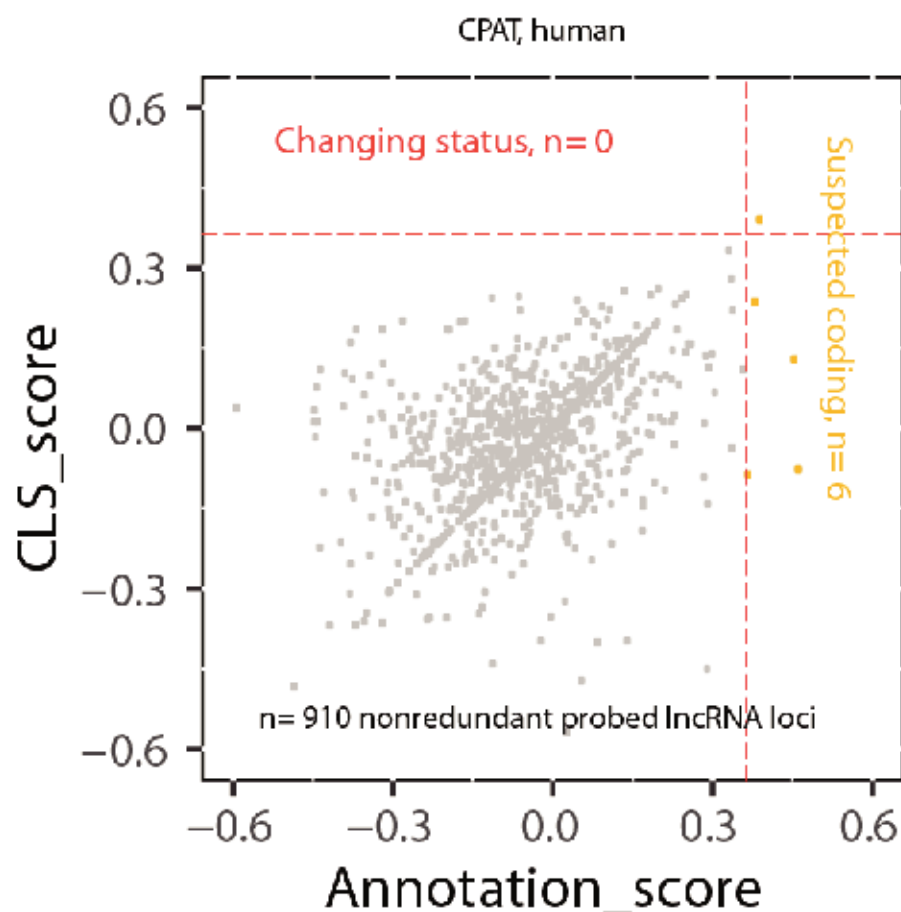


bioRxiv preprint doi: <https://doi.org/10.1101/105064>; this version posted June 16, 2017. The copyright holder for this preprint (which was not certified by peer review) is the author/funder, who has granted bioRxiv a license to display the preprint in perpetuity. It is made available under aCC-BY 4.0 International license.



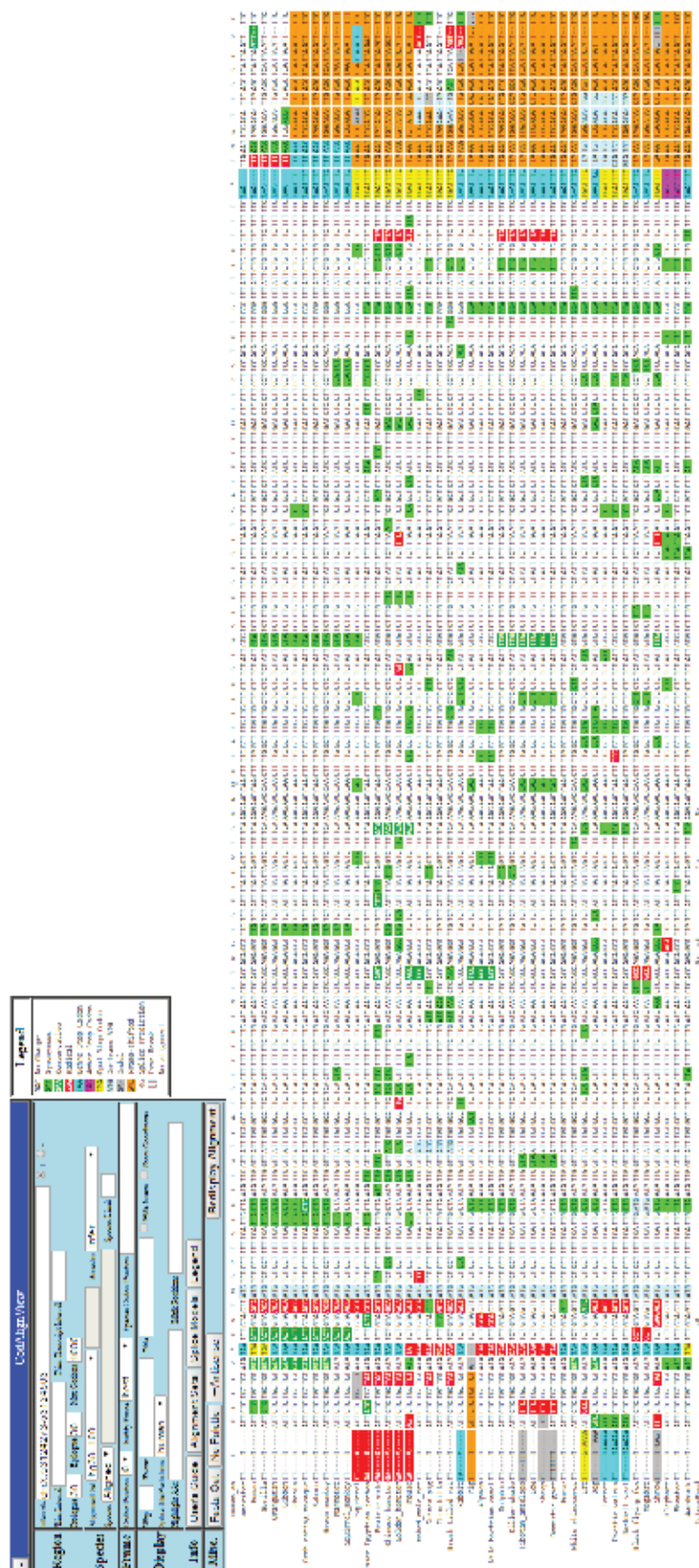
Supplementary Figure S43

bioRxiv preprint doi: <https://doi.org/10.1101/105064>; this version posted June 16, 2017. The copyright holder for this preprint (which was not certified by peer review) is the author/funder, who has granted bioRxiv a license to display the preprint in perpetuity. It is made available under aCC-BY 4.0 International license.



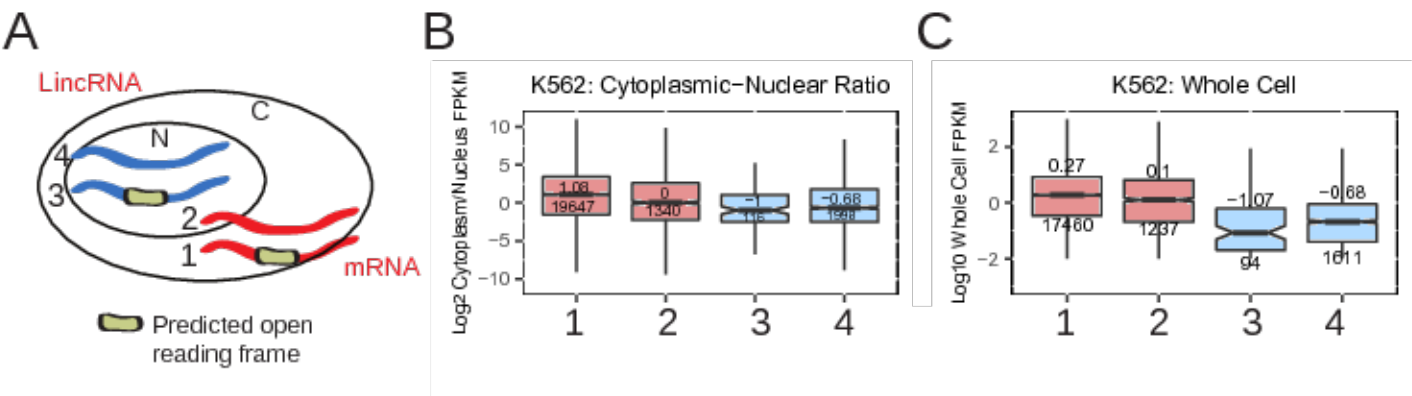
Supplementary Figure S44

bioRxiv preprint doi: <https://doi.org/10.1101/105064>; this version posted June 16, 2017. The copyright holder for this preprint (which was not certified by peer review) is the author/funder, who has granted bioRxiv a license to display the preprint in perpetuity. It is made available under aCC-BY 4.0 International license.



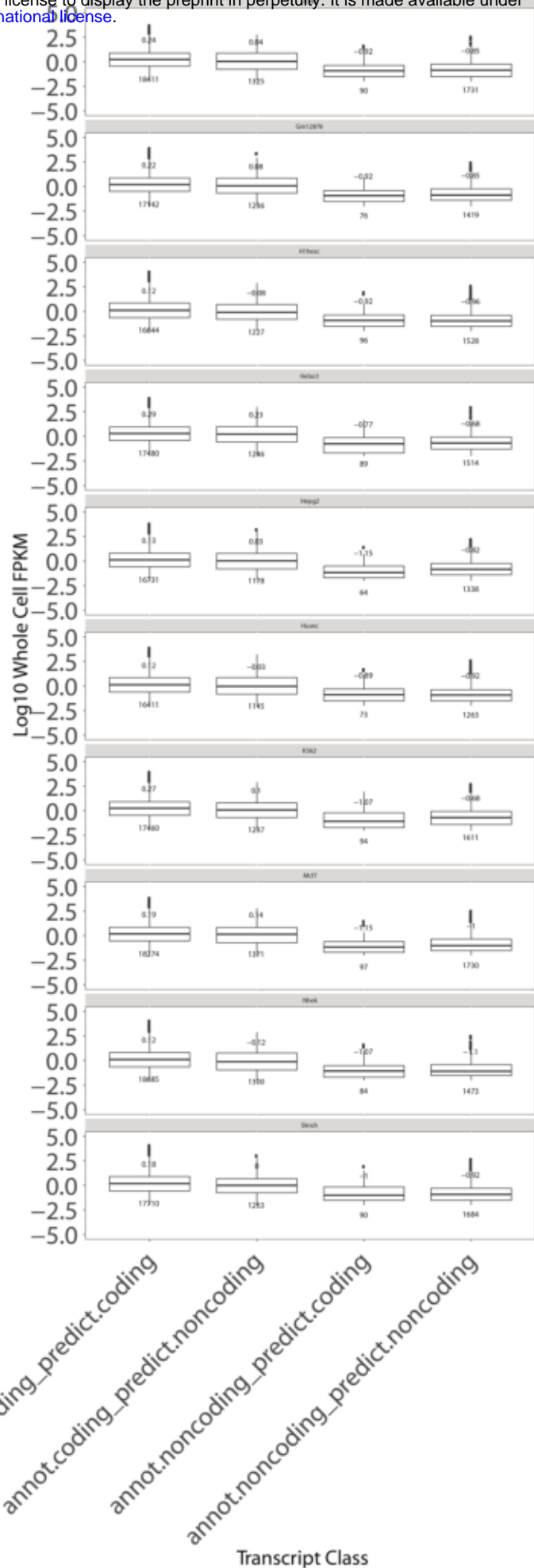
Supplementary Figure S45

bioRxiv preprint doi: <https://doi.org/10.1101/105064>; this version posted June 16, 2017. The copyright holder for this preprint (which was not certified by peer review) is the author/funder, who has granted bioRxiv a license to display the preprint in perpetuity. It is made available under aCC-BY 4.0 International license.



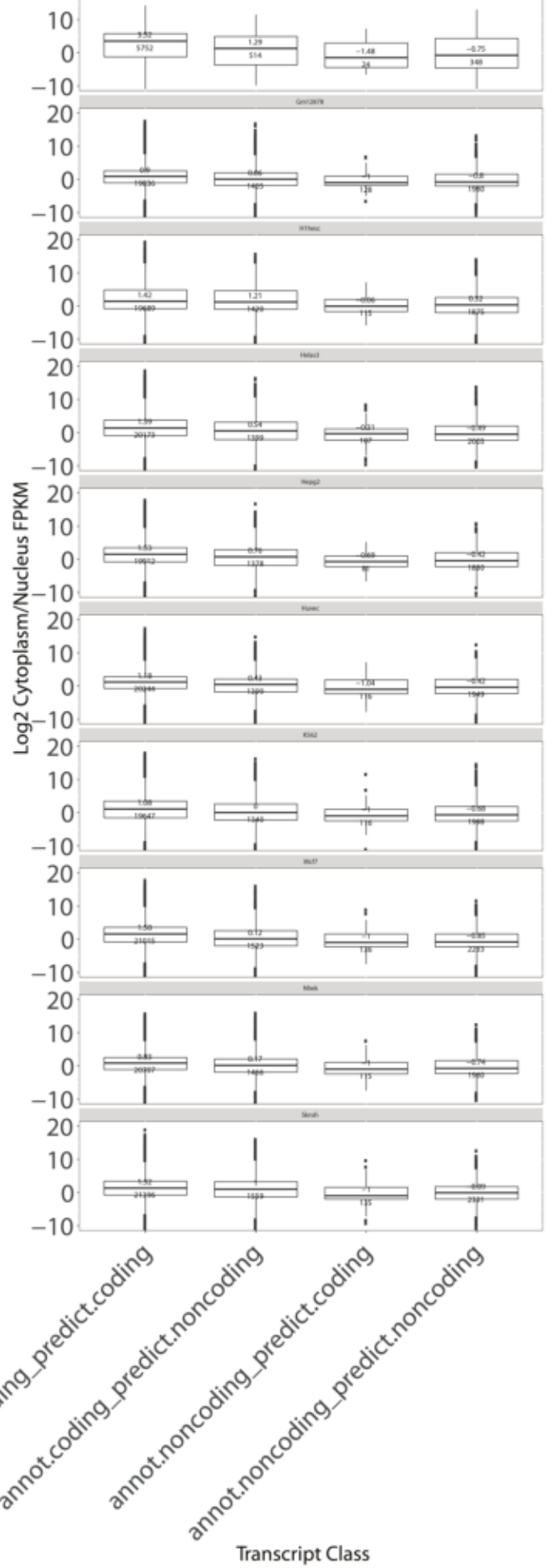
Supplementary Figure S46

bioRxiv preprint doi: <https://doi.org/10.1101/105064>; this version posted June 16, 2017. The copyright holder for this preprint (which was not certified by peer review) is the author/funder, who has granted bioRxiv a license to display the preprint in perpetuity. It is made available under aCC-BY 4.0 International license.



Supplementary Figure S47
 bioRxiv preprint doi: <https://doi.org/10.1101/105155>; this version posted November 10, 2016. The copyright holder for this preprint (which was not certified by peer review) is the author/funder, who has granted bioRxiv a license to display the preprint in perpetuity. It is made available under aCC-BY-NC-ND 4.0 International license.

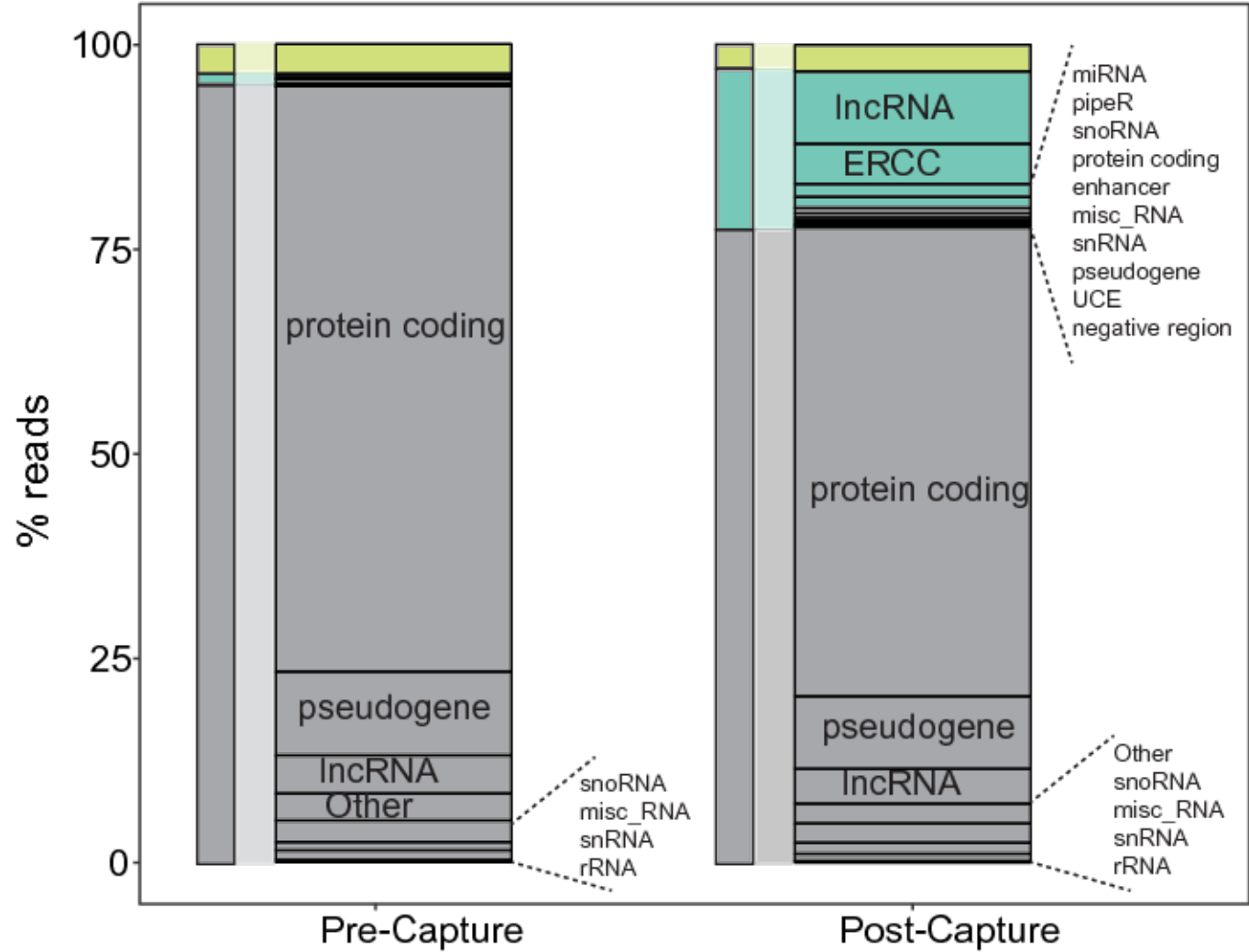
bioRxiv preprint doi: <https://doi.org/10.1101/105064>; this version posted June 16, 2017. The copyright holder for this preprint (which was not certified by peer review) is the author/funder, who has granted bioRxiv a license to display the preprint in perpetuity. It is made available under aCC-BY 4.0 International license.



Supplementary Figure S48

bioRxiv preprint doi: <https://doi.org/10.1101/105064>; this version posted June 16, 2017. The copyright holder for this preprint (which was not certified by peer review) is the author/funder, who has granted bioRxiv a license to display the preprint in perpetuity. It is made available under aCC-BY 4.0 International license.

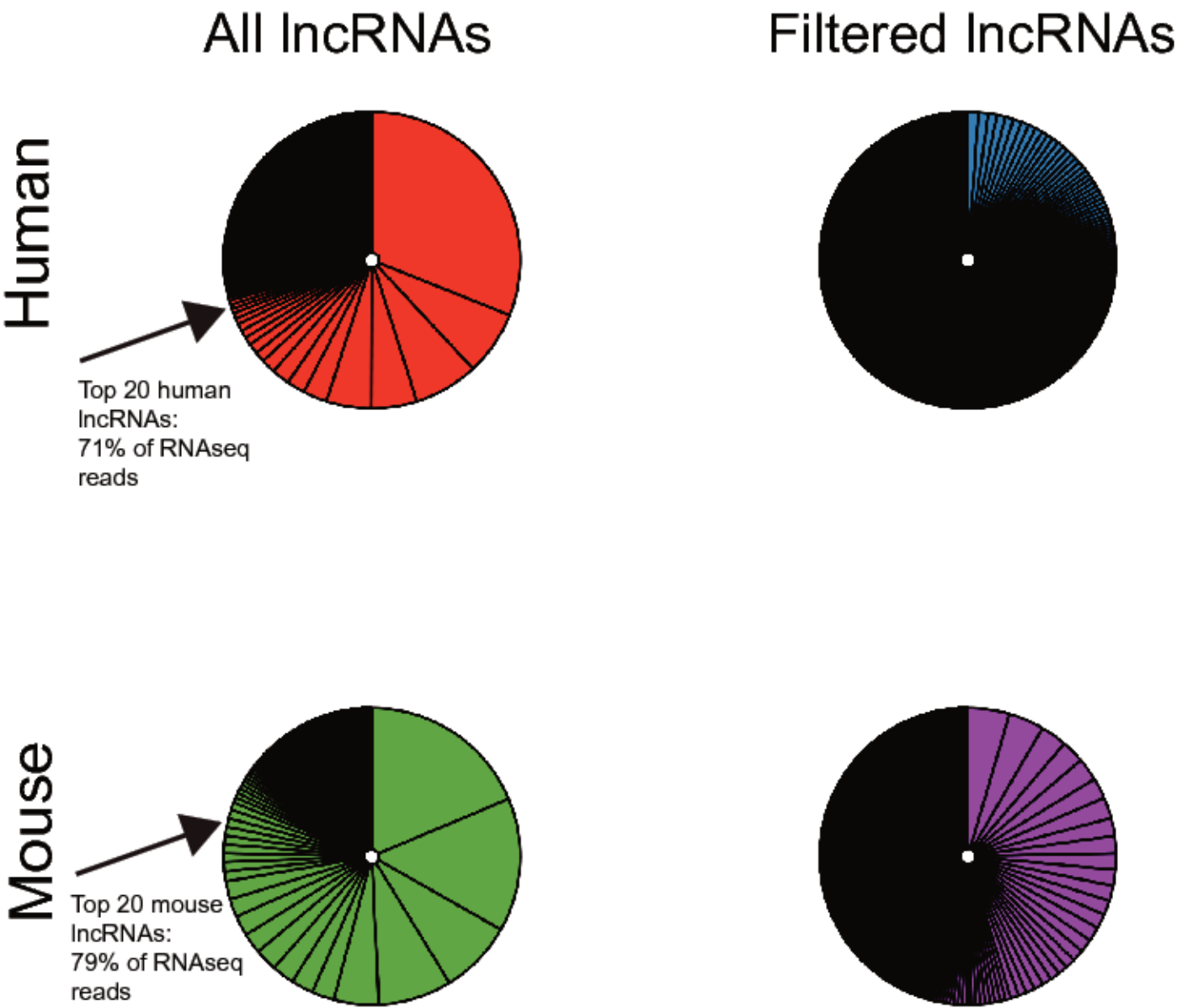
Mouse



Supplementary Figure S49

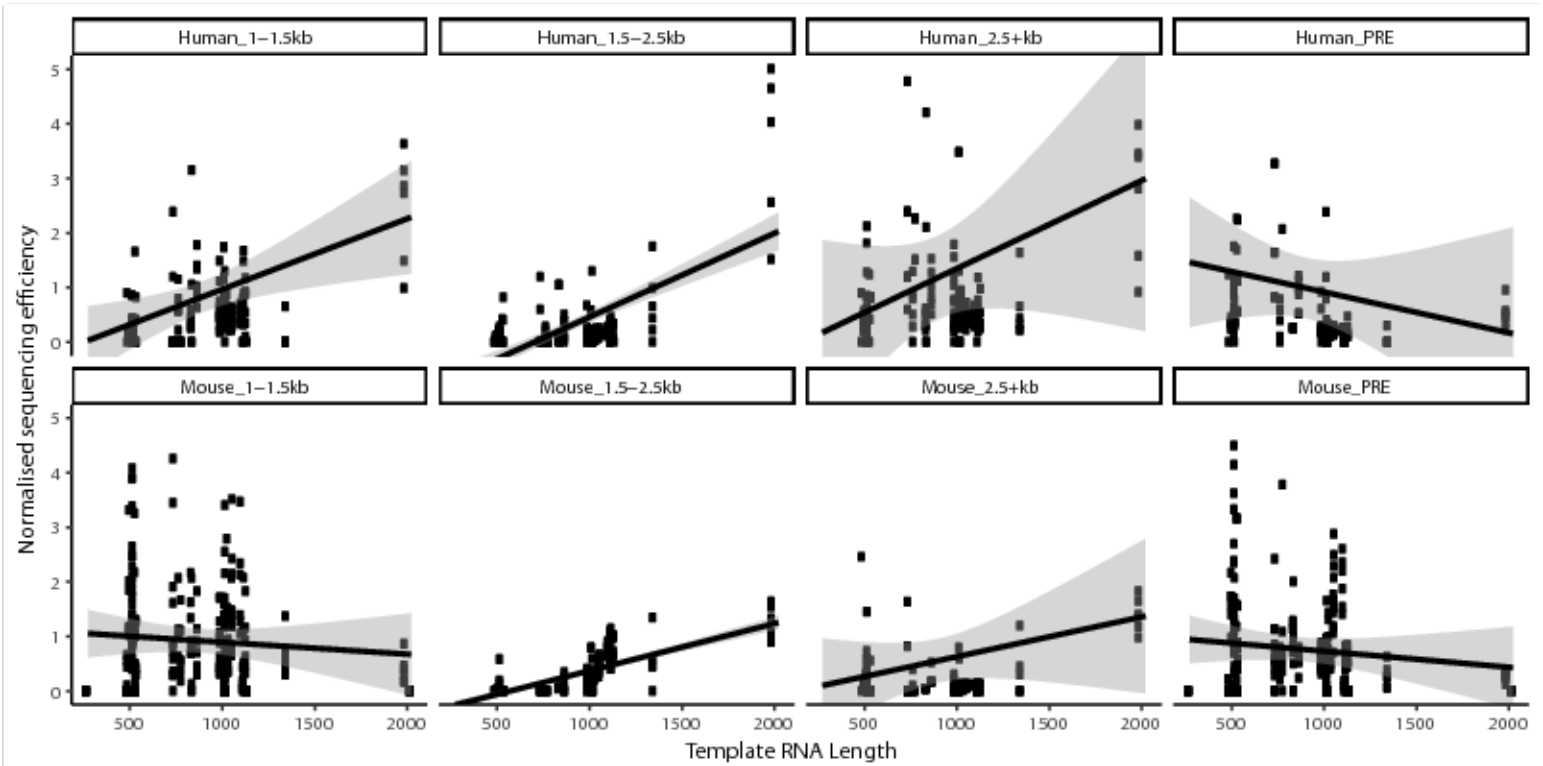
bioRxiv preprint doi: <https://doi.org/10.1101/105064>; this version posted June 16, 2017. The copyright holder for this preprint (which was not certified by peer review) is the author/funder, who has granted bioRxiv a license to display the preprint in perpetuity. It is made available under aCC-BY 4.0 International license.

Mapped Illumina RNAseq reads



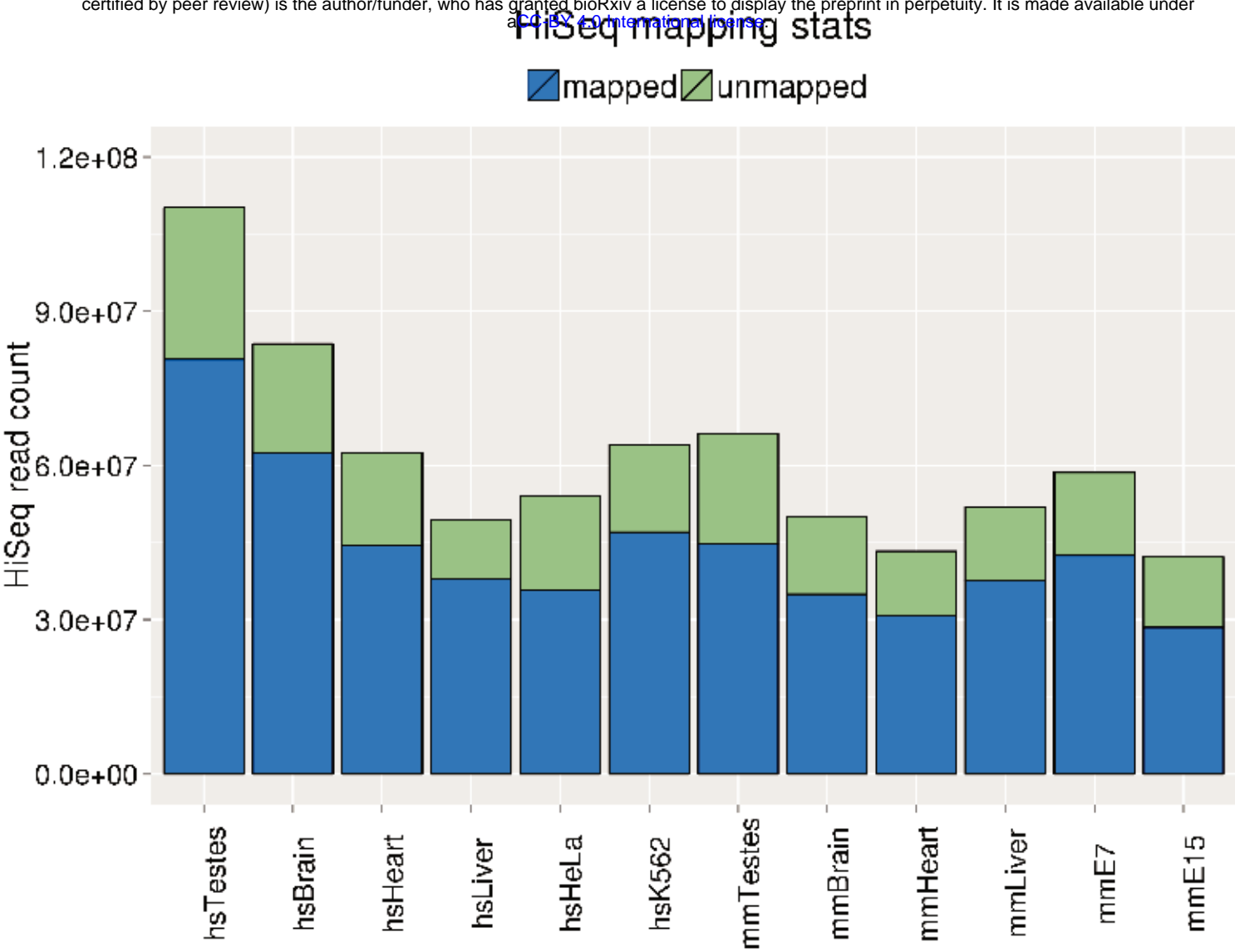
Supplementary Figure S50

bioRxiv preprint doi: <https://doi.org/10.1101/105064>; this version posted June 16, 2017. The copyright holder for this preprint (which was not certified by peer review) is the author/funder, who has granted bioRxiv a license to display the preprint in perpetuity. It is made available under aCC-BY 4.0 International license.



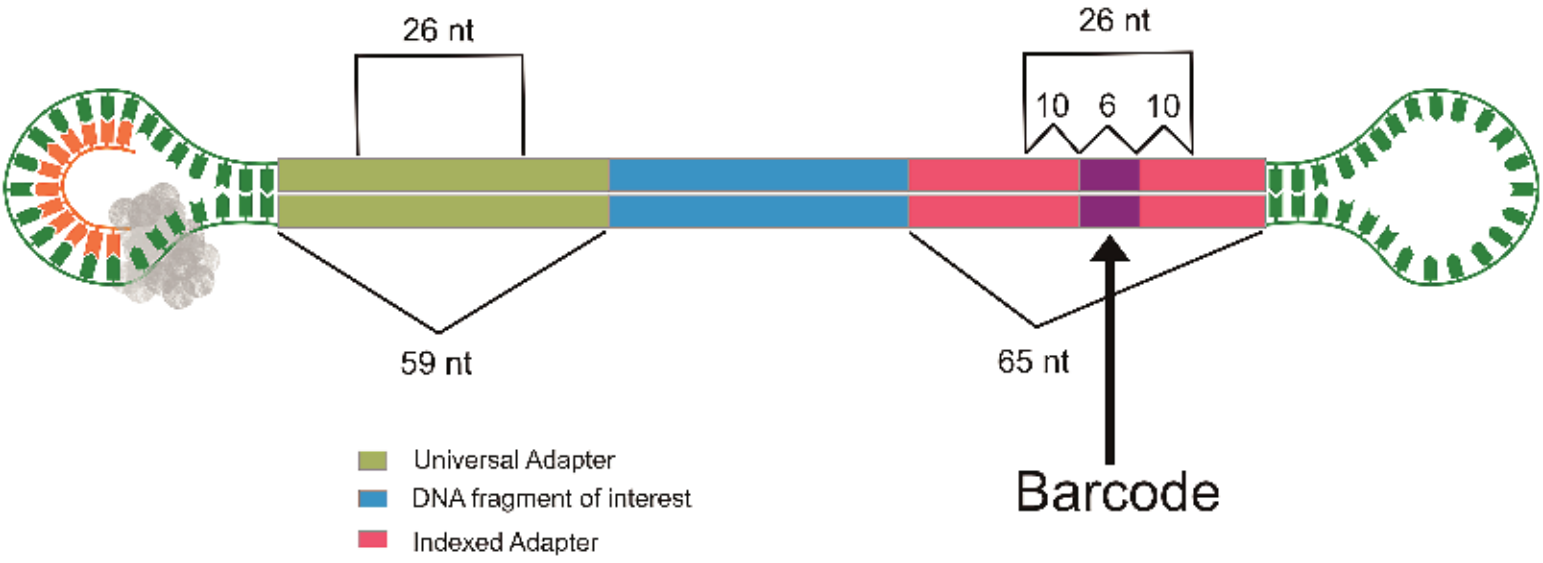
Supplementary Figure S51

bioRxiv preprint doi: <https://doi.org/10.1101/105064>; this version posted June 16, 2017. The copyright holder for this preprint (which was not certified by peer review) is the author/funder, who has granted bioRxiv a license to display the preprint in perpetuity. It is made available under aCC-BY 4.0 International license.



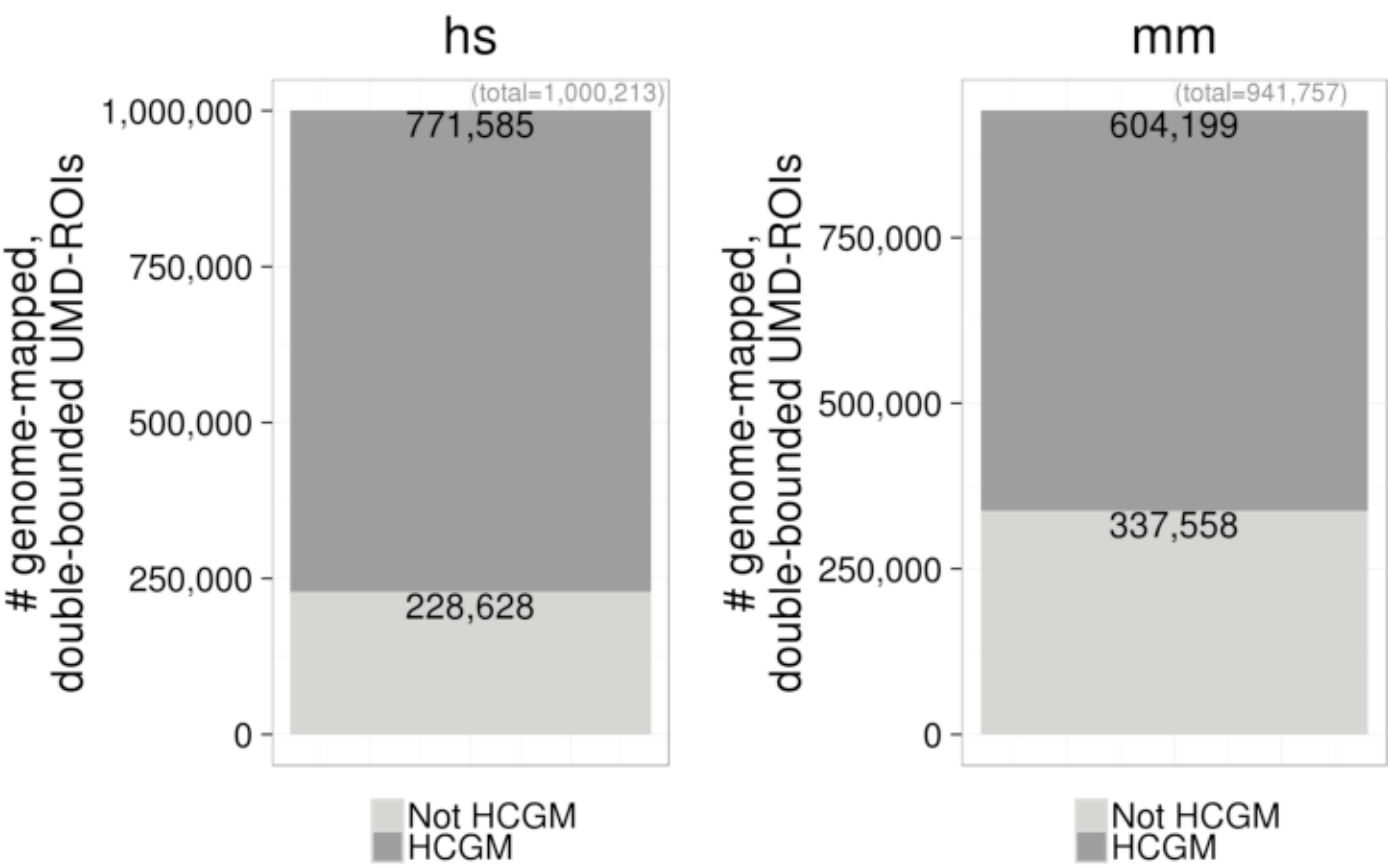
Supplementary Figure S52

bioRxiv preprint doi: <https://doi.org/10.1101/105064>; this version posted June 16, 2017. The copyright holder for this preprint (which was not certified by peer review) is the author/funder, who has granted bioRxiv a license to display the preprint in perpetuity. It is made available under aCC-BY 4.0 International license.



Supplementary Figure S53

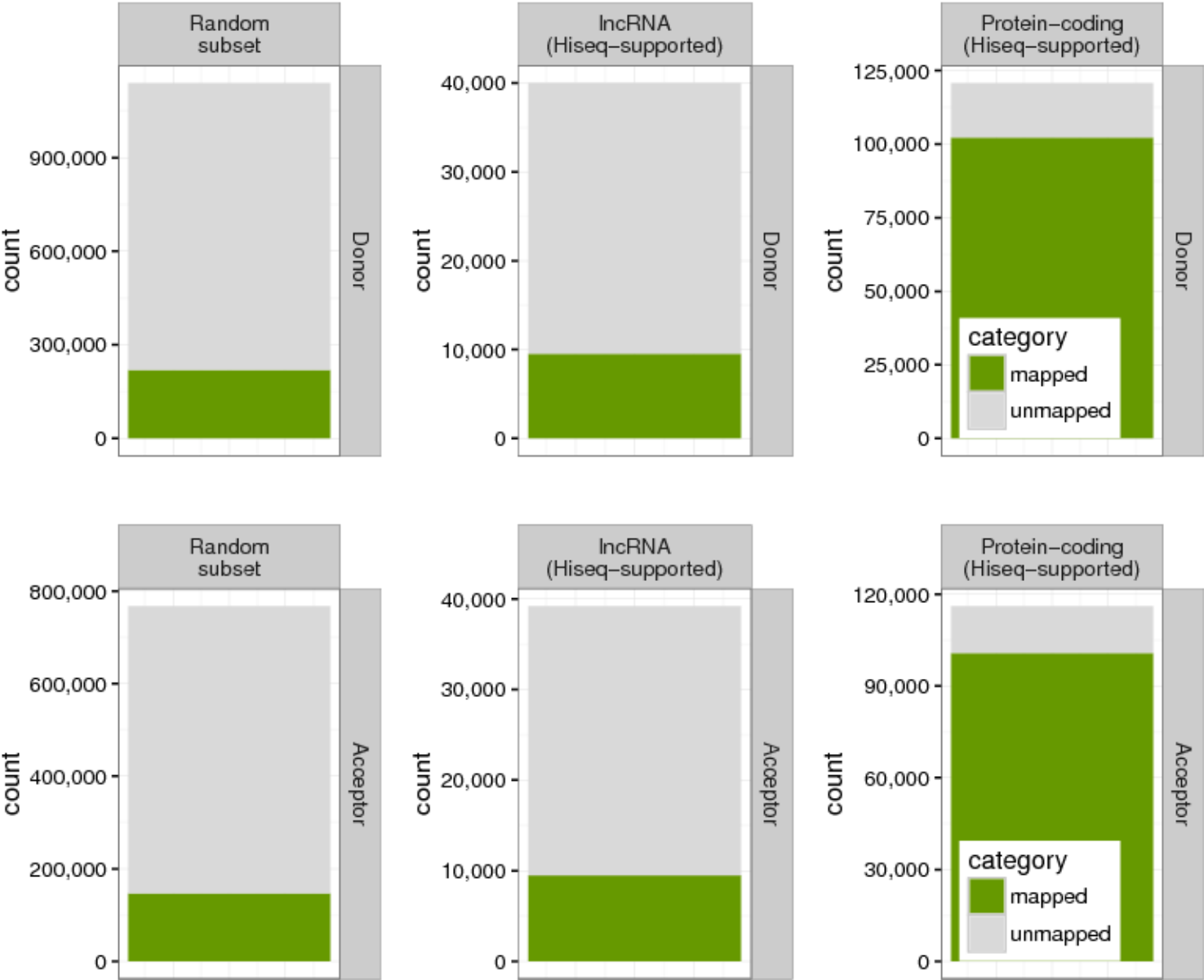
bioRxiv preprint doi: <https://doi.org/10.1101/105064>; this version posted June 16, 2017. The copyright holder for this preprint (which was not certified by peer review) is the author/funder, who has granted bioRxiv a license to display the preprint in perpetuity. It is made available under aCC-BY 4.0 International license.



Supplementary Figure S54

bioRxiv preprint doi: <https://doi.org/10.1101/105064>; this version posted June 16, 2017. The copyright holder for this preprint (which was not certified by peer review) is the author/funder, who has granted bioRxiv a license to display the preprint in perpetuity. It is made available under aCC-BY 4.0 International license.

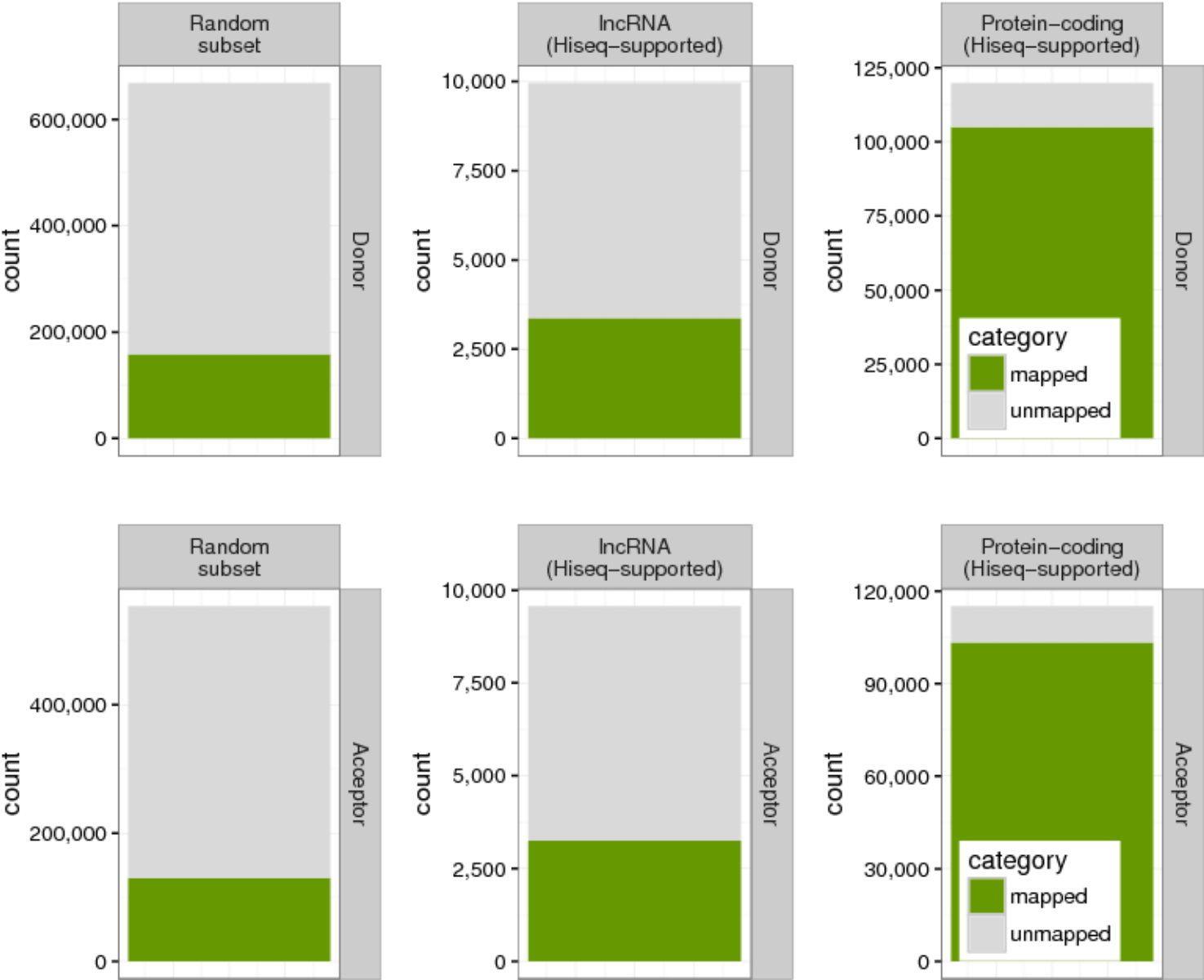
hg38 to mm10 splice site liftOver mappings stats



Supplementary Figure S55

bioRxiv preprint doi: <https://doi.org/10.1101/105064>; this version posted June 16, 2017. The copyright holder for this preprint (which was not certified by peer review) is the author/funder, who has granted bioRxiv a license to display the preprint in perpetuity. It is made available under aCC-BY 4.0 International license.

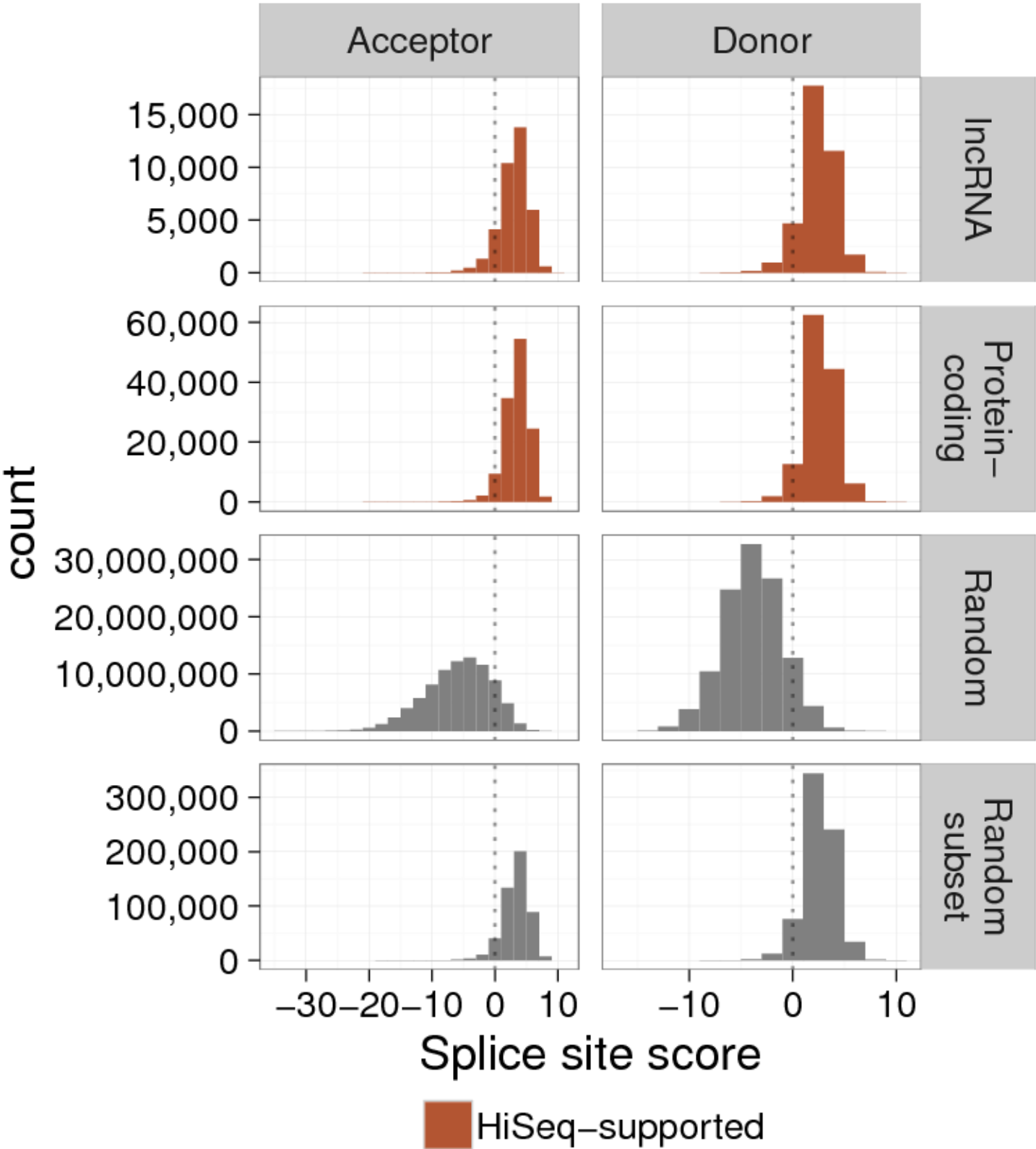
mm10 to hg38 splice site liftOver mappings stats



Supplementary Figure S56

bioRxiv preprint doi: <https://doi.org/10.1101/105064>; this version posted June 16, 2017. The copyright holder for this preprint (which was not certified by peer review) is the author/funder, who has granted bioRxiv a license to display the preprint in perpetuity. It is made available under aCC-BY 4.0 International license.

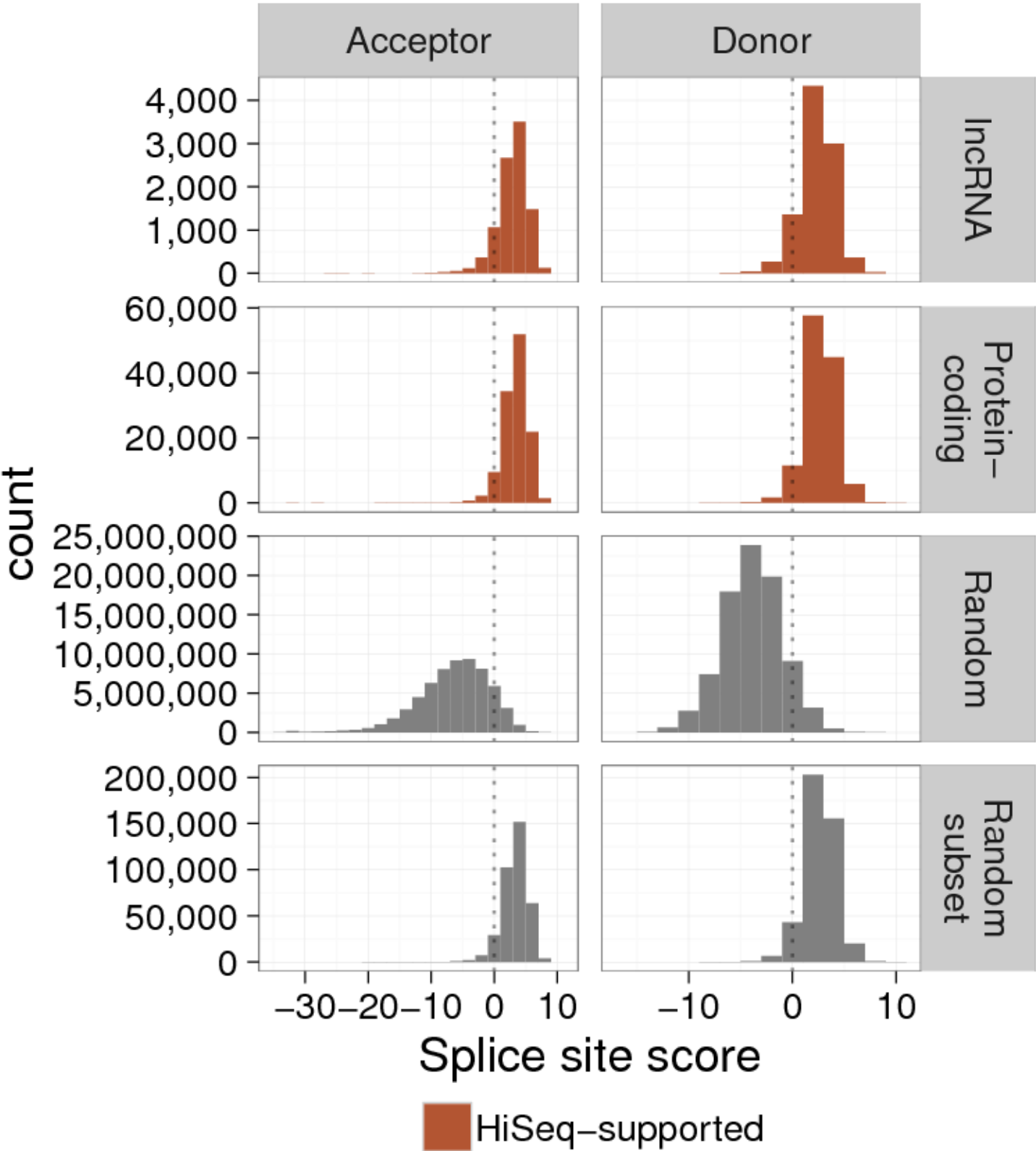
hs splice site scores



Supplementary Figure S57

bioRxiv preprint doi: <https://doi.org/10.1101/105064>; this version posted June 16, 2017. The copyright holder for this preprint (which was not certified by peer review) is the author/funder, who has granted bioRxiv a license to display the preprint in perpetuity. It is made available under aCC-BY 4.0 International license.

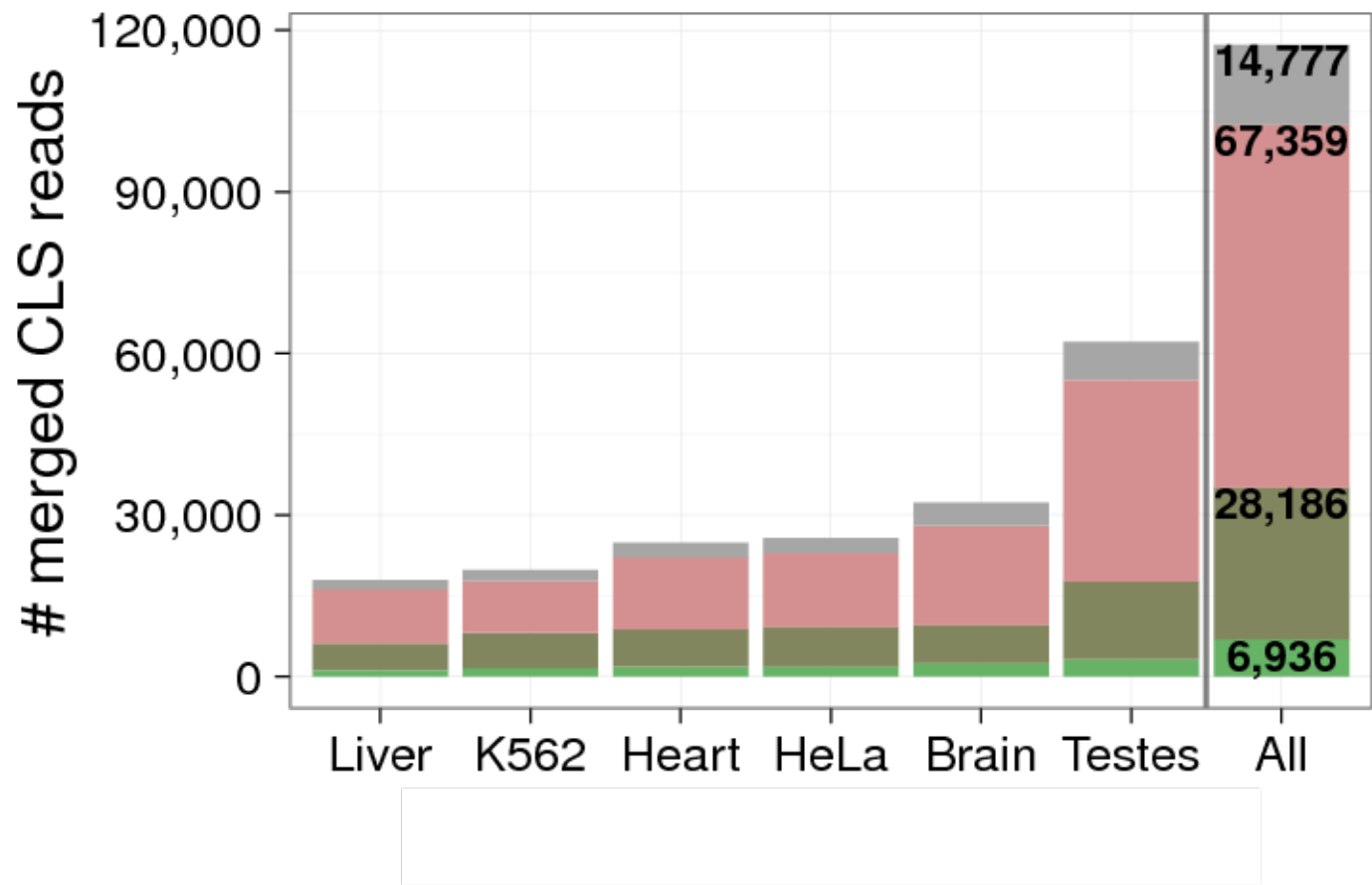
mm splice site scores



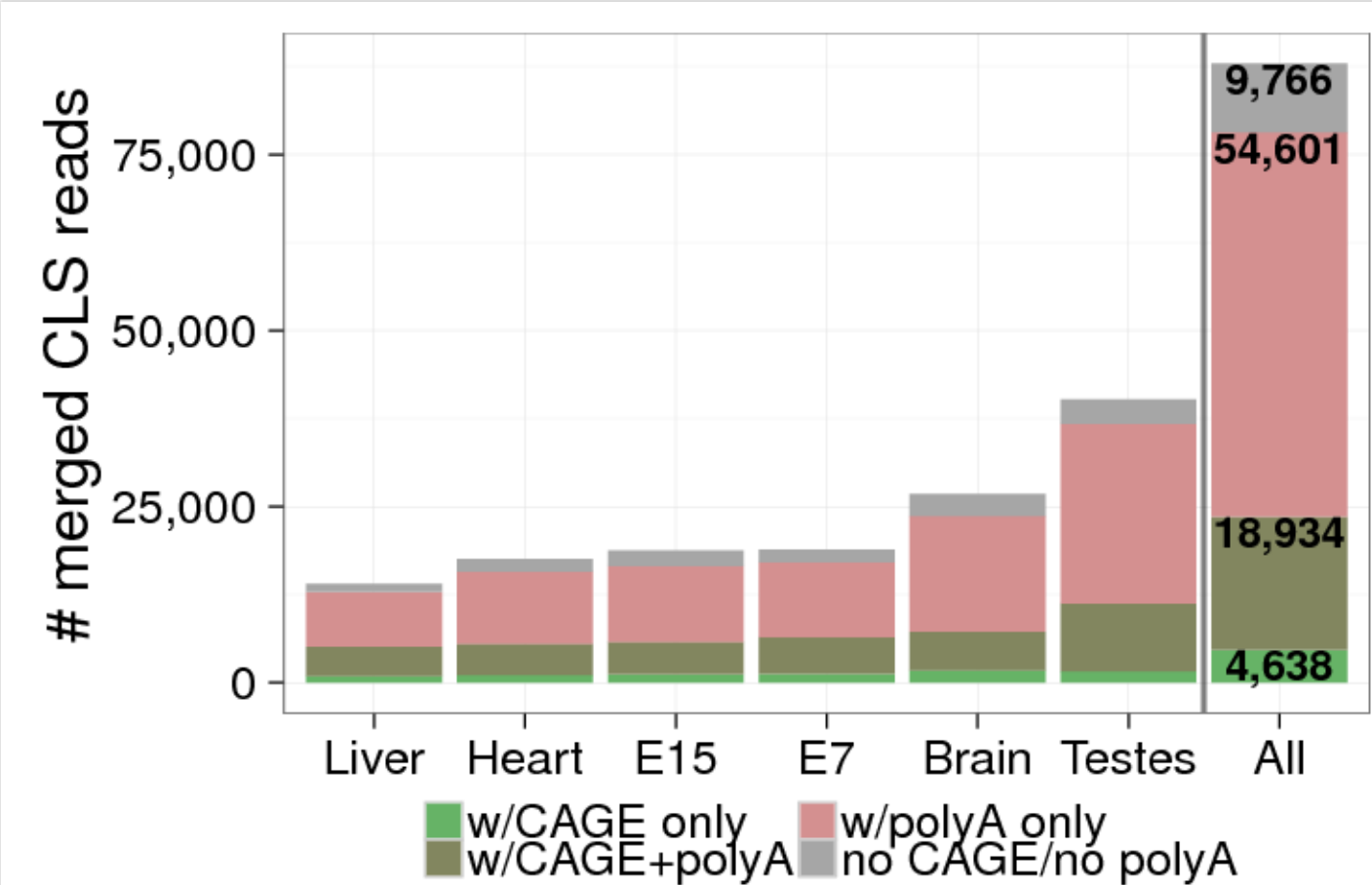
Supplementary Figure S58

bioRxiv preprint doi: <https://doi.org/10.1101/105064>; this version posted June 16, 2017. The copyright holder for this preprint (which was not certified by peer review) is the author/funder, who has granted bioRxiv a license to display the preprint in perpetuity. It is made available under aCC-BY 4.0 International license.

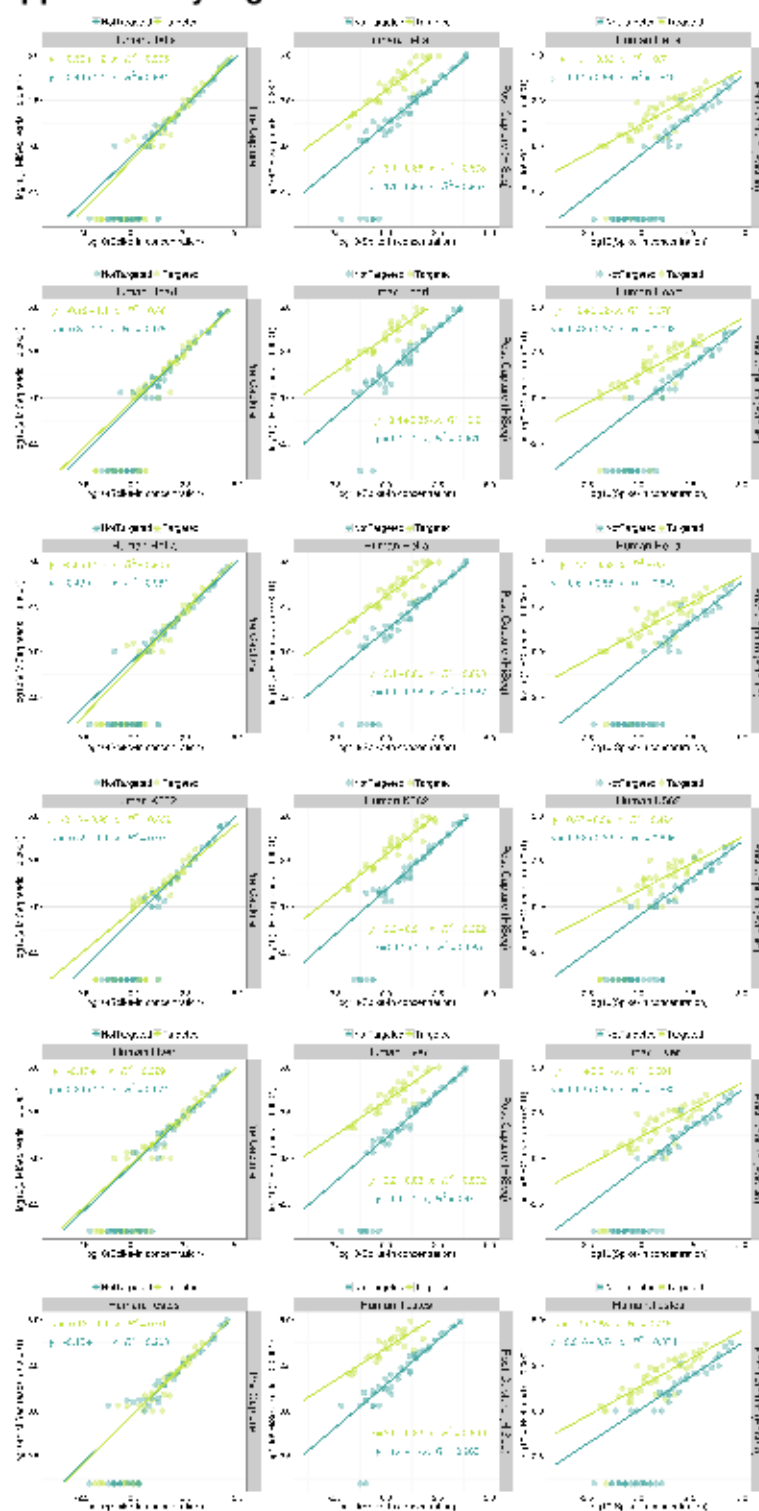
Human



Mouse

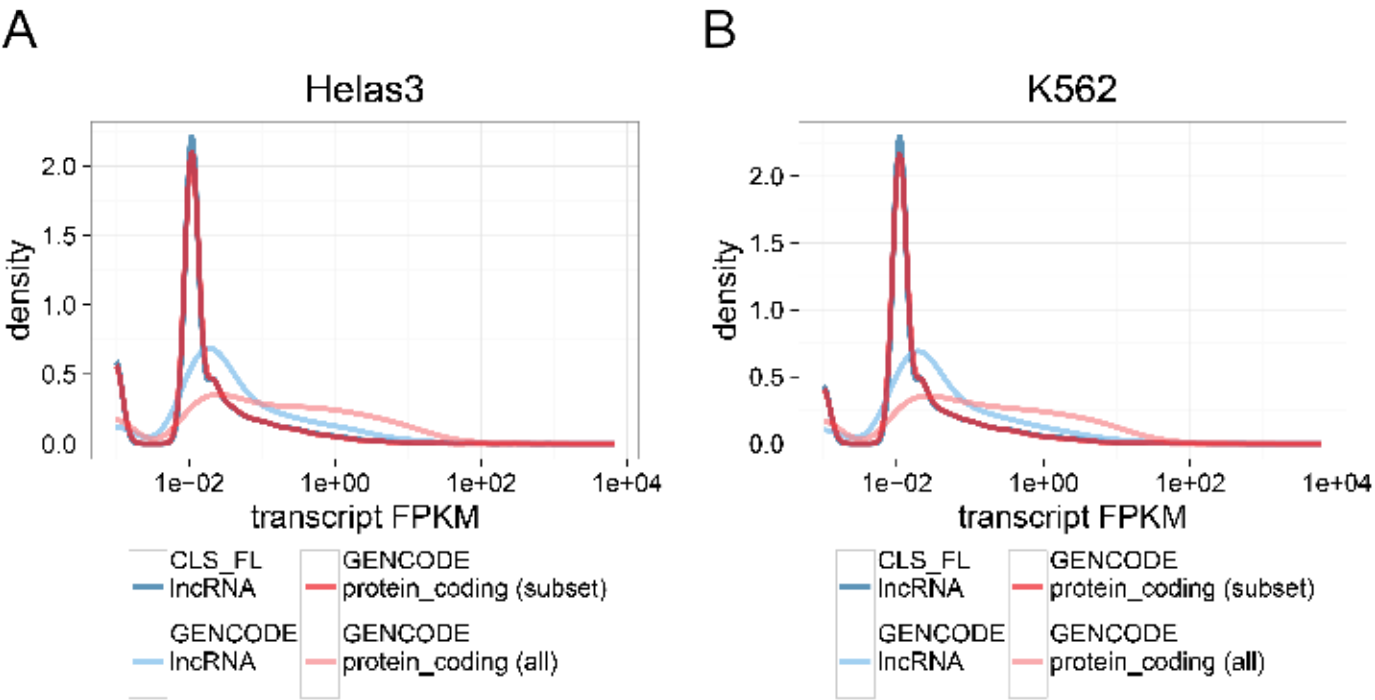


Supplementary Figure S59



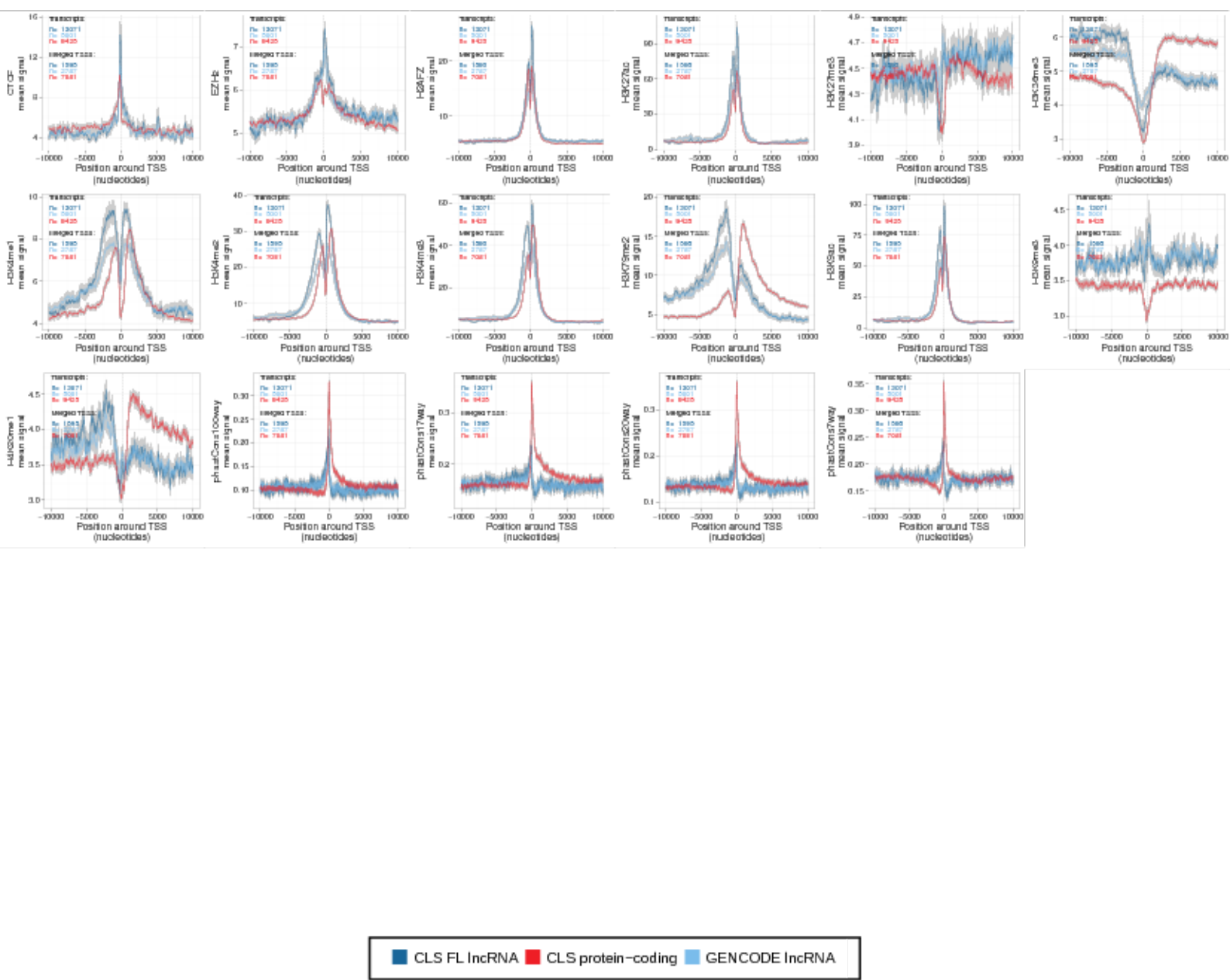
Supplementary Figure S60

bioRxiv preprint doi: <https://doi.org/10.1101/105064>; this version posted June 16, 2017. The copyright holder for this preprint (which was not certified by peer review) is the author/funder, who has granted bioRxiv a license to display the preprint in perpetuity. It is made available under aCC-BY 4.0 International license.



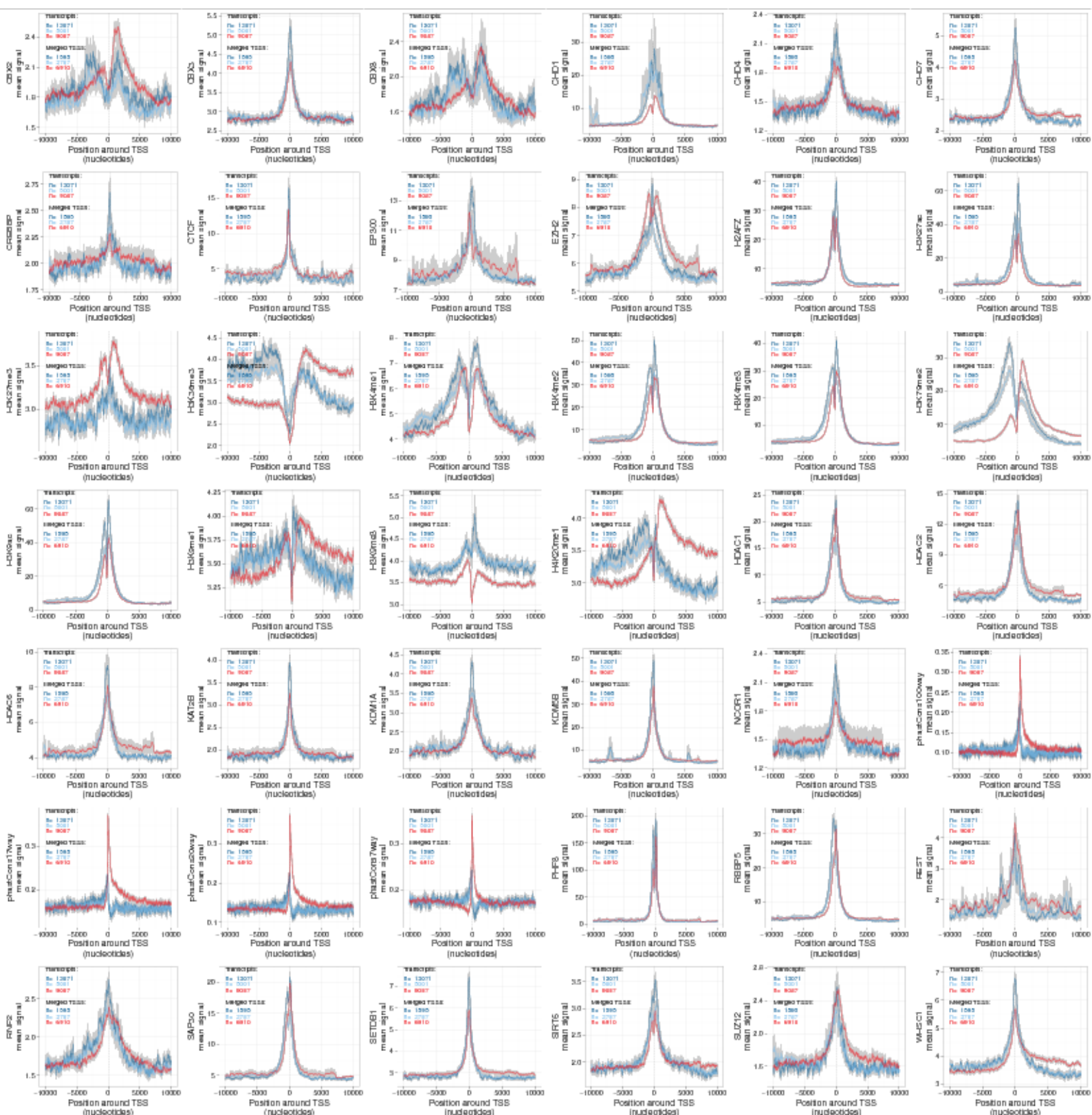
Supplementary Figure S61

bioRxiv preprint doi: <https://doi.org/10.1101/105064>; this version posted June 16, 2017. The copyright holder for this preprint (which was not certified by peer review) is the author/funder, who has granted bioRxiv a license to display the preprint in perpetuity. It is made available under aCC-BY 4.0 International license.



Supplementary Figure S62

bioRxiv preprint doi: <https://doi.org/10.1101/105064>; this version posted June 16, 2017. The copyright holder for this preprint (which was not certified by peer review) is the author/funder, who has granted bioRxiv a license to display the preprint in perpetuity. It is made available under aCC-BY 4.0 International license.



CLS FL lncRNA CLS protein-coding GENCODE lncRNA